UNIVERSITY OF CALIFORNIA SAN DIEGO

Thermally or Optically Powered Actuation of Liquid Crystal Elastomers

A dissertation submitted in partial satisfaction of the

requirements for the degree

Doctor of Philosophy

in

Materials Science and Engineering

by

Chi Hyung Ahn

Committee in charge:

Professor Shengqiang Cai, Chair
Professor Renkun Chen
Professor James R. Friend
Professor Darren Lipomi
Professor Zhaowei Liu

2018

The Dissertation of Chi Hyung Ahn is approved, and it is acceptable in quality and form for publication on microfilm and electronically:

_____

_____

_____

_____

_____

Chair

University of California San Diego

2018

DEDICATION

Dedicated to my beloved Wife, Daughter, and Parents whose unconditional love encourages me to go on every adventure in my life.

TABLE OF CONTENTS

LIST OF FIGURES

ACKNOWLEDGEMENTS

First of all, I would like to express my sincere gratitude to my Ph.D. advisor, Professor Shengqiang Cai, who has motivated me to plunge myself into soft materials science. Under his sincere guidance and support, I could complete my academic achievement. His knowledge inspired me to begin a new journey on my research every time I start a new project and enlightened the way to go.

I also want to give my appreciation to Dr. Xudong Liang whose deep knowledge and understandings on mechanics always fulfilled what I needed more on my study. Because of his help, my research could be enriched. Dr. Zhijian Wang also helped me a lot especially in the lab. His knowledges on Chemistry and the considerate attitude toward experiments are what I really wanted to learn from him. I also want to thanks to Qiguang He for his supports in many aspects of my life in the lab. He always helped me by providing several interesting ideas which inspired me to make a fast actuation system. I also sincerely appreciate Yang Wang for spending lots of time to discuss with me and solving my LCE motion problem. Zhaoqiang Song helped me a lot with making 3d structures by laser cutting instrument though he was busy. I also appreciate Dr. Kai Li who collaborated with me on LCE rolling project. Somaye Jafari and Yue Zheng whom I had no chance to work together, but I would remember the time we spent together in the group. I am also thankful to all other current or former group members who I really look forward to work together in the future.

I also deeply appreciate my committee members, Professor Renkun Chen, Professor James Friend, Professor Darren Lipomi, Professor Zhaowei Liu for their comments, suggestions, and advices to my research.

Lastly, I would like to express my deepest gratitude to my beloved parents, little Ellie, and

my loving wife for their endless love, endurance, and belief.

This work was funded by Haythornthwaite Foundation, National Science Foundation, and Office of Naval Research.

Chapter 2, in part or in full, is a reprint of the following material: C. Ahn, X. Liang, S. Cai "Inhomogeneous stretch induced patterning of molecular orientation in liquid crystal elastomers" Extreme Mechanics Letters, 5, pp. 30-36 (2015). The dissertation author was the primary investigator and author of this paper.

Chapter 4, in part or in full, is a reprint of the following material: C. Ahn, K. Li, S. Cai "Light or Thermally Powered Autonomous Rolling of an Elastomer Rod" ACS Applied Materials and Interfaces, 10, pp. 25689-25696 (2018). The dissertation author was the primary investigator and author of this paper.

Chapter 5, in part or in full, is a reprint of the following material: C. Ahn, X. Liang, S. Cai "Bioinspired design of light-powered crawling, squeezing and jumping of an untethered soft robot" (*Submitted*) (2018). The dissertation author was the primary investigator and author of this paper.

VITA

EDUCATION

2009 Bachelor of Science in Chemical Engineering, Hongik University

2011 Master of Science in Materials Science and Engineering, Seoul National University

2018 Doctor of Philosophy in Materials Science and Engineering, University of California San Diego

PUBLICATIONS

C. Ahn, X. Liang, S. Cai “Bioinspired design of light-powered crawling, squeezing and jumping of an untethered soft robot” *(submitted)*

C. Ahn, K. Li, S. Cai "Light or Thermally Powered Autonomous Rolling of an Elastomer Rod" ACS Applied Materials and Interfaces, 10, pp. 25689-25696 (2018)

S. Cui, C. Ahn, M. C. Wingert, D. Leung, S. Cai, and R. Chen, "Bio-inspired effective and regenerable building cooling using tough hydrogels" Applied Energy, 168, pp. 332-339 (2016)

C. Ahn, X. Liang, S. Cai “Inhomogeneous stretch induced patterning of molecular orientation in liquid crystal elastomers” Extreme Mechanics Letters, 5, pp. 30-36 (2015)

C. Ahn, J.-D. Jeon, and S.-Y. Kwak, “Photoelectrochemical effects of hyperbranched polyglycerol in gel electrolytes on the performance of dye-sensitized solar cells” Journal of Industrial and Engineering Chemistry, 18, pp. 2184-2190 (2012)

ABSTRACT OF THE DISSERTATION

Thermally or Optically Powered Actuation of Liquid Crystal Elastomers

by

Chi Hyung Ahn

Doctor of Philosophy in Materials Science and Engineering

University of California San Diego, 2018

Professor Shengqiang Cai, Chair

Soft actuator is a promising candidate for replacing a traditional rigid materials-based actuator when the actuating system requires human compatibility, large degree of freedom for the motion, low fabrication cost, and simple body structure. Among many soft materials, liquid crystal elastomer (LCE) is one of the most advantageous soft active material due to their large macroscopic deformability coupled with molecular level anisotropy. Patterning of LCE with precise control of molecular alignment can generate diverse actuations. In addition, different types of actuation of LCE can be induced by various external stimuli such as heat or light.

In this study, we demonstrate radially patterned LCE with predesigned stretch field using a strain engineering technique which is facile, effective, and does not require any sophisticated

setup. The radially patterned LCE exhibits fully reversible undulating deformation upon heating or swelling, attributed to the constrained expansion of radially patterned LCE in hoop direction. By applying the strain engineering technique, we design different LCE structures which exhibit diverse actuations like bending, rolling, crawling, or jumping. Incorporation of carbon nanotube (CNT) in the LCE allows photoresponsivity of LCE-CNT composite due to the photothermal effect of CNT. We prepare LCE-CNT rod with molecular alignment in its longitudinal direction which shows heliotropic behavior with multi-directional bending under the light irradiation rather than conventional uni- or bi-directional bending. The bending is induced by the contraction gradient of LCE-CNT rod in thickness which is maximized on the surface towards light, so the bending direction can be tuned by controlling the position of light source. Using the similar LCE or LCE-CNT rod, we show unusual rolling phenomena in which the LCE or LCE-CNT rod keeps rolling while maintaining its initial curvature in the same direction continuously induced by simply placing them on a homogeneously hot flat surface or under the visible light irradiation. Such non-intuitive autonomous rolling phenomena is induced by coupling of inhomogeneously distributed supporting force and gravity, which is triggered by continuous bending deformation of the rod during rolling. We also design a light-driven soft robot based on an arch shape LCE-CNT structure with magnet pieces on each end that performs crawling, squeezing, and jumping motions inspired by deformation traveling of inchworm locomotion and power amplification mechanism of jumping fly larva. The soft robot can perform different motions by switching its shape between arch and closed loop shape under different light irradiation modes, which enables fully reversible biomimetic motions.

Chapter 1 Introduction

1.1 Liquid crystal

Liquid crystal (LC) is a material that exhibits properties between conventional liquid and solid, which is usually consisted with organic molecule (*1, 2*). It flows like a liquid, but its molecules may be oriented in a crystal-like way as a function of temperature (*3*) (Fig 1.1a). Mesogen is a fundamental unit of an organic molecule that enables LC material to exhibit both liquid-crystal behavior. The shape of mesogen is usually rod-like which is constituted by rigid part with aromatic compounds and flexible part with aliphatic compounds (Fig 1.1b). In mesogen, the rigid part contributes molecular alignment in one direction whereas the flexible part induces fluidity in molecules like liquid. When viewed under a microscope using polarized light source, different liquid crystal phases will appear to have distinct textures which correspond to domains where the LC molecules are oriented in different directions. Within a domain, however, the molecules are well ordered. LC materials are not always in a liquid crystal phase and the phase transition can occur under different environmental conditions. LC materials can be divided into three different phases: thermotropic, lyotropic, and metallotropic (*2*). Thermotropic LC materials show phase transition as temperature changes while lyotropic LC materials exhibit its phase transition depending not only on temperature changes but also on their concentration change in a solvent. Different from thermotropic and lyotropic LC materials, both organic and inorganic molecules consist metallotropic LC materials which exhibit phase transition by the ratio between organic and inorganic molecules in addition to the change of temperature or concentration.

The LC phase can be characterized by different types of its ordering status. For example,

thermotropic LC can be an isotropic phase at a temperature higher than its phase transition temperature in which it is in an isotropic phase with a liquid like behavior with a random orientation of molecules. If the temperature is lower than the isotropic transition temperature, LC is in different types of anisotropic structure which exhibit orientational order with still having a fluidity like a liquid. Depending on the ordering phase, LC can be mainly divided into nematic, semectic, and chiral phases (*4, 5*) (Fig. 1.2). Nematic phase is most conventional LC phase in which mesogens can align in a long range directional order with their long axes roughly parallel and no positional order. Nematic LC have a similarity in terms of fluidity like liquid (isotropic phase), but it can be aligned into a certain direction under the external stimuli such as magnetic or electric field. Smectic phase LC can be found at lower temperatures than the nematic phase, which forms distinguishable layers that can slide over one another and positionally ordered along one direction. Based on the orientation profile, the smectic phase can be also divided into Smectic A and Smectic C phases. In Smectic A phase, mesogens are aligned normal to the layer while being tilted from the normal to the layer in Smectic C phase. Chiral phase which is also called as cholesteric phase occurs if there is no internal symmetric plane in mesogens. The characteristic of this phase is that the mesogens are twisted perpendicular to the preferred orientation, resulting in spiral twisting alignment structure normal to the layer.

Due to the anisotropy of LC material which enabling optical property changes under the electric field by controlling the alignment status of mesogens, LC material have been widely applied in liquid crystal display (LCD) industry for several decades. In addition to utilizing LC molecules itself, polymerized LC materials are emerging for the soft actuating applications which will be discuss in the following section.

1.2 Liquid crystal elastomer

Liquid crystal elastomer (LCE) is a crosslinked polymeric material mainly caused by polymerization of mesogens with other crosslinkable molecules (*6*-*8*). The principle characteristics of LCE is that the orientation of LC can be coupled to the macroscopic deformation of polymeric network (Fig. 1.3). In other words, the change in orientation of mesogens in molecular level induced by external stimuli such as temperature, electric, or magnetic field can generate macroscopic deformation in a whole polymeric material. In addition, by applying the mechanical stress on the LCE, the alignment status of LC molecules can be also changed since they can uptake mechanical strain with a crosslinked structure which is different from when they are in small molecules.

LCE can be divided into amorphous or crystalline structure according to the phase of LC molecules (Fig. 1.4). Amorphous LCE structure can be usually found above the temperature high enough to induce isotropic phase transition of LC molecules. At amorphous structure of LCE, the LC molecules are in an isotropic phase, therefore no alignment of LC can be found in the whole LCE structure. Below the isotropic phase transition temperature, LCE is in crystalline structure which also can be divided into two different configurations: monodomain and polydomain configuration. When the LCE is in a polydomain configuration, there are large number of small domains in the LCE structure in which LC molecules are aligned but disordered macroscopically. Therefore, there is no principal orientation in polydomain LCE and it does not generate any macroscopic contraction under external stimuli. On the other hand, in the LCE with monodoamin configuration with a single crystalline structure, LC molecules align in one direction macroscopically with a principal orientation, which enables LCE contract macroscopically along

the aligned direction under external stimuli. Therefore, to enable macroscopic spontaneous and reversible deformation of LCE under the external stimuli, LCE needs to be in a monodomain configuration.

Since LCE is composed of polymeric material with random coil structure, LCE synthesized from LC molecules without any careful treatment is conventionally in a polydomain configuration. Therefore, there have been many approached to prepared monodomain LCE. Firstly, Finkelmann prepared monodomain LCE using two-step crosslinking method which utilizes reaction kinetics difference between two functional group of LCE during the heat induced polymerization process (*9*). In this method, partially crosslinked LCE is prepared and uniaxial strain is applied to align LCE in one direction followed by further thermal reaction to obtain fully crosslinked monodomain LCE. Another method is utilizing alignment layer before LCE is synthesized (*10-12*). Alignment layer such as polyimide thin film is coated on substrate and LC molecules and other reactants are placed on the alignment layer. After long axis of LC molecules are oriented along the alignment layer, polymerization process is induced by UV or heat, results in the fully crosslinked monodomain LCE. Recently, Yakacki et al. introduced thiol-acrylate two step crosslinking method (Fig. 1.5) (*13*). Different from the previously reported two step crosslinking method utilizing kinetics difference during the thermal polymerization process, this method utilizes UV curing process for the second step crosslinking at room temperature. Therefore, monodomain LCE structures with various shape can be easily prepared by molding LCE before it is fully cured.

The monodomain and polydomain LCE can be easily distinguished due to their different optical property. Since the polydomain LCE induces light scattering, it is turbid whereas the monodomain LCE is transparent (Fig. 1.6a). Therefore, from the partially crosslinked polydomain LCE, we can observe gradual transparency change as the LCE changing from polydomain to

monodomain under uniaxial strain. Under the tensile test of the partially crosslinked polydomain LCE, we can also observe the transition of polydomain to monodomain. In the tensile test, we can observe a plateau in the middle of the curve accompanied by LC molecular rotation that is the sign of transition from polydomain to monodomain configuration under the uniaxial strain, which cannot be observed in the curve obtained from monodomain LCE. Fully crosslinked monodomain LCE also exhibits reversible thermal actuation. When the temperature is increased to 95 ℃, monodomain LCE shows significant large deformation with around 30% of contraction strain and recovers its original shape upon it is cooled to the room temperature (Fig. 1.6b). In addition, monodomain LCE swells anisotropically as it can swell more in the direction perpendicular to the initial orientation (Fig. 1.6c). Due to the large deformability, LCE can be applied on different types of soft actuators induced by heat, magnetic field, electric field, or light depending on its components.

1.3 Soft actuators

Soft actuators have been broadly and intensively studied in recent years, because of its potential advantages such as contact compliance, low fabrication cost, resistance to the mechanical damage, human compatibility with their similar modulus to the human skin, simple structure and large number of degrees of freedom for the actuation over the conventional rigid actuators (*14-16*). Because of its soft structure without any joint, soft actuators can exhibit continuous, large, and diverse deformation modes such as contraction (*17, 18*), bending (*19, 20*), twisting (*10, 21*), oscillation(*22*) with even simpler structure and various shapes. Based on the diverse deformation modes of soft actuators, they exhibit various types of actuating motions such as rolling,

manipulation, gripping, locomotion, swimming, crawling, and jumping. For instance, as shown in Fig. 1.7a cylindrical shape polymer coated with carbon nanotube (CNT) can roll under the light irradiation driven by torque obtained from gravity center change (*23*). Quadrupedal locomotion in a soft tetrapod robot has been reported with individually controllable legs with embedded pneumatic channels which allows independent deformation of each legs by inflation through each pneumatic channels (*24*) (Fig. 1.7b). Fig.1.7c shows LCE based disc driven by laser that can swim on the surface of water with a localized deformation which enables obtaining propulsion from water (*25*).

The power source for driving soft actuator needs to be carefully considered. So far, many types of energy source have been adopted for driving soft actuators such as air pressurizing, electricity, humidity, heat, and light (*14*). Soft actuators adopted with pneumatic channels are one of the most widely studied system, but they are usually bulky and the structure needs to be tethered. Similarly, the electrically powered soft actuators are usually wired, and the power source needs to be rigid which may also increase the weight of the soft actuator and make the actuating system inefficient. The advantage of humidity, heat, or light based soft actuators is their tetherless structure and the power source can be obtained from nature (*26-32*). However, the difficulty in controlling the power source makes them hard to be applied in practical applications. Soft actuators driven by different power sources have their own strength or weakness, and recent promising researches including power source based on graphene, organic polymers, and conductive fabric materials may potentially benefit for the practical applications of soft actuators in the future (*14*).

1.4 Light or heat induced soft actuators based on LCE

There have been different types of materials adopted to the base material for the soft actuator range such as silicone based materials, shape memory polymer, and other different types of polymers Among different types of materials, LCE is one of the most attractive materials for the soft actuator because of its large deformability based on the anisotropic nature, patterning processability for various actuation modes, and capability of using various of power sources with simple structure (*33, 34*). Recently, many studies have reported soft actuators using LCE triggered by heat (*31, 35*), magnetic field (*36, 37*), electricity (*38, 39*), and light(*40, 41*).

Among different types of power sources, heat and light driven LCE soft actuators are advantageous because of their tetherless and simple structures and easy fabrication process. Therefore, there have been many studies on heat or light induced LCE soft actuators from simple deformation to complicated robotic systems reported in recent years. For instance, LCE can oscillate under continuous light irradiation induced by the alternate light irradiation on the top and bottom surface (*22*). LCE film precisely patterned with digital patterning technique deforms from flat sheet to three-dimensional cone shapes upon heating (Fig. 1.8) (*12*). In addition, LCE can even swim, crawl, or roll driven by thermal or optical energy sources. Laser induced LCE fish has been reported that can swim on the surface of water under the localized laser irradiation with a swimming direction controllability (Fig. 1.9a) (*25*). LCE and polyethylene double layer structure can crawl under alternate UV and visible light irradiation by the variation of its frictional force with bending and unbending deformation (Fig. 1.9b) (*42*). An initially flat LCE film can roll under the light irradiation by deforming its shape into helical shape to generate torque (Fig. 1.9c) (*10*).

For the thermally driven LCE soft robots, any special strategy is not required to generate

actuation since LCE itself is sensitive to heat to get macroscopic deformation with disorder or reorientation of anisotropic mesogens constituting LCE structure. However, light-induced LCE soft actuator requires additional components that endows light-sensitivity on LCE. Therefore, LCE with azobenzene moiety or carbon materials have been commonly used to get photoactuation. LCE containing azobenzene moiety can be photosensitive attributed to the *trans-cis* isomerization under UV or visible light irradiation which triggers macroscopic deformation of LCE by the geometry alteration of LC molecules within LCE (*43, 44*). Another approach is incorporation of carbon materials such as CNT into the LCE matrix (*45, 46*). Because of the photothermal effect of CNT which converts incoming photo energy into thermal energy in the LCE, LCE can be either heat or photoresponsive upon mixed with CNT.

a

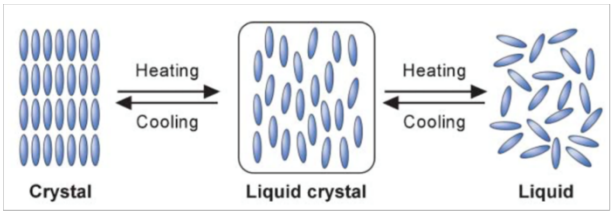

< LC phase transition >

b

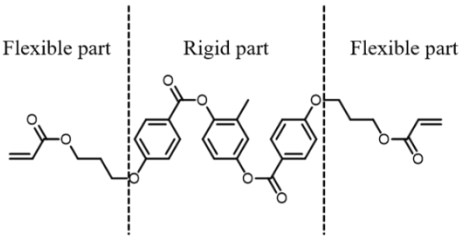

< Example of the mesogens strucutre >

Figure 1.1: (a) Phase transition of LC with temperature change (3). (b) Example of mesogens structure containing rigid part and flexible part.

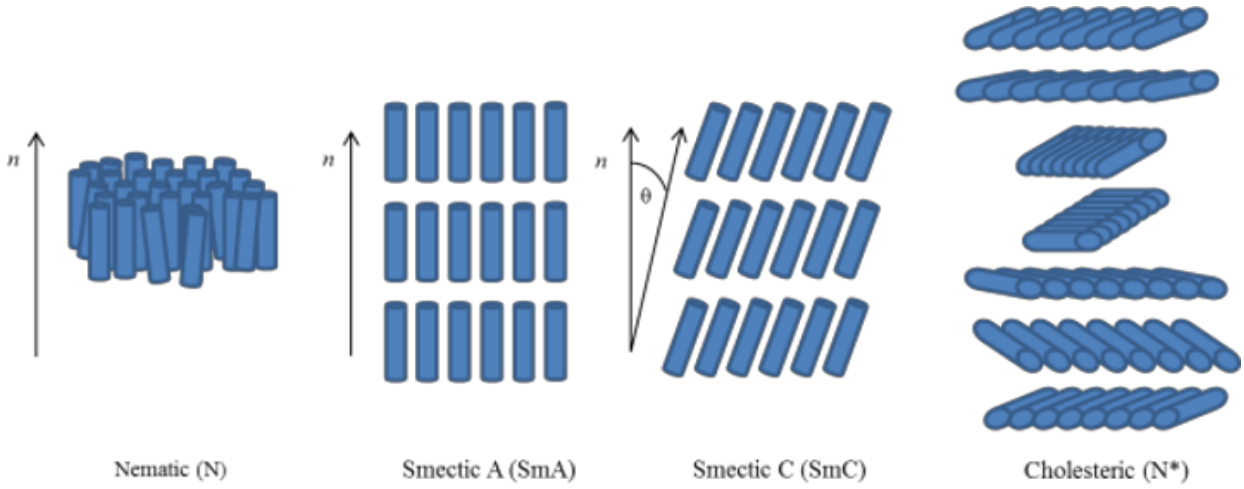

Figure 1.2: Thermotropic LC phases arranged from left to right in order of increasing order and decreasing temperature (*4*).

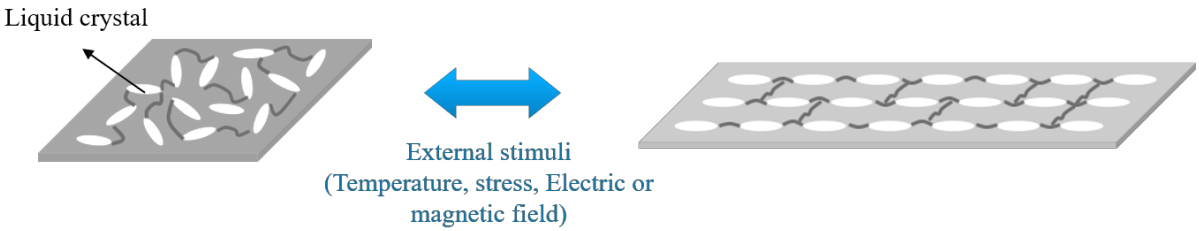

Figure 1.3: Schematic of coupling between the LC orientation and the macroscopic deformation in LCE.

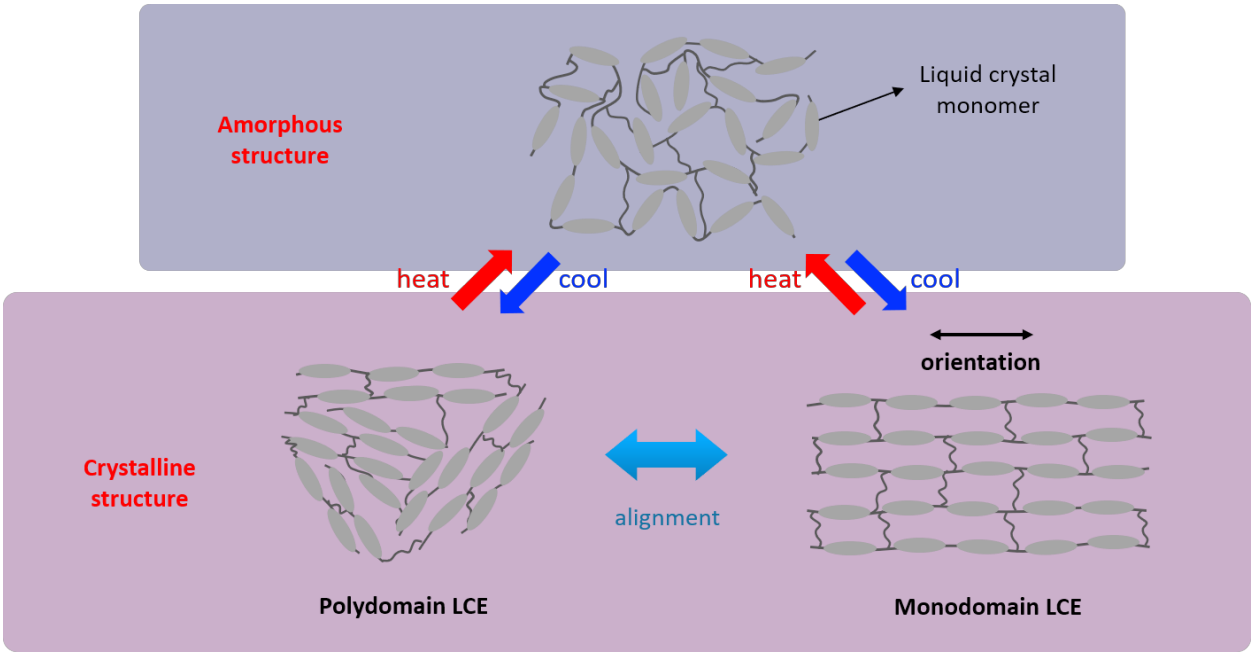

Figure 1.4: Schematic of LCE phase transition by change of temperature or alignment status.

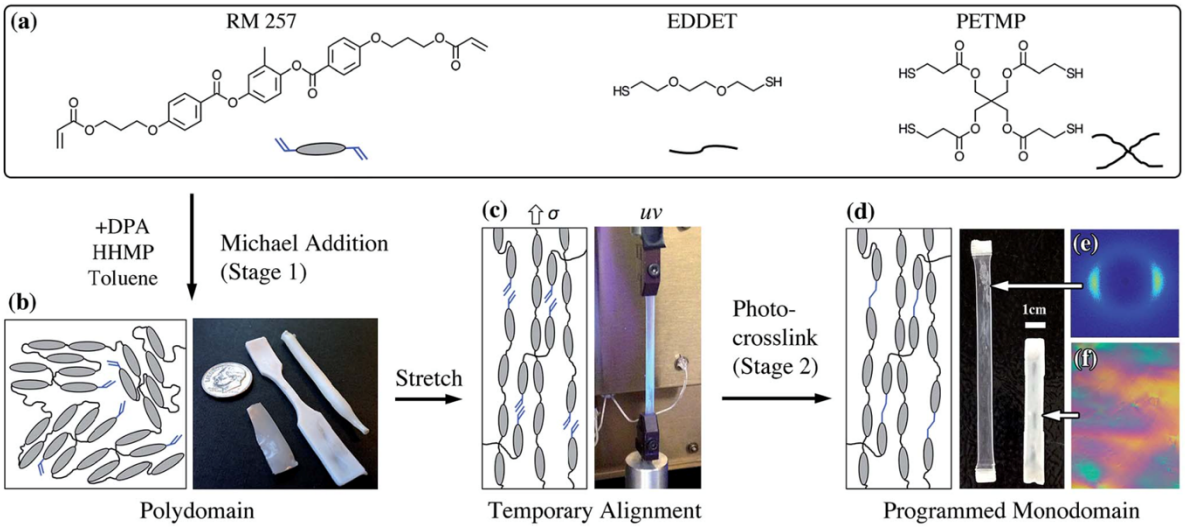

Figure 1.5: Thiol-acrylate Michael addition and photopolymerization reaction (TAMAP) two step crosslinking method for monodomain LCE (*13*).

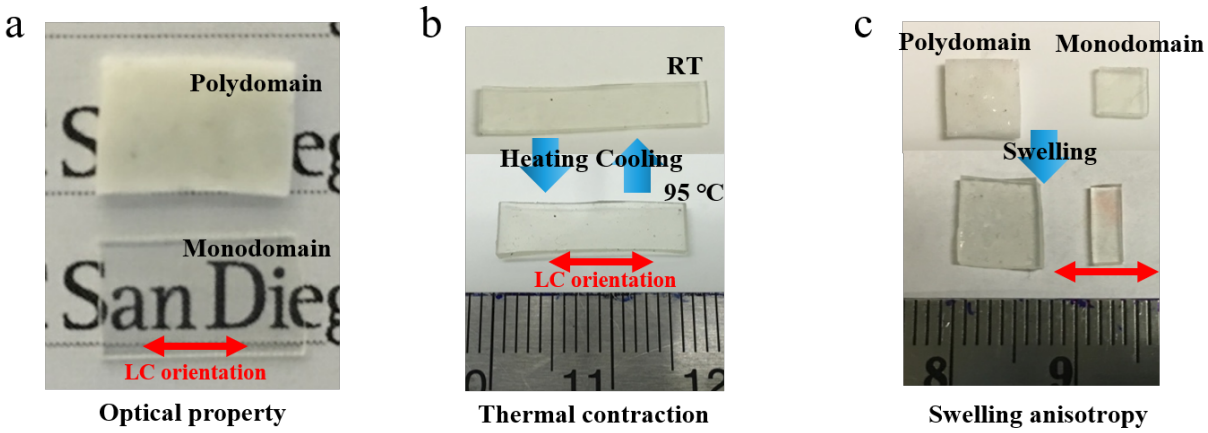

Figure 1.6: Intrinsic properties of monodomain LCE with (a) optical transparency, (b) thermal contraction behavior, and (c) swelling anisotropy.

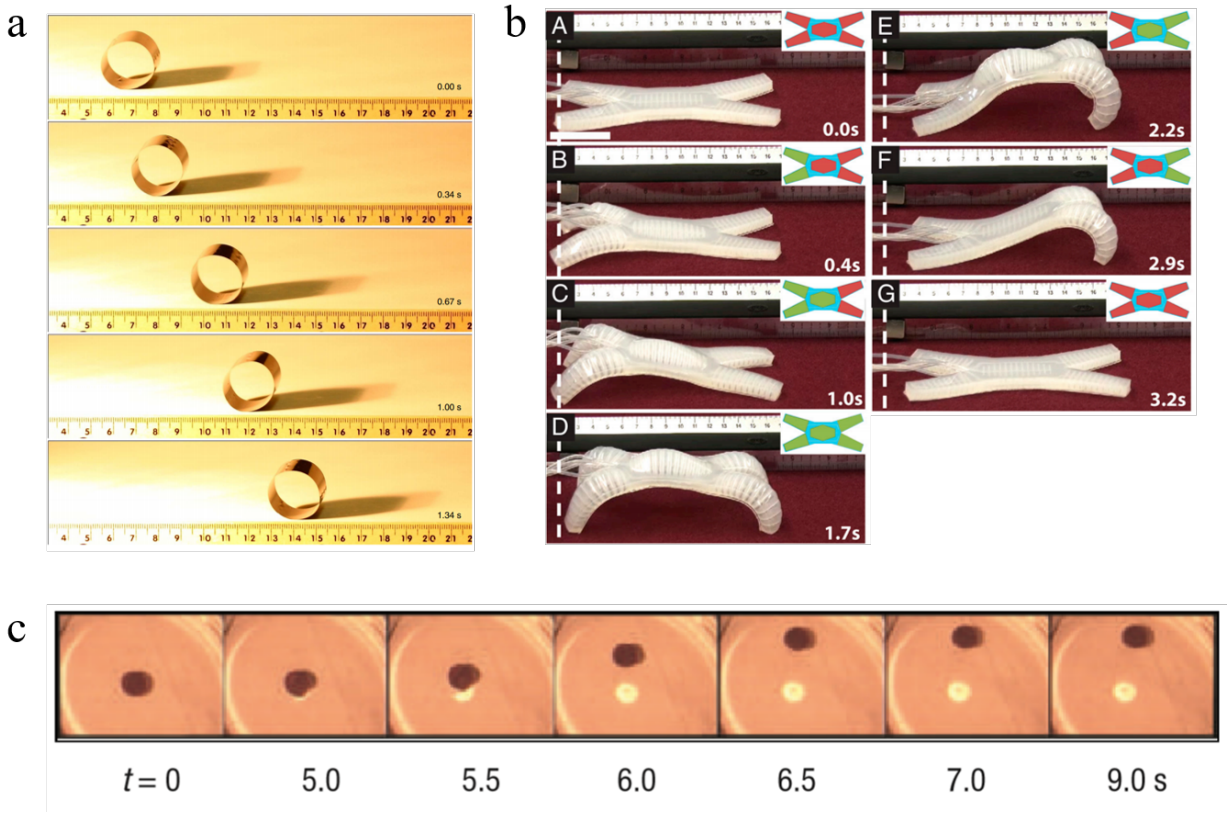

Figure 1.7: Different types of soft actuations (a) Light-induced rolling of CNT-polymer bilayer structure (*23*). (b) Quadrupedal locomotion in a soft tetrapod robot with embedded pneumatic channels (*24*). (c) Optically driven swimming LCE disk (*25*).

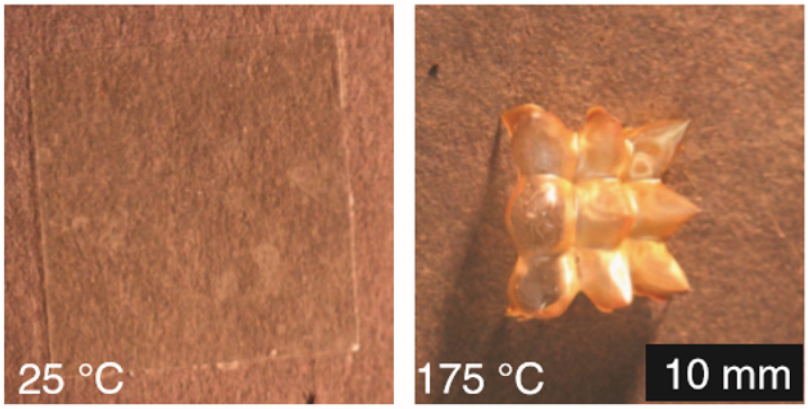

Figure 1.8: Thermally driven deformation of flat LCE sheet into 3D structure prepared by precise digital patterning technique (*12*).

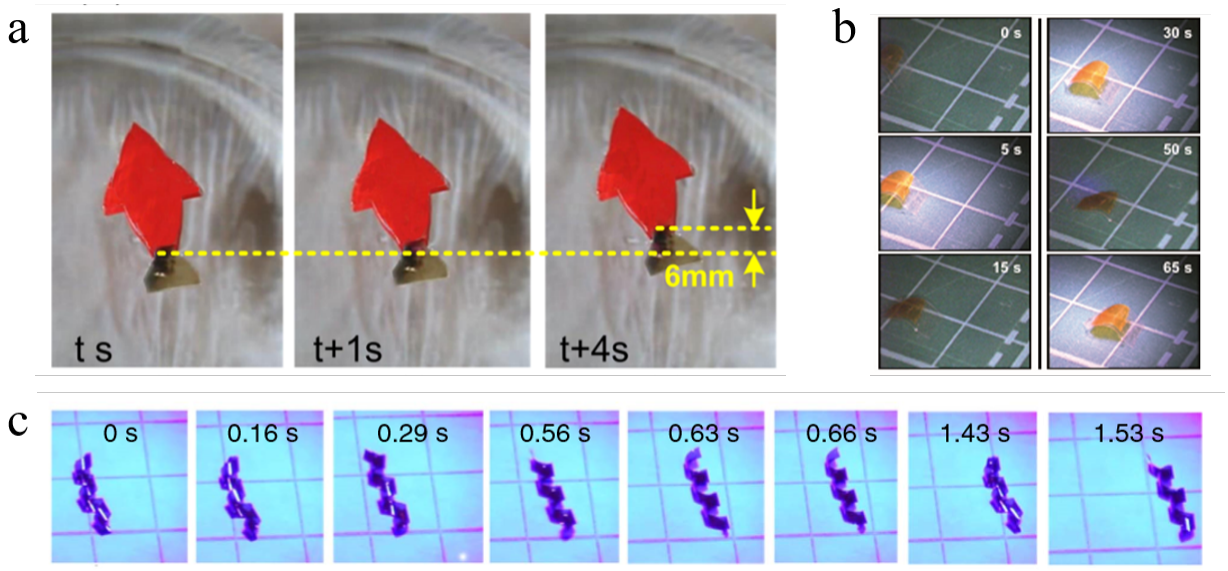

Figure 1.9: Light-driven soft actuation of LCE (a) Swimming motion of light-sensitive LCE fish with localized deformation (*47*). (b) Photomobile soft walker with LCE and PE double layer structure under alternate UV and visible light irradiation (*42*). (c) Rolling of LCE strip with a twisted nematic geometry induced by UV light (*10*).

1.5 References

1. S. Chandrasekhar, *Liquid Crystals*. (Cambridge University Press, ed. 2nd).

2. M. Barón, R. F. T. Stepto, Definitions of basic terms relating to polymer liquid crystals (IUPAC Recommendations 2001). *Pure Appl*. *Chem.* **74**, 493 (2002)

3. T. Kato, Y. Hirai, S. Nakaso, M. Moriyama, Liquid-crystalline physical gels. *Chem. Soc. Rev.* **36**, 1857 (2007).

4. J. G. Fernsler, University of Colorado Boulder (2007).

5. T. Matsui, *Numerical Simulation of Lasing Dynamics in Choresteric Liquid Crystal Based on ADE-FDTD Method*. (2011).

6. H. Finkelmann, A. Greve, M. Warner, The elastic anisotropy of nematic elastomers. *Eur. Phys. J. E* **5**, 281 (2001).

7. P. Xie, R. Zhang, Liquid crystal elastomers, networks and gels: advanced smart materials. *J. Mater. Chem.* **15**, 2529 (2005).

8. K. Urayama, Selected Issues in Liquid Crystal Elastomers and Gels. *Macromolecules* **40**, 2277 (2007).

9. J. Küpfer, H. Finkelmann, Nematic liquid single crystal elastomers. *Die Makromol. Chemie, Rapid Commun.* **12**, 717 (1991).

10. J. J. Wie, M. R. Shankar, T. J. White, Photomotility of polymers. *Nat. Commun*, **7**, 13260 (2016).

11. A. H. Gelebart, D. J. Mulder, M. Varga, A. Konya, G. Vantomme, E. W. Meijer, R. L. B. Selinger and D. J. Broer, Making waves in a photoactive polymer film. *Nature* **546**, 632 (2017).

12. T. H. Ware, M. E. McConney, J. J. Wie, V. P. Tondiglia, T. J. White, Voxelated liquid crystal elastomers. *Science* **347**, 982 (2015).

13. C. M. Yakacki, M. Saed, D. P. Nair, T. Gong, S. M. Reed, C. N. Bowman, Tailorable and Programmable Liquid-Crystalline Elastomers Using a Two-Stage Thiol–Acrylate Reaction. *RSC Adv.* ***5***, 18997 (2015)

14. D. Rus, M. T. Tolley, Design, fabrication and control of soft robots. *Nature* **521**, 467 (2015).

15. S. Kim, C. Laschi, B. Trimmer, Soft robotics: a bioinspired evolution in robotics. *Trends Biotechnol.* **31**, 287 (2013).

16. C. Laschi, B. Mazzolai, M. Cianchetti, Soft robotics: Technologies and systems pushing the boundaries of robot abilities. *Sci. Robot.* **1**, 3690 (2016).

17. T. Ikeda, J.-i. Mamiya, Y. Yu, Photomechanics of Liquid-Crystalline Elastomers and Other Polymers. *Angew. Chem. Int. Ed.* **46**, 506 (2007).

18. M.-H. Li, P. Keller, Artificial muscles based on liquid crystal elastomers *Phil. Trans. R. Soc. A*, 2763 (2006).

19. O. M. Wani, H. Zeng, A. Priimagi, A light-driven artificial flytrap. *Nat. Commun.* **8**, 15546 (2017).

20. Y. Yu, M. Nakano, T. Ikeda, Photomechanics: Directed bending of a polymer film by light. *Nature* **425**, 145 (2003).

21. S. Iamsaard, S. J. Aßhoff, B. Matt, T. Kudernac, J. J. L. M. Cornelissen, S. P. Fletcher, N. Katsonis, Conversion of light into macroscopic helical motion. *Nature Chem.* **6**, 229 (2014).

22. K. Kumar, C. Knie, D. Bleger, M. A. Peletier, H. Friedrich, S. Hecht, D. J. Broer, M. G. Debije and A. P.H.J. Schenning, A chaotic self-oscillating sunlight-driven polymer actuator. *Nat. Commun.* **7**, 11975 (2016).

23. X. Zhang, Z. Yu, C. Wang, D. Zarrouk, J.-W. T. Seo, J. C. Cheng, A. D. Buchan, K. Takei, Y. Zhao, J. W. Ager, J. Zhang, M. Hettick, M. C. Hersam, A. P. Pisano, R. S. Fearing and A. Javey, Photoactuators and motors based on carbon nanotubes with selective chirality distributions. *Nat. Commun.* **5**, 2983 (2014)

24. R. F. Shepherd, R. F. Shepherd, F. Ilievski, W. Choi, S. A. Morin, A. A. Stokes, A. D. Mazzeo, X. Chen, M. Wang and G. M. Whitesides, Multigait soft robot. *PNAS* **108**, 20400 (2011).

25. M. Camacho-Lopez, H. Finkelmann, P. Palffy-Muhoray, M. Shelley, Fast liquid-crystal elastomer swims into the dark. *Nat. Mater.* **3**, 307 (2004).

26. L. Zhang, X. Qiu, Y. Yuan, T. Zhang, Humidity- and Sunlight-Driven Motion of a Chemically Bonded Polymer Bilayer with Programmable Surface Patterns. *ACS Appl. Mater. Inter.* **9**, 41599 (2017).

27. Z. Lidong, N. Panče, Light- and Humidity-Induced Motion of an Acidochromic Film. *Angew. Chem. Inter. Ed.* **54**, 8642 (2015).

28. B. Shin, J. Ha, M. Lee, K. Park, G. H. Park, T. H. Choi, K.-J. Cho and H.-Y. Kim, Hygrobot:A self-locomotive ratcheted actuator powered by environmental humidity. *Sci. Robot.* **3**, 2629 (2018).

29. Y. Sawa, K. Urayama, T. Takigawa, A. DeSimone, L. Teresi, Thermally Driven Giant Bending of Liquid Crystal Elastomer Films with Hybrid Alignment. *Macromolecules* **43**, 4362 (2010)

30. X. Zhang, C. L. Pint, M. H. Lee, B. E. Schubert, A. Jamshidi, K. Takei, H. Ko, A. Gillies, R. Bardhan, J. J. Urban, M. Wu, R. Fearing and A. Javey, Optically- and Thermally-Responsive Programmable Materials Based on Carbon Nanotube-Hydrogel Polymer Composites. *Nano Lett*. **11**, 3239 (2011).

31. C. Ahn, K. Li, S. Cai, Light or thermally powered autonomous rolling of an elastomer rod. *ACS Appl. Mater. Inter.* **10**, 25689 (2018).

32. C. Ahn, X. Liang, S. Cai, Inhomogeneous stretch induced patterning of molecular orientation in liquid crystal elastomers. *Extrem. Mech. Lett.* **5**, 30 (2015).

33. T. Ube, T. Ikeda, Photomobile Polymer Materials with Crosslinked Liquid-Crystalline Structures: Molecular Design, Fabrication, and Functions. *Angew*. *Chem*. *Int*. *Ed*. **53**, 10290 (2014)

34. T. Ube, K. Kawasaki, T. Ikeda, Photomobile Liquid-Crystalline Elastomers with Rearrangeable Networks. *Adv. Mater.* **28**, 8212 (2016).

35. Y. Sawa, K. Urayama, T. Takigawa, A. DeSimone, L. Teresi, Thermally Driven Giant Bending of Liquid Crystal Elastomer Films with Hybrid Alignment. *Macromolecules* **43**, 4362 (2010).

36. H. M. Song, J. C. Kim, J. H. Hong, Y. B. Lee, J. Choi, J. I. Lee, W. S. Kim, J.-H. Kim and N. H. Hur, Magnetic and Transparent Composites by Linking Liquid Crystals to Ferrite Nanoparticles through Covalent Networks. *Adv. Funct. Mater.* **17**, 2070 (2007).

37. J. M. Haberl, A. Sanchez-Ferrer, A. M. Mihut, H. Dietsch, A. M. Hirt, R. Mezzenga, Liquid-Crystalline Elastomer-Nanoparticle Hybrids with Reversible Switch of Magnetic Memory. *Adv. Mater.* **25**, 1787 (2013).

38. Y. Hu, J. Liu, L. Chang, L. Yang, A. Xu, K. Qi, P. Lu, G. Wu, W. Chen and Y. Wu, Electrically and Sunlight-Driven Actuator with Versatile Biomimetic Motions Based on Rolled Carbon Nanotube Bilayer Composite. *Adv. Funct. Mater.* **27**, 1704388 (2017).

39. H. Finkelmann, M. Shahinpoor, Electrically-controllable liquid crystal elastomer-graphite composite artificial muscles. Society of Photo-Optical Instrumentation Engineers, Bellingham, WA, INTERNATIONAL. **4695**, 506 (2002)

40. H. Zeng, O. M. Wani, P. Wasylczyk, R. Kaczmarek, A. Priimagi, Self-Regulating Iris Based on Light-Actuated Liquid Crystal Elastomer. *Adv. Mater.* **89**, 1701814 (2017).

41. H. Zeng, O. M. Wani, P. Wasylczyk, A. Priimagi, Light-driven, caterpillar-inspired miniature inching robot. *Macromol. Rapid Commun.* **39**, 1700224 (2018).

42. M. Yamada, M. Kondo, R. Miyasato, Y. Naka, J.-i. Mamiya, M. Kinoshita, A. Shishido, Y. Yu, C. J. Barrett and T. Ikeda, Photomobile polymer materials—various three-dimensional movements. *J. Mater. Chem.* **19**, 60 (2009).

43. Z. Hao, W. Piotr, W. D. S., P. Arri, Light Robots: Bridging the Gap between Microrobotics and Photomechanics in Soft Materials. *Adv. Mater.* **30**, 1703554 (2018).

44. T. Yoshino, M. Kondo, J.-i. Mamiya, M. Kinoshita, Y. Yu, T. Ikeda, Three-Dimensional Photomobility of Crosslinked Azobenzene Liquid-Crystalline Polymer Fibers. *Adv. Mater.* **22**, 1361 (2010).

45. C. Li, Y. Liu, X. Huang, H. Jiang, Direct Sun-Driven Artificial Heliotropism for Solar Energy Harvesting Based on a Photo-Thermomechanical Liquid-Crystal Elastomer Nanocomposite. *Adv. Funct. Mater.* **22**, 5166 (2012).

46. C. Li, Y. Liu, C.-w. Lo, H. Jiang, Reversible white-light actuation of carbon nanotube incorporated liquid crystalline elastomer nanocomposites. *Soft Matter* **7**, 7511 (2011).

47. H. Tian, Z. Wang, Y. Chen, J. Shao, T. Gao and S. Cai, Polydopamine-Coated Main-Chain Liquid Crystal Elastomer as Optically Driven Artificial Muscle. *ACS Appl. Mater. Inter.* **10**, 8307 (2018).

Chapter 2 Stretch Induced Patterning of a Liquid Crystal Elastomer

Liquid crystal elastomer (LCE) is soft active material, which can have large deformation when subjected to various external stimuli. Due to the coupling between the orientation of liquid crystal (LC) molecules in the elastomer and the deformation of LCEs, mechanical behaviors of LCEs can be significantly modified by manipulating LC molecular orientation field in the material. In the letter, we demonstrate, for the first time, that inhomogeneous and anisotropic stretch field can be used to pattern LC molecular orientation in the LCE during its synthesis. We further show that different active deformation modes can be realized in LCE sheets with different patterns of LC molecules. The method developed in the letter to pattern LC molecular orientation field in the LCE is facile and effective, which may find wide applications in fabricating programmable materials and structures.

2.1 Introduction

A combination of liquid crystal (LC) and polymer network can form a new material-liquid crystal elastomer (LCE). The special molecular combination endows LCE with many unique properties such as soft or semi-soft elasticity *(1-4)* and multi-responsiveness *(5–9)*, which have led to myriad applications ranging from artificial muscle *(7,10)* to stretchable optical devices *(11–14)*. Recently, several biological materials such as actin filament network *(15)* and fibrillar collagens *(16)* have also been found to have similar molecular structure and behaviors as man-made LCEs.

A salient feature of LCE is that the orientation of LC molecules inside the elastomer is coupled with macroscopic deformation of polymer network and vice versa *(17–21)*. In another word, the change of the orientation of LC molecules can deform the elastomer. On the other hand, the deformation of the elastomer can induce reorientation of LC molecules. As a consequence, LC molecules with macroscopically uniform orientation (or monodomain LCE) can be achieved by applying uniaxial stretch onto a polydomain LCE sample, which has been utilized to synthesize monodomain LCEs as first developed by Finkelmann et al. *(22)*. In the experiment, uniaxial tension was applied onto a lightly-crosslinked polydomain LCE sample to align the LC molecules in one direction. The aligned orientation of LC molecules was further frozen in the LCE by the second-step crosslinking of the polymer network. The development of the synthesis of monodomain LCE has greatly broadened its applications *(23,24)*. The method developed by Finkelmann is still commonly adopted by different researchers to make monodomain LCE due to its robustness and generality.

Because of the coupling between the orientation of LC molecules and the network deformation, deformation of LCEs can be driven by various external stimuli such as temperature

change, light irradiation and magnetic or electric field *(25–28)*. Through fabricating different structures, diverse deformation modes in LCEs actuated by different stimuli have been observed in experiments *(29–31)*. For instance, bending, twisting or surface wrinkling in a bi- layered LCE have been realized by changing temperature *(32,33)*. As another example, LCEs containing photosensitive azobenzene moiety show three-dimensional photoactuated deformation under the light irradiation *(34–36)*.

Recently, photoalignment method has been developed to obtain pre-designed LC molecular orientation field in LCEs *(37)*. Different from fabricating LCE structures with different geometries, this method directly manipulates LC molecular orientation in a LCE using properly designed light or electric field. The developed experimental method has opened not only new research opportunities but also innovative applications of LCEs *(38,39)*. However, the corresponding experimental setup is usually complex and the method only work for synthesizing LCEs containing several particular kinds of LC molecules.

Within the context, in the paper, we develop a strain engineering technique to pattern LC molecular orientation in LCEs. Our method can be regarded as generalization of the experiment developed by Finkelmann et al. Instead of applying homogeneous stretch, we apply predesigned inhomogeneous and anisotropic stretch in a lightly-crosslinked LCE sample, which will result in patterned LC molecular orientation. The LC molecular orientation field will be further frozen by second-step crosslinking reaction in the LCE. Our method will be generally applicable to making LCEs with different chemistries and shapes. In the letter, we will use one example: radially patterned LCE, to illustrate our ideas. We further show that different undulation in the patterned LCE sheets can be induced by thermal actuation and solvent penetration.

2.2 Methods

2.2.1 Materials

LC monomer, 1,4-Bis-[4-(3-acryloyloxypropyloxy) benzoyloxy]-2-methylbenzene (95%, RM257) was purchased from Wilshire Technologies. Crosslinker, pentaerythritol-tetrakis(3-mercaptopropionate) (95%, PETMP) and spacer, 2,2′-(ethylenedioxy) diethanethiol (95%, EDDET), were purchased from Aldrich. Michael addition catalyst, dipropyl amine (98%, DPA) and the photoinitiator, (2-hydroxyethoxy)-2-methylpropiophenone (98%, HHMP) were purchased from Aldrich. All chemicals were used as received without any purification.

2.2.2 Synthesis of a radially aligned LCE

We followed the two-step crosslinking reaction method to prepare LCE recently developed by Yakacki et al. *(23)*. RM257 (LC monomer) and thiol monomers, PETMP (crosslinker) and EDDET (spacer) were dissolved in toluene by heating and vigorous mixing. The molar functionality composition of thiol monomers, PETMP and EDDET was fixed as 2:8 while that between thiol monomers and RM257 was fixed as 1:1.15, so that there was 15% excess molar functional group of RM257 to that of PETMP and EDDET. A value of 0.5 wt% of HHMP to RM257 and thiol monomers, and 1.1 wt% of DPA to thiol monomers were added in the solution. After the solution was homogeneously mixed, it was placed in the vacuum chamber to remove bubbles trapped inside the solution. The solution was transferred to the mold and left overnight at room temperature for the first-step reaction. During the first step reaction, RM257 reacted with PETMP and EDDET through thiol-acrylate Michael addition to form lightly-crosslinked polydomain LCE sheet. The polydomain LCE was ready for applying mechanical stretch and

second-step crosslinking reaction after the complete evaporation of toluene at 80 °C. In our experiment, the thickness of the LCE sheet after the first-step crosslinking reaction was 0.9 mm.

Orientation of LC molecules at a material point in a LCE depends on its stretch state. Qualitatively speaking, LC molecules tend to orient toward the direction with the largest tensile stretch as predicted by most models and demonstrated in experiments *(40–42)*. In the experiment, we generate inhomogeneous and anisotropic stretch in a LCE sheet by introducing stiff regions with different shapes into it as shown in Fig. 2.1.

To make a region in a lightly-crosslinked LCE sheet stiffer, we shed UV light onto a free-standing LCE sheet through a designed photomask as shown in Fig. 2.1. Under the UV light exposure, second-step crosslinking reaction proceeds and the region becomes dramatically stiffer. Subsequently, we manually stretch the LCE sheet in radial directions and fix the stretch field under the exposure of UV light. Due to the material inhomogeneity, the stretch field in the LCE sheet is inhomogeneous and anisotropic, so the LC molecular orientation in the LCE will also be inhomogeneous. In the second-step crosslinking step, UV light is generated by an 8 W UV lamp with the wavelength of 365 nm. The LCE sample is placed 10 cm away from the UV lamp for 10 min.

2.3 Results and Discussion

2.3.1 Inhomogeneous stress/stretch-induced patterning of LC molecular orientation

As described in the previous section, we radially stretch a lightly-crosslinked LCE sheet with a stiff region in the middle to orient LC molecules in the elastomer. Under the exposure of UV light, second-step crosslinking reaction proceeds in the stressed LCE and the patterned LC

molecules are frozen in the elastomer.

The pattern formation of LC molecules under the stretch can be qualitatively understood as following: We assume the stiff region deform negligibly when the LCE is stretched. Due to the constraint, the stretch along the hoop direction of the stiff region is close to one, while the stretch perpendicular to the edge of the stiff region can be much larger than one. Therefore, regardless of the shape of the stiff region, the LC molecules near the stiff region will be perpendicular to its edge. In the area far away from the stiff region, the stretch in the LCE will be close to the far-field stretch state. Therefore, by controlling the shape of the stiff region, we can obtain different patterns of LC molecules in a LCE.

Next, as an example, we quantitatively calculate the stretch distribution in a circular LCE sheet with a circular constraint in the middle. In the undeformed state, the radius of the LCE sheet is denoted by B and the radius of the circular constraint is denoted by A (see the inset of Fig. 2.2). We assume the circular constraint is much stiffer than the LCE with only the completion of first-step crosslinking reaction. Therefore, after stretch, the radius of the sheet becomes b while the circular constraint remains the same. A material point in the undeformed state with the distance R from the center moves to the position with r away from the center in the deformed state. Considering the radially symmetric deformation, we can calculate the radial stretch $\lambda_r(R)$ and hoop stretch $\lambda_\theta(R)$ by

$$\lambda_r = \frac{dr}{dR} \qquad (1)$$

$$\lambda_\theta = \frac{r}{R} \qquad (2)$$

The stress perpendicular to the LCE sheet is zero. Assuming the elasticity of the LCE can be captured by Neo-hookean model, we have the following stress–stretch relationship,

$$S_r = \mu\left(\lambda_r - \frac{1}{{\lambda_r}^3{\lambda_\theta}^2}\right) \qquad (3)$$

$$S_\theta = \mu\left(\lambda_\theta - \frac{1}{{\lambda_r}^2{\lambda_\theta}^3}\right) \qquad (4)$$

where S_r and S_θ are nominal stresses in radial and hoop direction respectively, and μ is small deformation shear modulus.

The Force balance in the radial direction is

$$\frac{dS_r}{dR} + \frac{S_r - S_\theta}{R} = 0 \qquad (5)$$

A combination of Eqs. (1)–(5) gives a second order ordinary differential equation of $r(R)$. The two boundary conditions of the ODE are:

$$r(A) = A$$

$$r(B) = b$$

Using Matlab, we numerically solve the ODE. The numerical results are shown in Fig. 2.2 In the calculation, we set B/A = 2 and b/B = 3, which are close to our experimental conditions. From Fig. 2.2, we can clearly see that the radial stretch is several times larger than the hoop stretch in the area close to the edge of the constraint. The two stretches gradually get closer to each other when the area is far away from the edge of the constraint, which is due to the radial stretch applied in far field. Therefore, the LC molecules will align along the radial direction of the LCE sheet as sketched in Fig. 2.3a

Due to the optical birefringence of LC molecules, the pattern of LC molecules sketched in Fig. 2.3a can be confirmed by taking polarized optical microscope (POM) images as shown in Fig. 2.3b and c. In Fig. 2.3b, the pattern with maximum brightness can be observed at around 45° with respect to the analyzer while the darkest pattern at around 0° and 90°. In Fig. 2.3c, the POM image

of the LCE rotated by 45° with respect to its original position is very similar to that in Fig. 2.3b. It is known that the maximum light transmittance can be found when the LC molecule is 45° between crossed polarizer and analyzer *(43)*. Therefore, we can confirm that LC molecules in the LCE are indeed along its radial direction as sketched in Fig. 2.3a.

To examine the effects of the shape of the constraint, we also introduced a stiff region with square shape in the LCE sheet. As discussed at the beginning of this section, LC molecules will align perpendicular to the edge of the stiff region when the LCE sheet is radially stretched in far field. Fig. 2.3d sketches the LC molecular patterns. Similarly, the expected LC molecular patterns are confirmed by the POMs of the LCE sheet at different rotational angle as shown in Fig. 2.3e and f. Different patterns shown in Fig. 2.3a and d are caused by the different shape of the stiff region: circular and square. The results clearly indicate that our experimental method can be readily used to obtain diverse LC molecular patterns through introducing stiff constraints with different shapes into the LCE.

As shown in Fig. 2.2, the stretch of the material point near the constraint is more anisotropic than the one close to the free edge. Therefore, the orientation of LC molecules in the LCE is not only anisotropic but also inhomogeneous along the radial direction. More specifically, the LC molecules in the LCE near the constraint should be more aligned than the molecules far away from the constraint.

To confirm the above assumption, we further conduct thermal-actuation experiments in the patterned LCE sample. In the experiment, we cut three small square LCE samples from two patterned LCE sheets with different constraint shapes along the radial direction with different distances away from the constraint as shown in the inset figure of Fig. 2.4a and b. As expected, upon being heated up to 80 °C, all the three square LCE samples contract parallel to the direction

of LC molecular orientation (radial direction) while expand in the perpendicular direction (hoop direction).

Fig. 2.4a plots the radial and hoop stretches of three square LCE samples from a patterned LCE sheet with a circular constraint. Because the LCE sheet is asymmetric, we cut the three square LCE samples from an arbitrary radial path in the LCE sheet in the experiment. Fig. 2.4b plots the radial and hoop stretches of three square LCE samples from a patterned LCE sheet with a square constraint. For the patterned LCE sheet with a square constraint, as shown in the inset figure of Fig. 2.4b, we cut the three LCE samples from two different radial paths, P1 and P2: P1 is from the center of square and perpendicular to an edge of the square constraint; P2 is along the connection between the center of the square and its vertex. The results in Fig. 2.4a and b clearly show that the LCE sample near the constraint has the maximum anisotropy of thermal-actuated strain, while the LCE sample near the free edge has the minimal anisotropy. The experimental results confirm our assumption that the LC molecules in the LCE near the constraint are more aligned than the molecules far away from the constraint. In addition, Fig. 2.4b also shows that, for the patterned LCE sheet with a square constraint, the anisotropy of thermal-actuated strain along the radial path passing through the square vertex is generally larger than the one in the radial path perpendicular to the edge of the square. This is the consequence of stress concentration caused by the sharp vertex of the square.

2.3.2 Reversible undulation in patterned LCEs driven by temperature variation and solvent penetration

Because LC molecules tend to be more and more randomly orientated with increasing temperature, upon being heated up, a patterned LCE will contract along the direction of LC

molecular orientation while expand in the perpendicular direction as shown in Fig. 2.4. In the experiment, when a flat patterned LCE sheet is heated up, due to the anisotropic actuation, multiple wrinkles form in the LCE sheet as shown in Fig. 2.5. In the experiment, we place the patterned LCE film on a hot plate with the temperature 80 °C, which is above the phase transition temperature of the LCE we synthesized. Multiple wrinkles appear in the patterned LCE film within a few seconds (Fig. 2.5a and b).

To quantitatively investigate the wrinkling instability induced by the temperature change, we further measure the winkling amplitude in a patterned LCE sheet at different temperatures as shown in Fig. 2.6. In the experiment, with increasing the temperature, the amplitude of wrinkles in the patterned LCE sheets increases while the wavenumber does not change. Fig. 2.6 shows that a noticeable wrinkling deformation can be observed in the experiment around 40 °C for both the LCE sheets with a circular constraint or square constraint. With different patterns of LC molecules, the wrinkling morphologies driven by temperature change are also different in the LCE sheets as shown in Fig. 2.5a and b. We would like to further point out that the mechanism of generating the undulation in the LCE sheet is different from that of the formation of wrinkles in a circular gel sheet undergoing inhomogeneous swelling *(44,45)*. The size of the LCE sheet reduces about 15% when the temperature increases as shown in Fig. 2.5a and b. In addition, when we remove the undulated LCE film from the hot plate to another plate with room tem- perature, the LCE sheet can fully recover back to flat shape within several seconds.

A patterned LCE also swells anisotropically in a solvent. When a patterned LCE is submerged into a solvent such as toluene, its swelling ratio along the direction of LC molecular orientation is much smaller than the perpendicular to the direction of LC molecular orientation. [22] Therefore, similar undulating deformation in the patterned LCE sheets can be also driven by

solvent penetration as shown in Fig. 2.7. The undulated LCE sheets can also recover to its original flat shape after it is dried out.

2.4 Conclusion

In recent years, programmable soft materials and structures have been intensively studied. The material includes hydrogels, shape memory polymers and biopolymers. In this study, we developed a facile and effective strain engineering technique to pattern LC molecules in a LCE. As a result, the patterned LCE can have different active deformation modes when subjected to various external stimuli, and thus realize different functions. Although only simple patterns in LCE sheets have been demonstrated in the letter, there should not be any intrinsic difficulties to generate more complex LC molecular patterns in a LCE by applying inhomogeneous stretch. We believe the strain engineering technique developed in the article can be directly used to fabricate programmable LCE structures, which is the ongoing research being conducted by us.

Chapter 2, in part or in full, is a reprint of the following material: C. Ahn, X. Liang, S. Cai "Inhomogeneous stretch induced patterning of molecular orientation in liquid crystal elastomers" Extreme Mechanics Letters, 5 (2015). The dissertation author was the primary investigator and author of this paper.

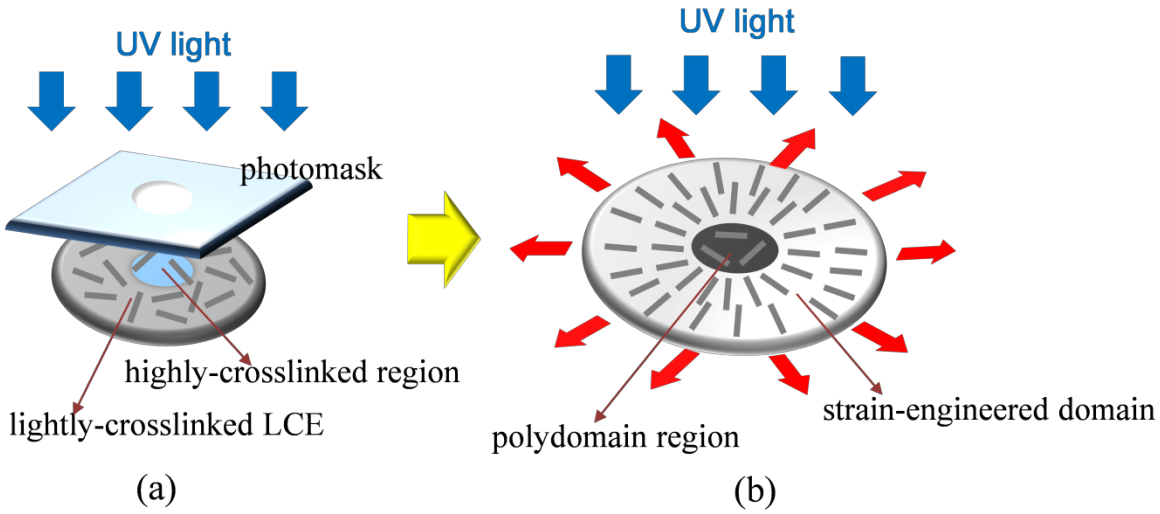

Figure 2.1: Schematics of the experimental steps for fabricating a patterned LCE sheet. (a) UV light is shed onto a LCE sheet through a designed photomask. When the region is exposed to UV light, second-step crosslinking reaction proceeds in the elastomer and the region becomes dramatically stiffer. (b) Subsequently, the LCE sheet is radially stretched under the exposure of UV light. Due to the material inhomogeneity, the stretch field in the LCE sheet is inhomogeneous and anisotropic, so the orientation of LC molecules in the LCE is patterned. The orientation field of LC molecules is frozen in the LCE through the second-step crosslinking reaction activated by the UV light.

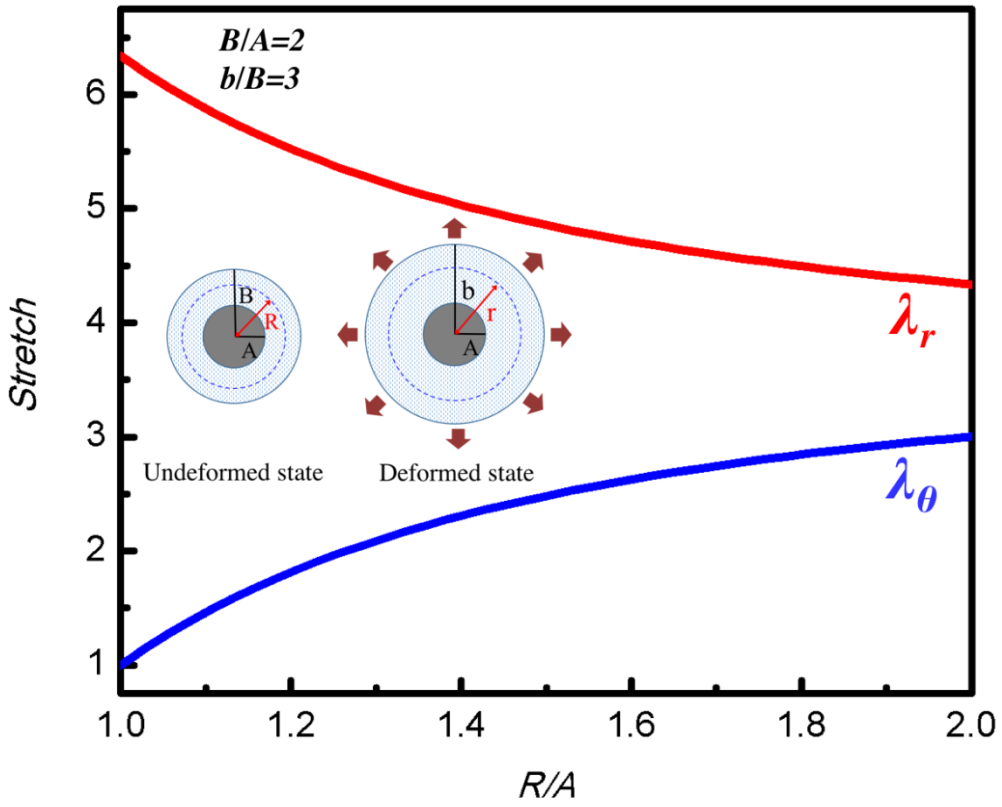

Figure 2.2: Stretch distribution in a radially stretched circular LCE sheet with a stiff circular region in the middle.

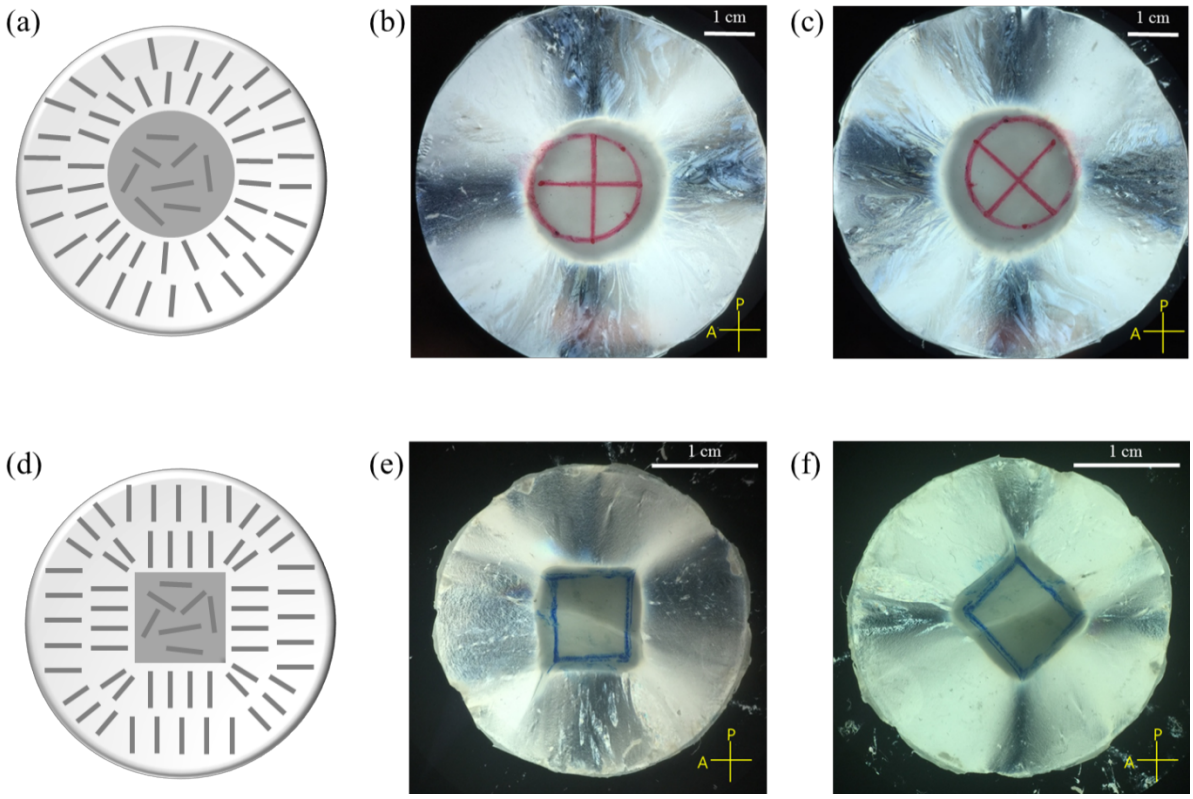

Figure 2. 3: (a) Schematic of LC molecular orientation in the LCE sheet with a circular stiff region in the middle. (b) and (c) are polarized optical microscope images of the LCE sheet with two different angles with respect to the analyzer. (d) Schematic of LC molecular orientation in the LCEsheet with a square stiff region in the middle. (e) and (f) are polarized optical microscope images of the LCE sheet with two different angles with respect to the analyzer.

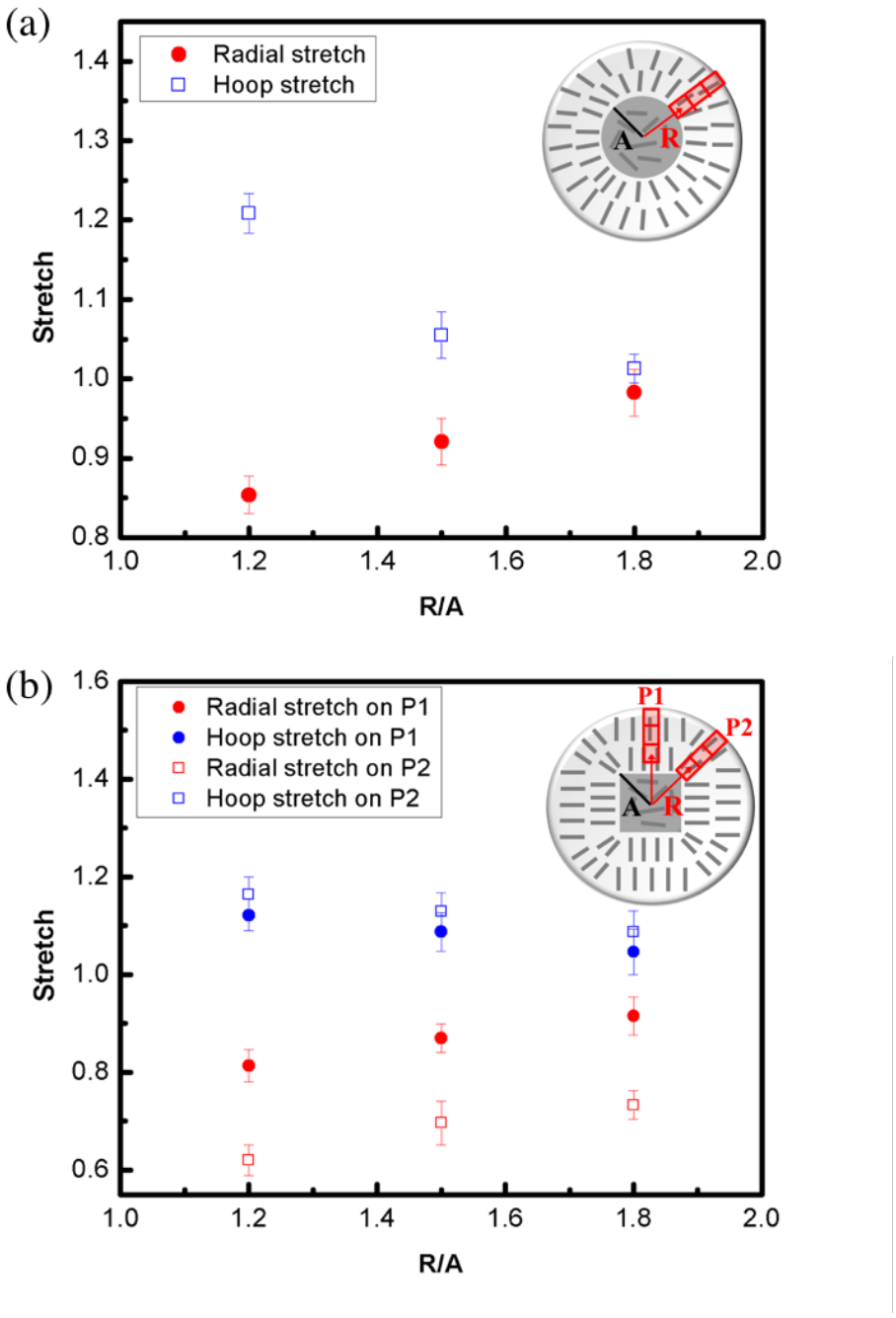

Figure 2.4: Thermally-actuated radial and hoop stretch on the patterned LCEs along radial directions with different distances away from the constraint. (a) Three LCE samples cut from an arbitrary radial path in a patterned LCE sheet with a circular constraint. (b) LCE samples cut from two different radial paths: P1 and P2 from a patterned LCE with a square constraint.

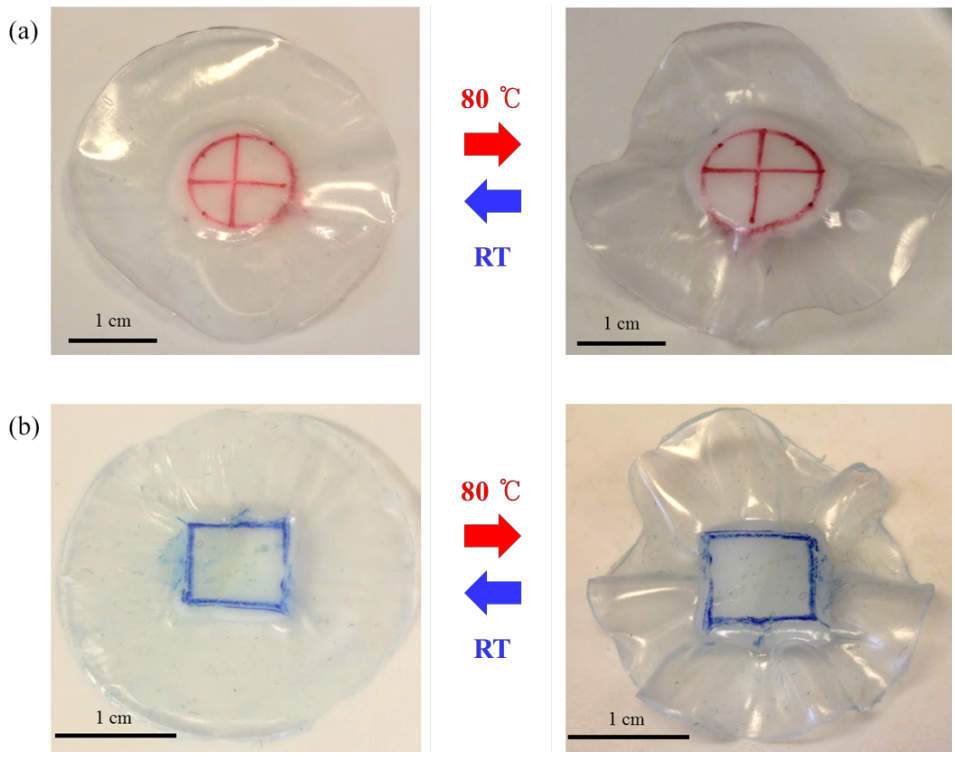

Figure 2.5: Reversible thermally driven undulation in patterned LCEs with a (a) circular constraint and (b) square constraint in the middle.

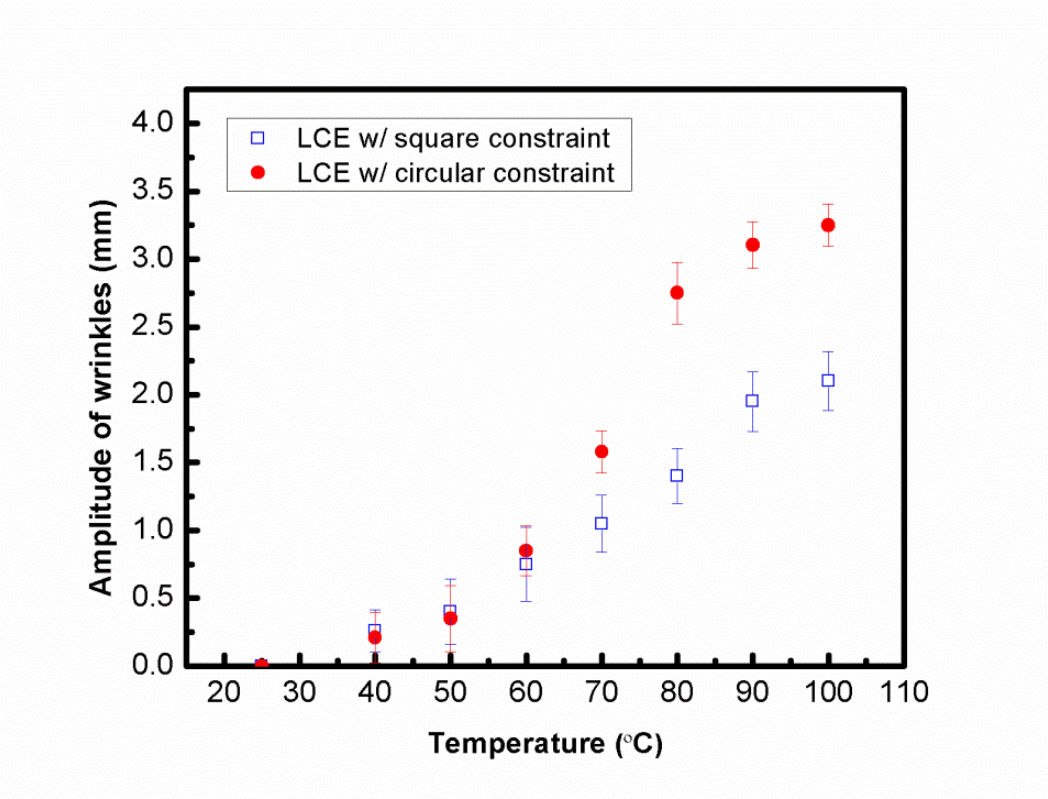

Figure 2.6: Evolution of the amplitude of wrinkles with the increase of temperature. For the LCE with a circular constraint, the amplitudes of different wrinkles are the same. For the LCE with a square constraint, we measure the amplitude of the wrinkle, which is perpendicular to the edge of the square.

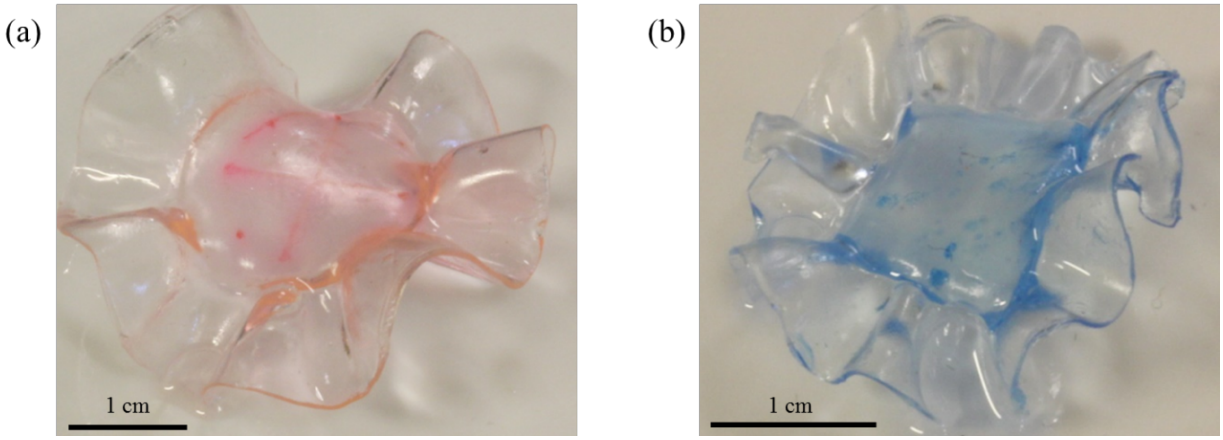

Figure 2.7: Solvent penetration driven undulation in patterned LCEs with a (a) circular constraint and (b) square constraint in the middle.

2.5 References

1. S. Dey, D. Agra-Kooijman, W. Ren, P. McMullan, A. Griffin, and S. Kumar, Crystals **3,** 363 (2013).

2. J. S. Biggins, M. Warner, and K. Bhattacharya, Journal of the Mechanics and Physics of Solids **60,** 573 (2012).

3. A. W. Brown, and J. M. Adams, Physical Review E **85,** 011703 (2012).

4. J. M. Adams, and M. Warner, Physical Review E **72,** 011703 (2005).

5. D. Corbett, and M. Warner, Liquid Crystals **36,** 1263 (2009).

6. N. J. Dawson, M. G. Kuzyk, J. Neal, P. Luchette, and P. Palffy-Muhoray, Journal of Optical Society of America B **28**, 2134 (2011).

7. H. Finkelmann and M. Shahinpoor, 2002, Smart Structures and Materials: Electroactive Polymer Actuators and Devices (Eapad) **4695,** 459 (2002).

8. S. Petsch, R. Rix, P. Reith, B. Khatri, S. Schuhladen, D. Ruh, R. Zentel, and H. Zappe, IEEE 27th International Conference on Micro Electro Mechanical Systems (MEMS), 905 (2014).

9. H. Xing, J. Li, J. Guo, and J. Wei, Journal of Materials Chemistry C **3,** 4424 (2015).

10. M. H. Li and P. Keller, Philosophical Transactions of the Royal Society a-Mathematical Physical and Engineering Sciences **364,** 2763 (2006).

11. J. Schmidtke, S. Kniesel, and H. Finkelmann, Macromolecules **38,** 1357 (2005).

12. J. Schmidtke, W. Stille, H. Finkelmann, and S. T. Kim, Advanced Materials **14,** 746 (2002).

13. N. J. Dawson, M. G. Kuzyk, J. Neal, P. Luchette, and P. Palffy-Muhoray, Optics Communications **284,** 991 (2011).

14. S. V. Shilov, H. Skupin, F. Kremer, K. Skarp, P. Stein, and H. Finkelmann, H., Liquid Crystals: Physics, Technology, and Applications, 62 (1998).

15. P. Dalhaimer, D. E. Discher, and T. C. Lubensky, Nature Physics **3,** 354 (2007).

16. D. P. Knight, and F. Vollrath, Philosophical Transactions of the Royal Society B: Biological Sciences **357,** 155 (2002).

17. C. Li, Y. Liu, C.-w. Lo, and H. Jiang, Soft Matter **7,** 7511 (2011).

18. K. Urayama, S. Honda, and T. Takigawa, Macromolecules **39,** 1943 (2006).

19. A. Agrawal, A. C. Chipara, Y. Shamoo, P. K. Patra, B. J. Carey, P. M. Ajayan, W. G. Chapman, and R. Verduzco, Nature Communication **4,** 1739 (2013).

20. H. Schüring, R. Stannarius, C. Tolksdorf, and R. Zentel, Macromolecules **34,** 3962 (2001).

21. R. Diaz-Calleja, P. Llovera-Segovia, E. Riande, and A. Quijano López, Applied Physics Letters **102,** 052901 (2013).

22. J. Küpfer, and H. Finkelmann, Die Makromolekulare Chemie, Rapid Communications **12,** 717 (1991).

23. C. M. Yakacki, M. Saed, D. P. Nair, T. Gong, S. M. Reed, and C. N. Bowman, RSC Advances **5,** 18997 (2015).

24. F. Brömmel, D. Kramer, and H. Finkelmann, Liquid Crystal Elastomers: Materials and Applications, W. H. de Jeu, ed., 1 (2012).

25. W. Lehmann, H. Skupin, C. Tolksdorf, E. Gebhard, R. Zentel, P. Kruger, M. Losche, and F. Kremer, Nature **410,** 447 (2001).

26. T. Ikeda, M. Nakano, Y. Yu, O. Tsutsumi, and A. Kanazawa, Advanced Materials **15,** 201 (2003).

27. N. Torras, K. E. Zinoviev, J. Esteve, and A. Sanchez-Ferrer, Journal of Materials Chemistry C **1,** 5183 (2013).

28. M. Brehmer, and R. Zentel, Macromolecular Rapid Communications **16,** 659 (1995).

29. C. Ohm, M. Brehmer, and R. Zentel, Advanced Materials **22,** 3366 (2010).

30. M. Yamada, M. Kondo, R. Miyasato, Y. Naka, J.-i. Mamiya, M. Kinoshita, A. Shishido, Y. Yu, C. J. Barrett, and T. Ikeda, Journal of Materials Chemistry **19,** 60 (2009).

31. Y. Yu, M. Nakano, and T. Ikeda, Nature **425,** 145 (2003).

32. A. Agrawal, T. Yun, S. L. Pesek, W. G. Chapman, and R. Verduzco, Soft Matter **10,** 1411 (2014).

33. A. Agrawal, P. Luchette, P. Palffy-Muhoray, S. L. Biswal, W. G. Chapman, and R. Verduzco, Soft Matter **8,** 7138 (2012).

34. T. Yoshino, M. Kondo, J.-i. Mamiya, M. Kinoshita, Y. Yu, and T. Ikeda, Advanced Materials **22,** 1361 (2010).

35. R. Yin, W. Xu, M. Kondo, C.-C. Yen, J.-i. Mamiya, T. Ikeda, and Y. Yu, Journal of Materials Chemistry **19,** 3141 (2009).

36. S. Iamsaard, S. J. Aßhoff, B. Matt, T. Kudernac, J. L. M. CornelissenJeroen, S. P. Fletcher, and N. Katsonis, Nature Chemistry **6,** 229 (2014).

37. T. Seki, Polymer Journal **46,** 751 (2014).

38. T. H. Ware, M. E. McConney, J. J. Wie, V. P. Tondiglia, and T. J. White, Science **347,** 982 (2015).

39. L. T. de Haan, C. Sánchez-Somolinos, C. M. W. Bastiaansen, A. P. H. J. Schenning, and D. J. Broer, Angewandte Chemie International Edition **51,** 12469 (2012).

40. Z. Wei, S. Michael, and P. Peter, Physical Review E **83,** 051703 (2011).

41. P. Bladon, EM. Terentjev, M. Warner, Physical Review E **47,** 3838 (1993).

42. S. Conti, A. DeSimone, G. Dolzmann, Journal of the Mechanics and Physics of Solids **50,** 1431 (2002).

43. A. Komp, J. Rühe, and H. Finkelmann, Macromolecular Rapid Communications **26,** 813 (2005).

44. J. Kim, J. A. Hanna, M. Byun, C. D. Santangelo, and R. C. Hayward, Science **335,** 1201 (2012).

45. Z. Liu, S. Swaddiwudhipong, and W. Hong, Soft Matter **9,** 577 (2013).

Chapter 3 Optically Controllable Multi-Directional Bending of a Liquid Crystal Elastomer

Soft actuation is advantageous over traditional rigid material-based actuation due to its easy fabrication, large degree of freedom, and human compatibility. Among many actuation mode, bending is more conventional and fundamental deformation mode because it can be utilized directly in the artificial muscle application or potentially enables further complex motions. However, multi-directional bending deformation is still challenging using conventionally studied film structured soft actuators. In this study, we report light-driven multi-directional bending deformation of soft actuator through the polymer rod structure with circular shape cross-section. We prepared carbon nanotube (CNT) incorporated liquid crystal elastomer (LCE) rod which can be photoresponsive under the visible light. The LCE-CNT rod shows reversible heliotropic behavior upon the light irradiation, which makes the structure always bend toward light in any direction. In addition, the bending deformation of LCE-CNT rod can be amplified and localized using laser irradiation which enables precise controlling of the deformation. Using a combined structure of LCE-CNT rod and arch shape LCE-CNT, we further show light-driven soft gripper with a manipulating function.

3.1 Introduction

Soft actuating structures have been intensively studied in recent years because of their simple geometry, large degree of freedom, and human compatibility (*1-7*). Among different types of deformation of soft actuators, bending deformation is one of the most commonly studied, but considerably important deformation mode since it is one of the fundamental function required to generate different types of motions such as oscillation (*8*), locomotion (*9, 10*), swimming (*11, 12*), jumping (*13*), and rolling (*14*) with a proper manipulation of structure. Therefore, bending deformation in soft actuation is fundamental to achieve more complex and sophisticated motions.

Different strategies have been applied for the bending of soft actuators using pneumatic channel (*15*), heat (*16*), magnetic field (*17*), humidity (*18*), or light (*19*). Among different types of external stimuli, light can be preferable since it enables simplification of soft actuator structure by removing wires and the capability of controlling direction and intensity when applied on the soft actuator. Previous studies have reported light-induced deformation of soft actuators with different types of soft materials with various approaches (*20-26*). A thin polycarbonate membrane/CNT double layered structure shows bending deformation under the visible light attributed to the different thermal expansion coefficients between each layers (*27*). A flexible Cr/Au bilayer microstructure with a polymer trigger layer on the top can bend upon the irradiation of laser on the polymer due to the expansion of polymer layer (*28*).

Among different soft materials, LCE is one of the promising candidate for the bending actuation, due to its high anisotropy which can induce large deformation upon light irradiation. Many studies have applied photoisomerization with azobenzene moiety (*29, 30*) or photothermal effect (*31*) with carbon based materials like CNT (*32, 33*) for obtaining light induced bending

deformation of LCE. The light-induced bending deformation of LCE can be obtained when the thickness of the LCE structure is larger than the light penetration depth in order to generate inhomogeneous contraction of LCE along the thickness. Yu et al. reported a precisely controllable directed bending of a LCE film with azobenzene moiety using linearly polarized light (*19*). In addition, direct sun-driven bendable system constituted by CNT incorporated LCE films can collect sunlight more effectively (*33*).

Most of studies on light-driven bending deformation presented so far, however, are limited to exhibit bending deformation in one or two directions since the soft actuating structures are usually in film structure. In this study, hereby, we report multi-directional light driven bending deformation of soft actuator in rod shape. By using LCE-CNT rod structure with a circular shape cross-sectional area, we can obtain heliotropic bending behavior which always bends toward light in any direction reversibly rather than limited in one or two directions. Furthermore, we demonstrate soft gripper actuation with a manipulating function using LCE-CNT rod and arch shape LCE-CNT structure which shows practical grasping performance driven by light.

3.2 Methods

3.2.1 Materials

LC monomer, 1,4-Bis-[4-(3-acryloyloxypropyloxy)benzoyloxy]-2-methylbenzene (95%, RM257) is purchased from Wilshire Technologies. Crosslinker, pentaerythritol tetrakis(3-mercaptopropionate) (95%, PETMP), spacer, 2,2'-(ethylenedioxy) diethanethiol (95%, EDDET), catalyst, dipropyl amine (98%, DPA), photoinitiator, (2-hydroxyethoxy)-2-methylpropiophenone (98%, HHMP), and multi-walled carbon nanotubes (98%, CNTs) are purchased from Aldrich. The

molecular structures of materials constituting are shown in Fig. 3.1a. LCE All chemicals are used as received without any purification.

3.2.2 Fabrication of LCE-CNT rods

LCE-CNT rods are prepared by the two-step crosslinking reaction according to the method previously reported by Yakacki et al (*34*). The LCE monomer mixture is prepared by dissolving RM257 (LC monomer), PETMP (crosslinker), EDDET (spacer), and HHMP (photoinitiator) in toluene followed by heating above LC phase transition temperature and vigorous mixing. The composition of the mixture consists of 53.0 wt% of RM257, 2.5 wt% of PETMP, 12.5 wt% of EDDET, 0.2 wt% of CNTs, and 0.4 wt% of HHMP in toluene. After the mixture becomes homogeneous, 0.2 wt% of DPA (catalyst) is added to trigger the reaction. The mixture is placed in the vacuum chamber to remove bubbles trapped inside, followed by being transferred into a cylindrical mold as shown in Fig. 3.1b. The mixture is left overnight at room temperature to be loosely-crosslinked by the thiol-acrylate Michael addition reaction. The loosely-crosslinked LCE rod is placed in the oven at 80 ℃ for 24 h for the evaporation of residual solvent. After the LCE rod is dried, it is subjected to uniaxial stretch to achieve monodomain state[15,42] and under the UV light (365 nm, UVP B-100AP/R) irradiation for 1 h to be fully-crosslinked. Finally, the LCE rod in a cylindrical shape with different diameters can be obtained.

3.2.3 Fabrication of light-driven soft gripper

Light-driven soft gripper consisted by two parts were prepared from the same LCE-CNT solution as LCE-CNT rods. We use the LCE-CNT rod as a top part of the soft gripper following

the procedure discussed in the previous section. The bottom part of soft gripper was prepared in arch shape prepared from the partially crosslinked rectangular shape LCE-CNT with around 1.8 mm in thickness. The partially crosslinked rectangular shape LCE-CNT was molded into arch shape using circular shape glass substrate under uniaxial strain followed by UV curing to obtain fully crosslinked LCE-CNT. The top and bottom part of soft grippers are simply combined together using electrical tape.

3.3 Results and Discussion

3.3.1 Multi-directional bending of LCE-CNT

Upon the visible light irradiation from the right, LCE-CNT rod bends concave toward the light while the pristine LCE rod remains almost same as its initial shape as shown in Fig. 3.2a. The different deformation behavior under the same light irradiation environment for pristine LCE rod and LCE-CNT rod can be attributed to the photothermal effect of CNT. The electrons within CNT excited under the light irradiation relax through the electron-phonon interaction resulting in the heat dissipation into surrounding LCE matrix [XX]. Therefore, only LCE-CNT rod exhibits obvious bending deformation under the light whereas the pristine LCE deforms slightly due to the thermal convection from heat generated by the light source. As the thickness of the LCE-CNT rod used in this study is thicker than the light penetration depth, only the CNTs on the surface or near-surface towards light source on the LCE-CNT rod can convert incoming light into heat. Consequently, the LC molecules in the LCE matrix close to the surface to the light source are more likely affected by the photothermal effect of CNT to be disordered by heating. Since there would be temperature gradient decreasing from the surface toward light to the opposite surface of LCE-

CNT rod, the LCE-CNT contracts most at the surface toward light, and the opposite surface of LCE-CNT may contract less. The inhomogeneous contraction of LCE-CNT rod generates strain gradient along the direction thickness of LCE-CNT rod, resulting in the bending deformation of whole structure (Fig. 3.2b). As the disordered LCs constituting LCE-CNT rod can recover its original anisotropy with temperature decrease, the LCE-CNT rod can become an initial straight rod shape when it is cooled after the light is removed.

Different from other bendable soft actuating structures conventionally in film shape, the LCE-CNT rod prepared in this study is solid and bulky shape with circular shape cross-section with homogeneous and larger thickness in any direction than the light penetration. Therefore, the LCE-CNT rod can bend towards in any direction following the light, showing heliotropism like sunflower behavior. Fig 3.3 shows the heliotropic motion of LCE-CNT rod under the light illumination in four different directions. LCE-CNT rod is glued on the substrate to be stand vertically perpendicular to the bottom with straight shape. Under the light irradiation, LCE-CNT rod shows bending deformation toward the light and recovers its original straight shape when the light is turned off. Since the whole surface area of the LCE-CNT rod towards the light source is illuminated by the light, the bending deformation occurs along the longitudinal direction of the whole LCE-CNT rod. Since the deformation is triggered by the heating process of the LCE matrix, the bending begins upon the light irradiation and the bending angle increases gradually until the contraction of the LCE towards light is saturated within a few seconds. The recovery process takes more time until it fully changed into its original shape as it need to be cooled to the room temperature through the heat dissipation process.

In addition to the unbounded light-induced deformation, more sophisticated deformation can be obtained on the LCE-CNT rod using the nIR laser (Fig. 3.4). Different from the light, the

laser is highly concentrated and having a smaller focal point with around 1 mm in diameter, larger power with localized external stimuli can be applied on the LCE-CNT rod. Therefore, upon the laser is placed on the surface of LCE-CNT rod, localized and larger bending deformation can be obtained. Due to the larger power of the laser, LCE-CNT rod exhibits faster and much larger deformation up to 90°. Furthermore, the deformation of the LCE-CNT rod is highly localized under the laser irradiation, so that the bending direction and location on the longitudinal direction on LCE-CNT can be precisely tuned. The bending point of the LCE-CNT rod can be altered at any different positions on its longitudinal direction corresponding to the position of the focal point of the laser on the surface of LCE-CNT rod range from the bottom right to the top right, or on the middle left. Similar to the light induced deformation, the direction of the bending can be tuned by controlling the direction of the laser.

3.3.2 Optically driven soft gripper

The multidirectional bending ability of LCE-CNT rod enables the LCE structure to be applied as a light driven manipulator. In addition to the manipulating function, LCE-CNT rod can be combined with another LCE-CNT structure but in different shape for more practical purpose. Using the LCE-CNT rods and other LCE-CNT structure in arch shape, soft gripper with manipulating function fully driven by light can be prepared. The optically driven soft gripper is constituted by LCE-CNT rod on the top and the arch shape LCE-CNT at the bottom, for enabling light only driven gripping and manipulating performance. The LCE-CNT rod in the middle plays a manipulating role which enables the whole structure bends in any directions towards the light. In addition to bending, by illuminating light on both right and left surface of LC-CNT rod simultaneously, the LCE-CNT rod contract along its axial direction which enabling the whole

structure moves up and down by turning on and off light. The arch shape LCE-CNT located at the bottom part can broaden its opening with the light illumination on its outer surface and recovers the opening to be decreased with the removal of light, which enabling gripping function by placing the opening on an object when it is being enlarged, and grip an object by fixing it at each ends of the gripper. Unlike other soft grippers limited to perform gripping and releasing, The LCE-CNT soft gripper can grip an object and move it to another location fully driven by light. In the Fig. 3.5, the LCE-CNT soft gripper moves a small piece of PDMS block from the back to the front substrate. Initially, the whole structure is contracted under the simultaneous light irradiation on the left and right of manipulating part followed by selective light irradiation on the lower back surface of the manipulating part to bend the whole structure toward back. Meanwhile, as the light is illuminated at the lower part of the manipulator, the outer surface of the gripper is under the effect of the light as well, so the gripper can broaden its opening. Consequently, the block is placed within an opening area of the gripper under the light irradiation and can be fixed by the gripping part once the light is removed. After the block is grasped by the soft gripper, the light is placed on the middle front part of the manipulator, resulting in the whole structure bends to the front and the gripper with the block is located on the front substrate. Finally, the light is placed on the gripping part again, and the block is released from the gripper by broadening of the opening and the soft gripper returns back to its original position once the light is removed.

3.4 Conclusion

In the study, light-induced multi-directional bending LCE-CNT rod is demonstrated using a simple preparation method. The LCE-CNT rod exhibits fully reversible heliotropic deformation under the visible light due to the inhomogeneous contraction of LCE in any direction towards the

light source. Therefore, the bending direction of the LCE-CNT rod can be intentionally tuned by positioning a light source. In addition, faster, larger, and localized bending deformation of LCE-CNT rod can be obtained using nIR laser, which enables precise control of the bending behavior. Soft gripper with manipulating function using LCE-CNT rod and arch shape LCE-CNT structure is also demonstrated fully driven by the light. The LCE-CNT soft gripper can perform the full process including gripping, moving, and releasing of an objective only driven by light. Because of the simple fabrication process and multi-directional bending performance, we expect that the LCE-CNT rod has a potential to be adopted in other types of practical applications.

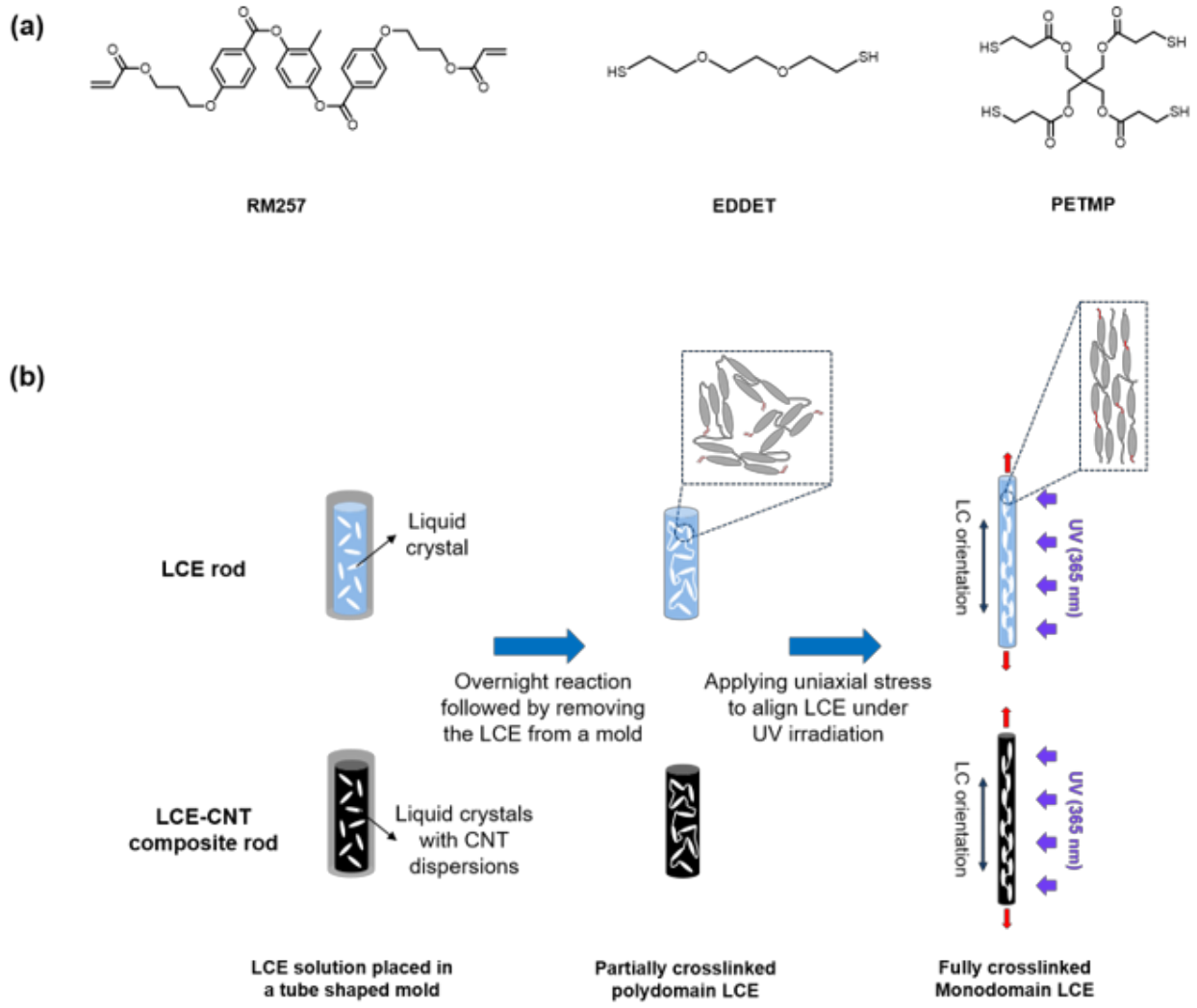

Figure 3.1: Schematic illustration of the process for the LCE rod preparation. (a) Chemical structures of the components for synthesizing a LCE rod. (b) LCE solution is poured into a cylindrical shape mold and left at room temperature to form partially crosslinked LCE rod. The partially crosslinked LCE rod is subjected to the uniaxial stretch under UV irradiation to be fully crosslinked with a monodomain configuration.

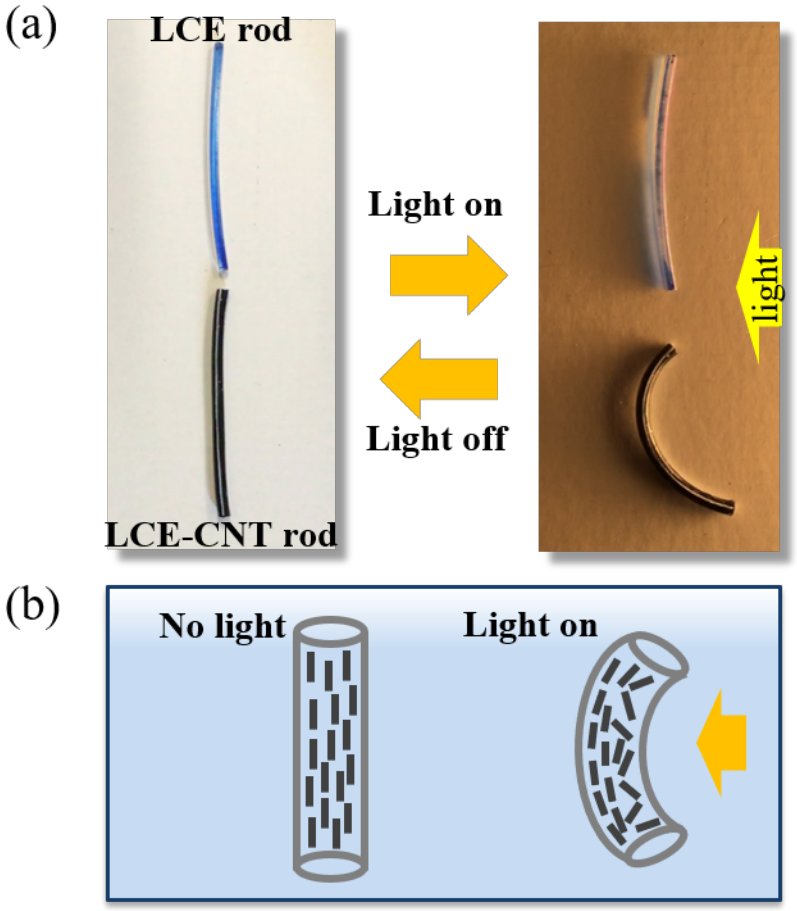

Figure 3.2: Bending deformation behavior of LCE and LCE-CNT rod. (a) Under the light irradiation with 300 mW/cm^2, LCE-CNT rod only bends concave toward to the light. (b) Schematic of LCE-CNT rod bending which is induced by photothermal effect of CNT that causes strain gradient on the rod in thickness.

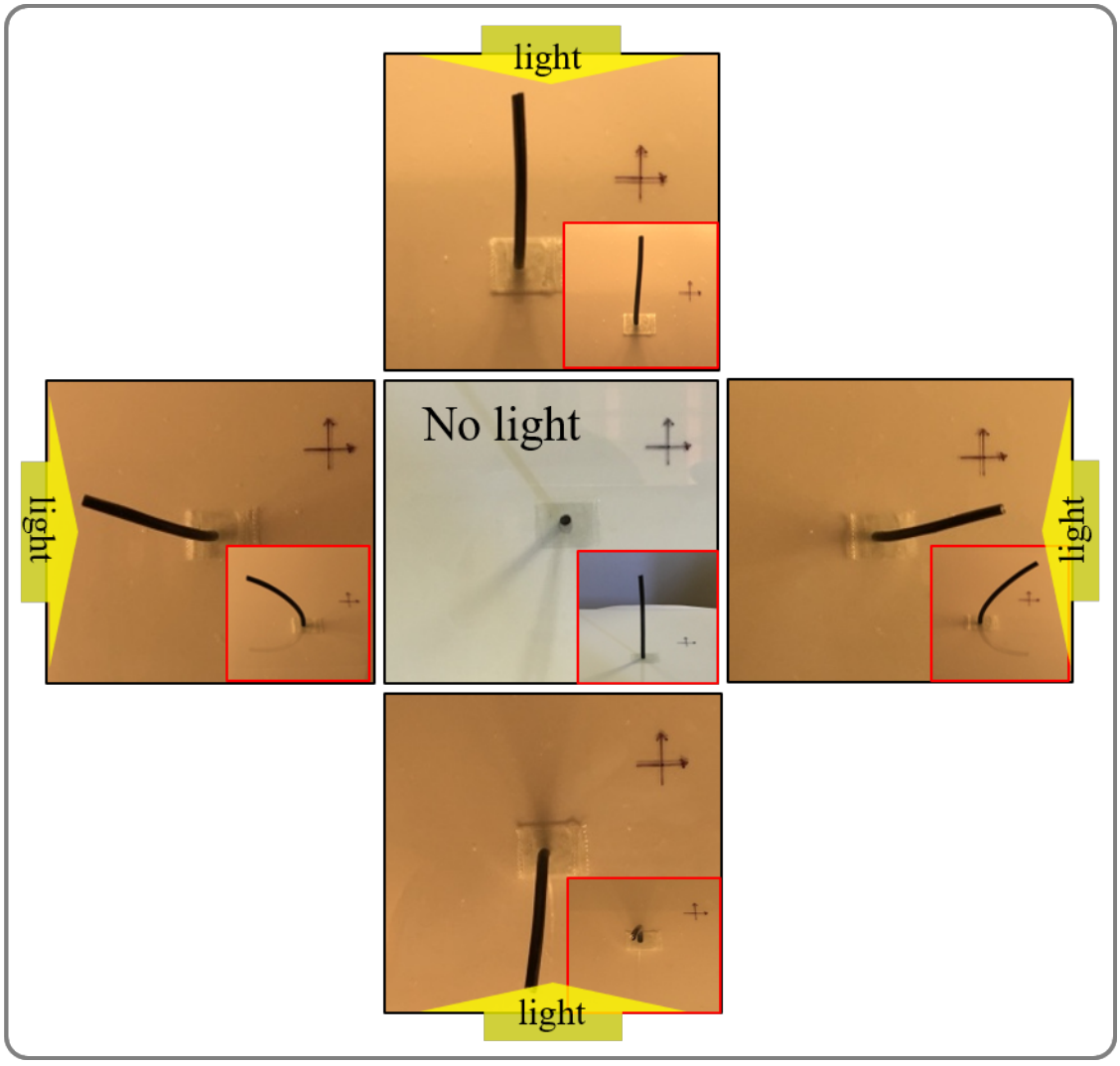

Figure 3.3: Multi-directional bending deformation of LCE-CNT rod under the light irradiation.

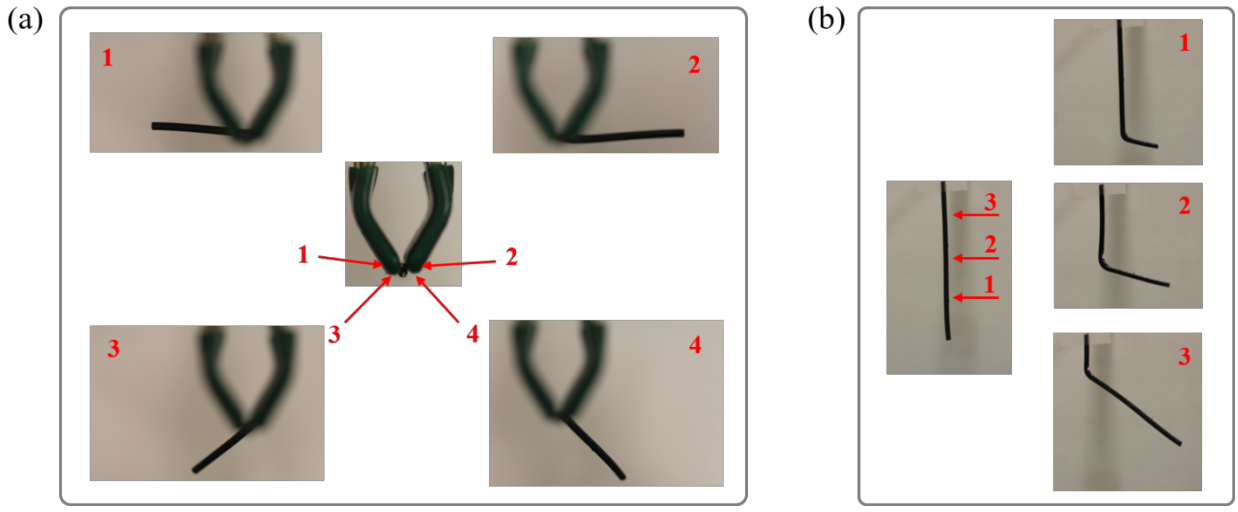

Figure 3.4: Bending deformation of LCE-CNT rod induced by nIR laser. (a) The direction of deformation can be tuned by the position of the laser. (b) Controllable localized deformation along the longitudinal direction of LCE-CNT rod.

Figure 3.5: Soft gripper prepared from LCE-CNT rod and LCE-CNT arch structure. The soft gripper can fully light-driven gripping and manipulation which enables moving a PDMS piece from the rear to the front plate.

3.5 References

1. D. Rus, M. T. Tolley, Design, fabrication and control of soft robots. *Nature* **521**, 467 (2015).

2. W. G. M., Soft robotics. *Angewandte Chemie International Edition* **57**, 4258 (2018).

3. C. Laschi, B. Mazzolai, M. Cianchetti, Soft robotics: Technologies and systems pushing the boundaries of robot abilities. *Sci. Robot.* **1**, 3690 (2016).

4. X. Zhang, Z. Yu, C. Wang, D. Zarrouk, J.-W. T. Seo, J. C. Cheng, A. D. Buchan, K. Takei, Y. Zhao, J. W. Ager, J. Zhang, M. Hettick, M. C. Hersam, A. P. Pisano, R. S. Fearing and A. Javey, Photoactuators and motors based on carbon nanotubes with selective chirality distributions. *Nat. Commun.* **5**, 2983 (2014)

5. H. Ying, L. Zhe, L. Tian, C. Wei, Photoactuators for Direct Optical-to-Mechanical Energy Conversion: From Nanocomponent Assembly to Macroscopic Deformation. *Adv. Mater.* **28**, 10548 (2016).

6. S. Kim, C. Laschi, B. Trimmer, Soft robotics: a bioinspired evolution in robotics. *Trends Biotechnol.* **31**, 287 (2013).

7. W. Jiang, D. Niu, H. Liu, C. Wang, T. Zhao, L. Yin, Y. Shi, B. Chen, Y. Ding, and B. Lu, Photoresponsive soft-robotic platform: biomimetic fabrication and remote actuation. *Adv. Funct. Mater.* **24**, 7598 (2014).

8. K. Kumar, C. Knie, D. Bleger, M. A. Peletier, H. Friedrich, S. Hecht, D. J. Broer, M. G. Debije and A. P.H.J. Schenning, A chaotic self-oscillating sunlight-driven polymer actuator. *Nat. Commun.* **7**, 11975 (2016).

9. W. Hu, G. Z. Lum, M. Mastrangeli, M. Sitti, Small-scale soft-bodied robot with multimodal locomotion. *Nature* **554**, 81 (2018).

10. M. Rogóż, H. Zeng, C. Xuan, D. S. Wiersma, P. Wasylczyk, Light-driven soft robot mimics caterpillar locomotion in natural scale. *Adv. Opt. Mater.* **4**, 1689 (2016).

11. M. Camacho-Lopez, H. Finkelmann, P. Palffy-Muhoray, M. Shelley, *Nat. Mater.* **3**, 307 (2004)

12. H. Tian, Z. Wang, Y. Chen, J. Shao, T. Gao and S. Cai, Polydopamine-Coated Main-Chain Liquid Crystal Elastomer as Optically Driven Artificial Muscle. *ACS Appl. Mater. Inter.* **10**, 8307 (2018).

13. H. Lee, C. Xia and N. X. Fang, First jump of microgel; actuation speed enhancement by elastic instability. *Soft Matter*. **6**, 4342 (2010)

14. C. Ahn, X. Liang, S. Cai, Inhomogeneous stretch induced patterning of molecular orientation in liquid crystal elastomers. *Extreme Mechanics Letters* **5**, 30 (2015).

15. R. F. Shepherd, R. F. Shepherd, F. Ilievski, W. Choi, S. A. Morin, A. A. Stokes, A. D. Mazzeo, X. Chen, M. Wang and G. M. Whitesides, Multigait soft robot. *PNAS* **108**, 20400 (2011).

16. Y. Sawa, K. Urayama, T. Takigawa, A. DeSimone, L. Teresi, Thermally Driven Giant Bending of Liquid Crystal Elastomer Films with Hybrid Alignment. *Macromolecules* **43**, 4362 (2010).

17. H. M. Song, J. C. Kim, J. H. Hong, Y. B. Lee, J. Choi, J. I. Lee, W. S. Kim, J.-H. Kim and N. H. Hur, Magnetic and Transparent Composites by Linking Liquid Crystals to Ferrite Nanoparticles through Covalent Networks. *Adv. Funct. Mater.* **17**, 2070 (2007).

18. Z. Lidong, N. Panče, Light- and Humidity-Induced Motion of an Acidochromic Film. *Angewandte Chemie International Edition* **54**, 8642 (2015).

19. Y. Yu, M. Nakano, T. Ikeda, Photomechanics: Directed bending of a polymer film by light. *Nature* **425**, 145 (2003).

20. W. Liu, L.-X. Guo, B.-P. Lin, X.-Q. Zhang, Y. Sun and H. Yang, Near-Infrared Responsive Liquid Crystalline Elastomers Containing Photothermal Conjugated Polymers. *Macromolecules* **49**, 4023 (2016).

21. J. E. Marshall, E. M. Terentjev, Photo-sensitivity of dye-doped liquid crystal elastomers. *Soft Matter*. 9, 8547 (2013)

22. T. Ikeda, M. Nakano, Y. L. Yu, O. Tsutsumi, A. Kanazawa, Anisotropic bending and unbending behavior of azobenzene liquid-crystalline gels by light exposure. *Adv. Mater.* **15**, 201-205 (2003).

23. C. L. van Oosten, C. W. M. Bastiaansen, D. J. Broer, Printed artificial cilia from liquid-crystal network actuators modularly driven by light. *Nat. Mater.* **8**, 677 (2009).

24. E. Wang, M. S. Desai, S.-W. Lee, Light-Controlled Graphene-Elastin Composite Hydrogel Actuators. *Nano Lett.* **13**, 2826 (2013).

25. Z. Cheng, T. Wang, X. Li, Y. Zhang, H. Yu, NIR–Vis–UV Light-Responsive Actuator Films of Polymer-Dispersed Liquid Crystal/Graphene Oxide Nanocomposites. *ACS Appl. Mater. Interfaces* **7**, 27494 (2015).

26. H. Zeng, O. M. Wani, P. Wasylczyk, A. Priimagi, Light-driven, caterpillar-inspired miniature inching robot. *Macromol. Rapid Commun.* **39**, 1700224 (2018).

27. X. Zhang, Z. Yu, C. Wang, D. Zarrouk, J.-W. T. Seo, J. C. Cheng, A. D. Buchan, K. Takei, Y. Zhao, J. W. Ager, J. Zhang, M. Hettick, M. C. Hersam, A. P. Pisano, R. S. Fearing and A. Javey, Photoactuators and motors based on carbon nanotubes with selective chirality distributions. *Nat. Commun.* **5**, 2983 (2013).

28. K. E. Laflin, C. J. Morris, T. Muqeem, D. H. Gracias, Laser triggered sequential folding of microstructures. *Applied Physics Letters* **101**, 131901 (2012).

29. K. M. Lee, H. Koerner, R. A. Vaia, T. J. Bunning, T. J. White, Light-activated shape memory of glassy, azobenzene liquid crystalline polymer networks. *Soft Matter* **7**, 4318 (2011).

30. T. Yoshino, M. Kondo, J.-i. Mamiya, M. Kinoshita, Y. Yu, T. Ikeda, Three-Dimensional Photomobility of Crosslinked Azobenzene Liquid-Crystalline Polymer Fibers. *Adv. Mater.* **22**, 1361 (2010).

31. H. K. Bisoyi, A. M. Urbas, Q. Li, Soft Materials Driven by Photothermal Effect and Their Applications. *Adv. Opt. Mater.* **6**, 1800458 (2018).

32. C. Li, Y. Liu, C.-w. Lo, H. Jiang, Reversible white-light actuation of carbon nanotube incorporated liquid crystalline elastomer nanocomposites. *Soft Matter* **7**, 7511 (2011).

33. C. Li, Y. Liu, X. Huang, H. Jiang, Direct Sun-Driven Artificial Heliotropism for Solar Energy Harvesting Based on a Photo-Thermomechanical Liquid-Crystal Elastomer Nanocomposite. *Adv. Funct. Mater.* **22**, 5166 (2012).

34. C. M. Yakacki, M. Saed, D. P. Nair, T. Gong, S. M. Reed and C. N. Bowman, Tailorable and programmable liquid-crystalline elastomers using a two-stage thiol–acrylate reaction. *RSC Adv.* **5**, 18997 (2015).

Chapter 4 Light or Thermally Powered Autonomous Rolling of an Elastomer Rod

Specially arranged external stimuli or carefully designed geometry are often essential for realizing continuous autonomous motion of active structures without self-carried power. As a consequence, it is usually very challenging to further integrate those structures as active building blocks into a system with complex form and multifunction. In this letter, we report an autonomous motion of a surprisingly simple setup: a cylindrical elastomer rod on a flat hot surface or under homogenous illumination of visible light. We further show that the rod can roll continuously without any sign of a pause after six hours, if an obstacle is put in front of it. We demonstrate that such non-intuitive autonomous rolling results from a combination of large thermal actuation of the elastomer and heat transfer between the rod and its surroundings. Using the autonomous rolling rods as main building blocks, we further design and fabricate a light-powered vehicle and a thermally-powered conveyor for mass transport in both air and water environment.

4.1 Introduction

Controlled movement of tether-less structures, driven by different external stimuli such as light, humidity, heat and magnetic field, have been recently extensively explored *(1-10)*, thanks to their potential applications in robotics, biomimetic systems, and energy harvesting devices. To maintain continuous motion of those structures, it is usually required to either introduce spatially heterogeneous stimuli (*11*) or dynamically control the external stimuli *(12, 13)*. For example, a photo-sensitive polymeric thin film can swim away from a light source on the surface of water, when the light is periodically turned on and off *(14, 15)*. Hygrobot fabricated from humidity-sensitive polymer can move along the gradient of environmental humidity *(16)*. A self-walking gel robot can walk automatically driven by internal self-oscillating reactions *(17)*.

Recently, novel structures and devices have been fabricated, which can move ceaselessly under the action of static stimuli *(8, 18-20)*. Autonomous movement of most of those structures relies on carefully designed geometries *(7, 24, 25)*, customized material *(1, 8, 23)* and/or specially arranged external stimuli *(3, 22)*. For example, in most light-driven autonomous moving structures, the light has to be illuminated from certain direction to the active structure *(8, 13, 23)*. Although unusual capabilities and intriguing performance of those structures have been demonstrated, it is very challenging to assemble those delicate structures as active building blocks to a system with complex forms and multifunction.

In this article, we report autonomous rolling of a cylindrical monodomain liquid crystal elastomer (LCE) rod on a flat plate with homogenously elevated temperature or under homogenous light illumination. Due to the large and reversible actuation strain, high stretchability and excellent programmability, LCE has been recently developed into diverse structures to realize various

deformation and motion, triggered by thermal *(24-28)*, optical *(3, 29-35)* and magnetic stimuli *(36, 37)*. Different from all the previous studies, continuous and autonomous rolling of an LCE rod observed in current study does not rely on any complex geometrical design, special patterning of mesogenic molecules and inhomogeneous or dynamic external stimuli. Autonomous rolling in the current work means no dynamic control of stimuli is involved, which is also often categorized as self-regulating motion *(10)*. Based on our understandings of the autonomous rolling mechanism of the LCE rod, we can realize controlled rod rolling through a combination of thermal and optical stimuli. Using autonomous rolling rods as the main building blocks, we further design and fabricate light-powered weight-carrying vehicle and thermally-powered conveyor for mass transport in both air and water.

4.2 Methods

4.2.1 Materials

LC monomer, 1,4-Bis-[4-(3-acryloyloxypropyloxy)benzoyloxy]-2-methylbenzene (95%, RM257) is purchased from Wilshire Technologies. Crosslinker, pentaerythritol tetrakis(3-mercaptopropionate) (95%, PETMP), spacer, 2,2'-(ethylenedioxy) diethanethiol (95%, EDDET), catalyst, dipropyl amine (98%, DPA), photoinitiator, (2-hydroxyethoxy)-2-methylpropiophenone (98%, HHMP), and multi-walled carbon nanotubes (98%, CNTs) are purchased from Aldrich. All chemicals are used as received without any purification.

4.2.2 Fabrication of LCE rods

LCE rods are prepared by the two-step crosslinking reaction according to the method previously reported by Yakacki et al. *(38)*. The LCE monomer mixture is prepared by dissolving RM257 (LC monomer), PETMP (crosslinker), EDDET (spacer), and HHMP (photoinitiator) in toluene followed by heating above LC phase transition temperature and vigorous mixing. The composition of the mixture consists of 53.0 wt% of RM257, 2.5 wt% of PETMP, 12.5 wt% of EDDET, and 0.4 wt% of HHMP in toluene. After the mixture becomes homogeneous, 0.2 wt% of DPA (catalyst) is added to trigger the reaction. For LCE-CNT composite, 0.2 wt% of CNTs are also added in the mixture. The mixture is placed in the vacuum chamber to remove bubbles trapped inside, followed by being transferred into a cylindrical mold . The mixture is left overnight at room temperature to be loosely-crosslinked by the thiol-acrylate Michael addition reaction. The loosely-crosslinked LCE rod is placed in the oven at 80 ℃ for 24 h for the evaporation of residual solvent. After the LCE rod is dried, it is subjected to uniaxial stretch to achieve monodomain state *(15,38)* and under the UV light (365 nm, UVP B-100AP/R) irradiation for 1 h to be fully-crosslinked. Finally, the LCE rod in a cylindrical shape with different diameters can be obtained.

4.2.3 Heat and light-induced rolling

The temperature of the hot plate (Corning PC-420D) is set up as a desired temperature and then LCE rod is placed on the top of it to initiate heat-induced rolling motion. For the light-induced rolling, LCE-CNT rod is placed below a white light source (Hubbell QLI500, halogen lamp) with distance about 20 cm. The LCE-CNT rod begins to move once the light is turned on.

4.2.4 Light-induced rolling reversal

The rolling direction of the LCE rod can be reversed by irradiation of visible light (Hubbell QLI500, halogen lamp) on the convex surface of the LCE rod. The light was turned on 20 cm away from the LCE rod while it is rolling. Once the rolling direction of the LCE rod is reversed, no further light irradiation is required.

4.2.5 Fabrication of LCE rod-based active structures

Two pairs of LCE-CNT rods, as wheels of the light-powered LCE vehicle, are connected by aluminum wires with diameter of 0.3 mm. A supporting frame structure is built on the connecting wires. For the weight-carrying LCE-CNT rod under water, an LCE-CNT rod is placed under water and two laser-cut acrylic structures connected by a transparent acrylic sheet are placed on the top of it. LCE-CNT rod rolls and drag the structure move forward under water, when a laser is scanned along the length of the rod. The thermally-driven LCE conveyor is made by placing five LCE rods I n parallel on the top of a hot surface. Two acrylic structures with five holes are placed at each end of the LCE rods to prevent the translation.

4.3 Results and Discussion

We find in the experiment that a cylindrical (monodomain) LCE rod with 70.0 mm length and 2.6 mm diameter rolls to one direction immediately after it is placed on the top of a flat hot surface with homogenous temperature around 100 ˚C. Its rolling speed is around 6 mm/s as shown in Fig. 4.1a. Inspired by the thermally-induced rolling, we further show that similar autonomous

rolling can also be powered by homogenous light illumination for an LCE-carbon nanotube (CNT) composite rod as shown in Fig 4.1b. In the experiment, we shed a white light (Hubbell QLI500, halogen lamp) from the top onto the LCE-CNT composite rod with the same size as the pristine LCE rod, which is laid on a flat surface at room temperature. The rod begins to roll to one direction at the speed around 0.3 mm/s, immediately after the light exposure. During the rolling of the elastomer rod as illustrated in Fig. 4.1a and b, no sliding between the rod and the surface is observed.

The LCE rod can even roll up on a hot surface with a tilting angle around 11° as shown in Fig. 4.2a. In this case, the rolling speed of the rod decreases to 3 mm/s, compared to 6 mm/s on a flat surface. With a blockage in front of the LCE rod, it can continuously spin with no sign of stopping after six hours, though its angular velocity slightly decreases from 2.05 rad/s to 1.75 rad/s as shown in Fig. 4.2b.

According to our knowledge, the autonomous rolling of an elastomer rod for such a simple setup as described above has never been reported before. We next provide a qualitative interpretation for the phenomenon and later develop a quantitative thermo-mechanics model for it. In terms of molecular structure, LCE can be regarded as an integration of mesogenic molecules into a polymer network. Large contraction along the aligning direction of the mesogens can be realized in a monodomain LCE upon heating, caused by the increased disorder of aligned mesogens with temperature increase. Reversible thermal actuation of an monodomain LCE film used in the current work is shown in Fig. 4.3. For an LCE-CNT composite, similar contraction can be achieved by light illumination due to photo-thermal effects, as shown in many previous studies *(39-42)*. We believe the light or thermally-powered autonomous rolling of the LCE rod described above are due to the combination of large thermal actuation of LCE material and heat transfer

between the elastomer and ambient environment. In the following, we discuss how the LCE rod starts to roll as well as maintains the continuous and steady rolling.

Because the external stimuli, namely the high temperature and light irradiation, are nearly homogenous in the lateral direction, breaking the geometrical symmetry of a cylindrical rod is necessary for initiating its rolling. In our experiments, we believe it is the initial curvature of the rod (introduced during its fabrication) that breaks the symmetry. Through careful examinations, we find that the degree of curvature of an as-prepared LCE rod as shown in Fig 4.4a, can be as large as 10˚, if no special attention is paid during the fabrication. In the autonomous rolling experiments, if we rotate the LCE rod by 180˚ with respect to its longitudinal axis, the rod rolls to the opposite direction under the same experimental condition, which also indicates the geometric asymmetry of the rod. Moreover, to directly validate the above explanations, we also fabricate LCE rods extremely carefully to significantly reduce their initial bending as shown in Fig. 4.4b. We find that those much straighter LCE rods cannot roll spontaneously when they are put onto the same hot surface.

The moment which drives the LCE rod to roll can be understood in the following force/moment analysis: when a cylindrical LCE rod is placed on a flat plate at room temperature, its gravity is distributed homogenously along its length. Likewise, the distribution of the supporting force provided by the plate is also homogenous. Therefore, the supporting force and gravity are balanced with each other as illustrated in Fig. 4.5a. When the temperature of the plate is raised to above the phase transition temperature of the mesogens in the LCE, the bottom of the LCE rod directly in contact with the plate is heated up to a higher temperature than the top of the rod as shown in Fig. 4.5b. Because the contraction of the LCE increases with the increase of temperature, the bottom of the LCE rod tends to contract more along the axial direction than its

top part, resulting in an internal bending moment which tends to bend up the middle segment of the rod. As a consequence, the homogenously distributed supporting force provided by the plate gets more and more concentrated toward the two ends of the rod. In an extreme case, if the LCE rod is clamped by its two ends as shown in Fig. 4.6a, due to the bending deformation of the LCE rod, the supporting force finally becomes two point-forces applied onto the two ends.

Because of the redistribution of the supporting force and the curved shape of the rod, the gravitational force of the rod and the supporting force provided by the plate can form a couple which drives the rod to roll to the direction which it is convex to, as shown in Fig. 4.5b. After the rolling of the LCE rod is started, the rolling can be maintained because the side of the rod opposite to the rolling direction is always hotter than the other side (Fig. 4.5b), which automatically maintains the lateral bending of the rod. For those straight LCE rods prepared much more carefully as mentioned previously, which cannot spontaneously roll on the hot plate, they can maintain the rolling without requiring any external force or torque, once the rolling is triggered. Therefore, the initial bending of an LCE rod is not critical for the maintenance of the continuous rolling.

Based on the mechanism proposed above, we can easily understand the light-powered rolling of the LCE-CNT composite rod. With a light radiation from the top, the top surface of the rod is heated up and tends to contract due to the photo-thermal effect. As a result, the two ends of the LCE rod has the tendency of bending up, causing the supporting force being concentrated on the middle of the rod. Light-induced bending deformation of a LCE-CNT composite rod is shown in Fig. 4.6b. The concentrated supporting force and gravity of the rod can also form a couple which drives the rod to roll to its concave direction as shown in Fig. 4.5c, which is opposite to the thermally-powered rolling as discussed above. Such prediction completely agrees with experimental observations.

According to the understandings of the autonomous rolling mechanism of the elastomer rod, rolling direction of the rod is determined by the direction of its curvature. We next use a light source to induce the reversal of the rolling direction of an LCE-CNT composite rod on a hot plate. In the experiment, an LCE-CNT composite rod first rolls on a hot plate with homogenous temperature of 100 °C. At a moment, we turn on a light remotely, which makes the rod slow down, stop and roll to the opposite direction as shown in Fig. 4.7. Such light-induced reversal of rod rolling can be easily understood based on the mechanism proposed above. As explained previously, before the light is turned on, the rod rolls on a hot surface to its convex direction. When a light is irradiated onto the LCE rod from its moving direction, the side of the rod facing to the light can absorb light, convert it to heat and tend to contract. As a consequence, the curvature of the rod, and thus its rolling direction, are both reversed to the opposite direction as shown in Fig. 4.7. Although only light-induced reversal of the rolling is demonstrated in the current work, it is reasonable to expect that by applying inhomogeneous light irradiation onto the LCE-CNT composite rod, we can realize many different rolling paths of the rod on a hot surface, which will be investigated in a following-up work.

Due to the simplicity of the autonomous rolling of an LCE rod discovered by us, we next assemble the LCE rods to three different functional devices which can be powered by heat or light, respectively. The first device is a light-powered weight-carrying vehicle as shown in Fig. 4.8a. The vehicle is simply composed of four LCE-CNT composite rods as active wheels connected to a wire as supporting structure. Rolling of the four wheels can finally result in translational motion of the vehicle. In the experiment as shown in Fig. 4.8a, we put a weight of roughly two times of the weight of the LCE rods on a supporting structure. Under the illumination of white light, the LCE vehicle can move forward with a speed around 0.2 mm/s.

To demonstrate the robustness of the autonomous rolling, we further show that a similar light-powered LCE vehicle can move underwater (Fig. 4.8b). In the design, a single LCE-CNT composite rod is used as the driving wheel for the vehicle. With a continuous nIR-laser scanning along the axial direction of the rod from the top, the vehicle can move under water with a speed around 2.0 mm/s while carrying a small weight.

The third device is a thermally-powered LCE conveyor as shown in Fig. 4.8c. Five LCE rods are placed parallel on the top of a hot surface. To prevent translational motion, both ends of each rod are constrained by small holes of rigid frames, which are glued onto the substrate. Blocks of different shapes can be transported on the conveyor from one side to the other side with the speed around 1.7 mm/s. Each block has a weight comparable to that of an LCE rod.

The three functional devices shown in Fig. 4.8 clearly demonstrate the potential applications of the light or thermally-driven autonomous rolling of LCE rods discovered in the current study. Due to the simple geometry and high robustness of the rolling mechanism, advanced active structures of more complex forms and with multiple functionalities can also be constructed based on various combinations of LCE rods.

4.4 Conclusion

In this article, we report a discovery of autonomous rolling phenomenon in a surprisingly simple setup: a cylindrical elastomer rod on a flat hot surface with homogenous temperature or under homogenous illumination of light. We find that a combination of thermally-driven active deformation of the elastomer and heat transfer between the rod and its surrounding is the key for the autonomous rolling of the rod. Based on our understanding, we successfully use a white light

source to induce the reversal of thermally-powered rod rolling. In addition, using the autonomous rolling rods as the active building blocks, we design and fabricate a light-powered weight-carrying vehicle, and a thermally-powered conveyor.

Chapter 4, in part or in full, is a reprint of the following material:

C. Ahn, X. Liang, S. Cai "Light or Thermally Powered Autonomous Rolling of an Elastomer Rod", *ACS Appl. Mater. Interfaces,* ***2018****, 10,* (2017). The dissertation author was the primary investigator and author of this paper.

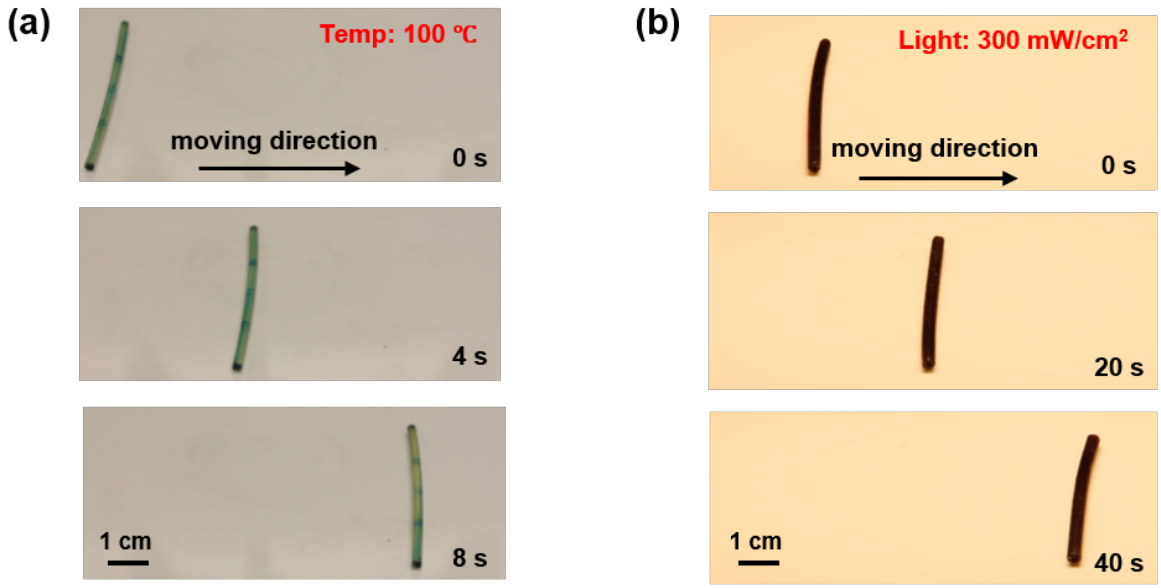

Figure 4.1: Autonomous rolling of an LCE rod on a plate with homogenously elevated temperature or under homogeneous light illumination. (a) A cylindrical LCE rod rolls autonomously on a hot plate with homogenous temperature around 100°C. (b) A cylindrical LCE-CNT composite rod rolls autonomously under homogenous illumination of white light with power density of 300 mW/cm^2.

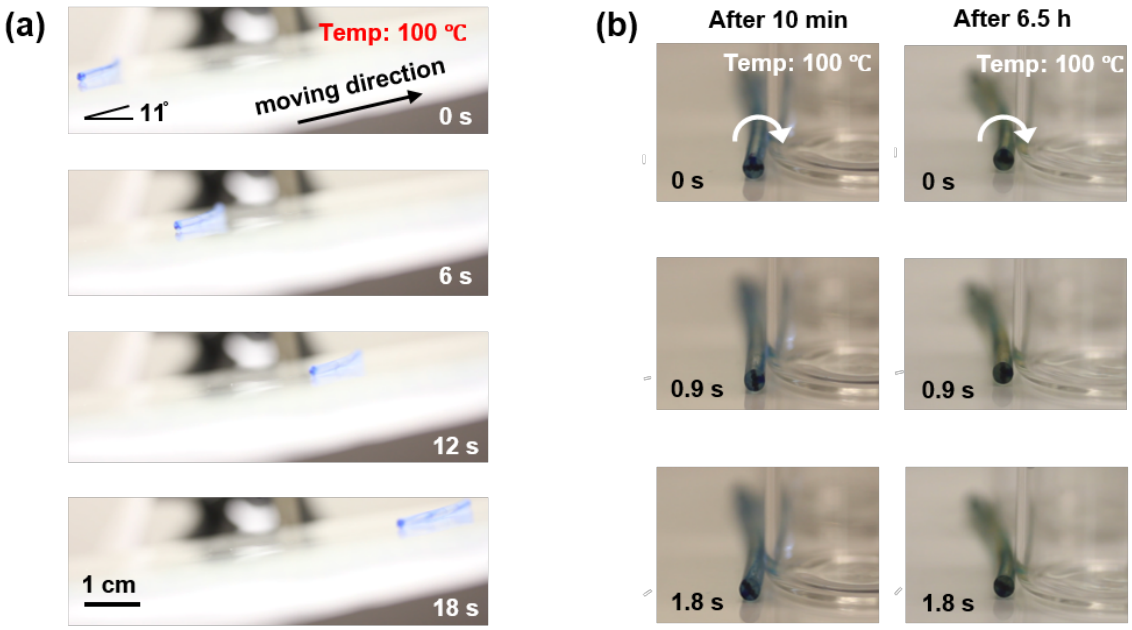

Figure 4.2: (a) Autonomous climbing LCE rod on a tilted hot surface. (b) Spinning of the same LCE rod blocked by a glass bottle on a hot surface with temperature of 100 ºC. 10 mins after the start of the spinning of the LCE rod, its spinning angular velocity of the rod is around 2.05 rad/s. After 6.5 hours, the spinning angular velocity of the rod decreases to 1.75 rad/s.

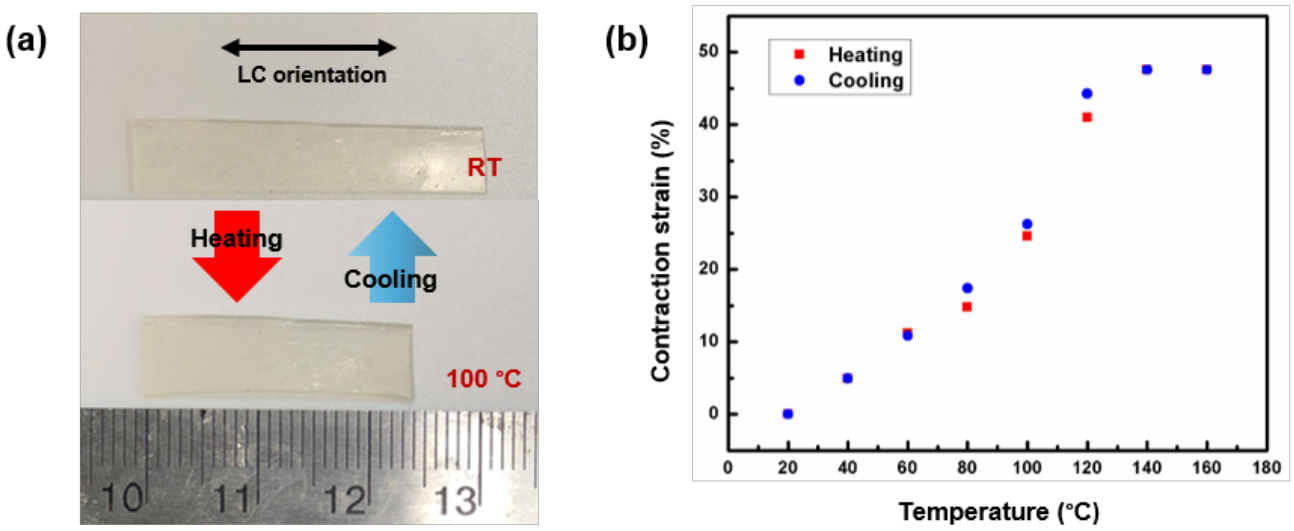

Figure 4.3: Reversible thermal actuation of a LCE film. (a) Photos of reversible actuation of a LCE film with temperature change. (b) Contraction strain of LCE film as a function of temperature with continuous heating and cooling process between 20 °C and 160 °C.

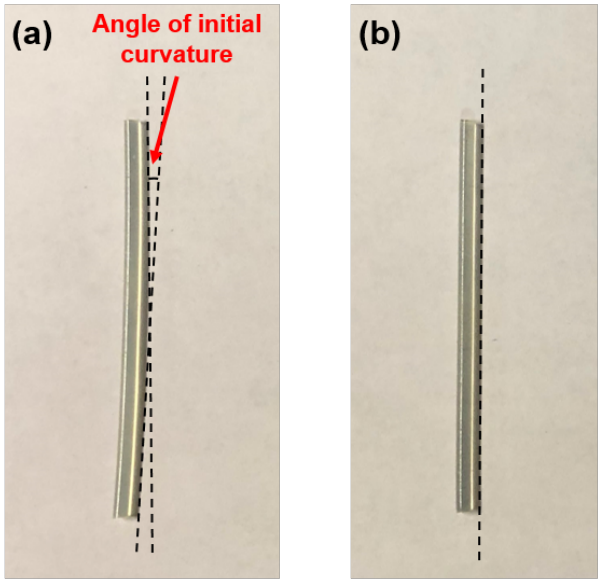

Figure 4.4: Photos of (a) an as-prepared LCE rod with initial bending angle, and (b) much straighter one, prepared with special effort.

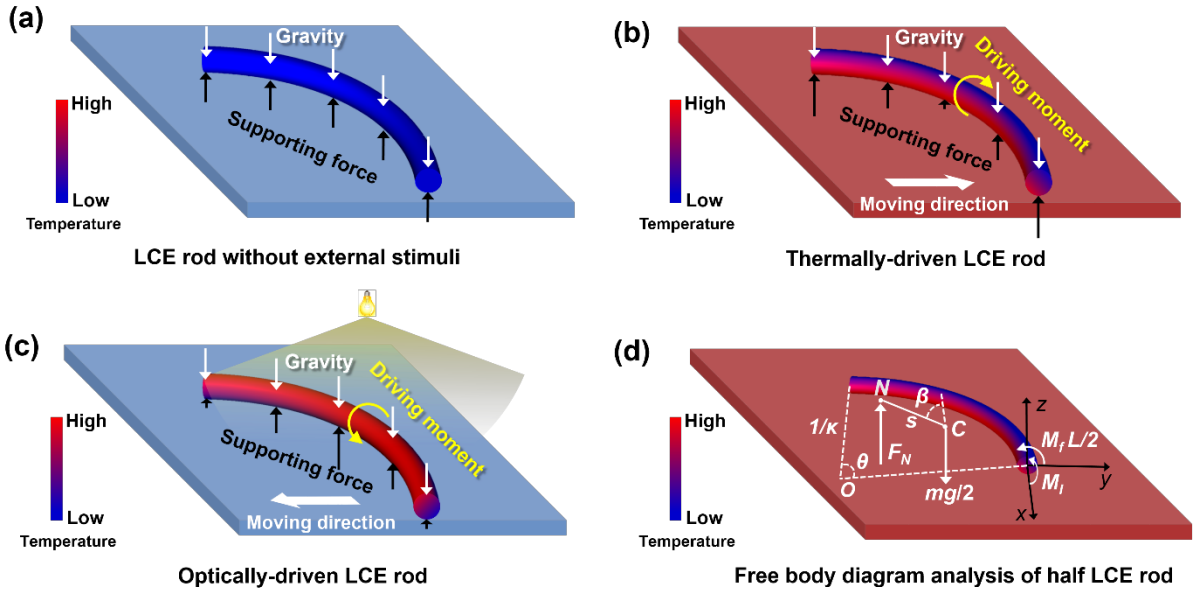

Figure 4.5: Schematic illustration of the mechanism of autonomous rolling of an LCE rod on a hot surface or under homogenous light illumination. (a) Initially, for an LCE rod lying on a surface at room temperature, its gravity distributes homogenously along its length, which is balanced by the supporting force provided by the surface. (b) When the temperature of the surface is elevated, an inhomogeneous temperature field in the LCE rod results in inhomogeneous actuating strain, which tends to bend the middle part of the rod up, and the supporting force gets highly concentrated on the two ends of the rod. Finally, the gravitational force and the supporting force generate a moment driving the LCE rod roll to the direction which it is convex toward. (c) With a light irradiation from the top, the LCE-CNT composite rod has the tendency of bending its two ends up due to the photothermal effect of CNTs which generate thermal gradient along the thickness of the rod. As a result, the supporting force provided by the surface gets concentrated to the middle part of the rod, and the moment generated by the supporting force and gravity drives the rod rolls to its concave direction. (d) Free body diagram analysis of half of the rod, which steadily rolls on a hot plate.

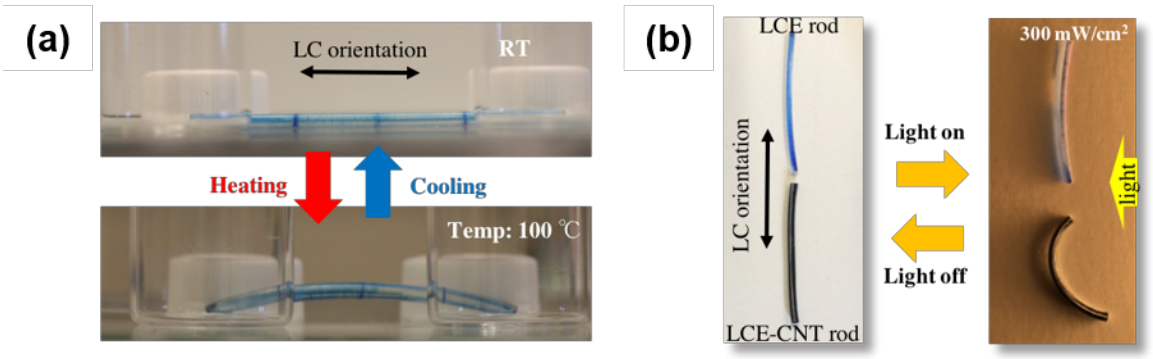

Figure 4.6: Bending deformation of an LCE rod and LCE-CNT composite rod induced by (a) bottom heating and (b) visible light illumination.

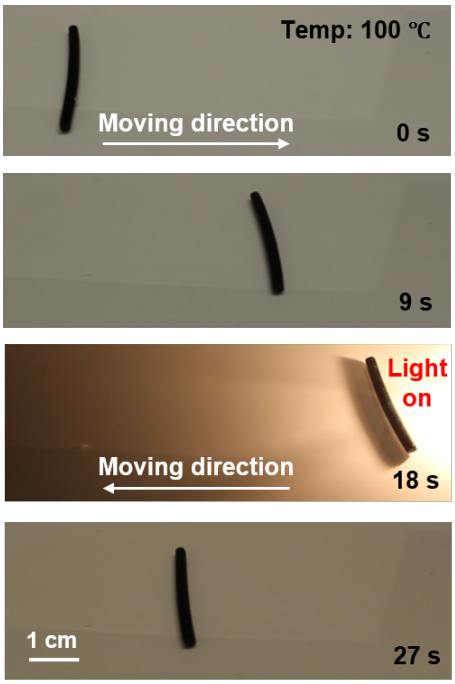

Figure 4.7: Light-induced reverse rolling of an LCE-CNT composite rod on a flat hot surface. An LCE-CNT composite rod rolls autonomously to its convex direction on a flat hot surface. When we turn on a light, the middle of the rod bends opposite to its rolling direction, and consequently, the rolling of the rod slows down, stops and then reverses. The rod moves to the opposite direction steadily after the light is turned off.

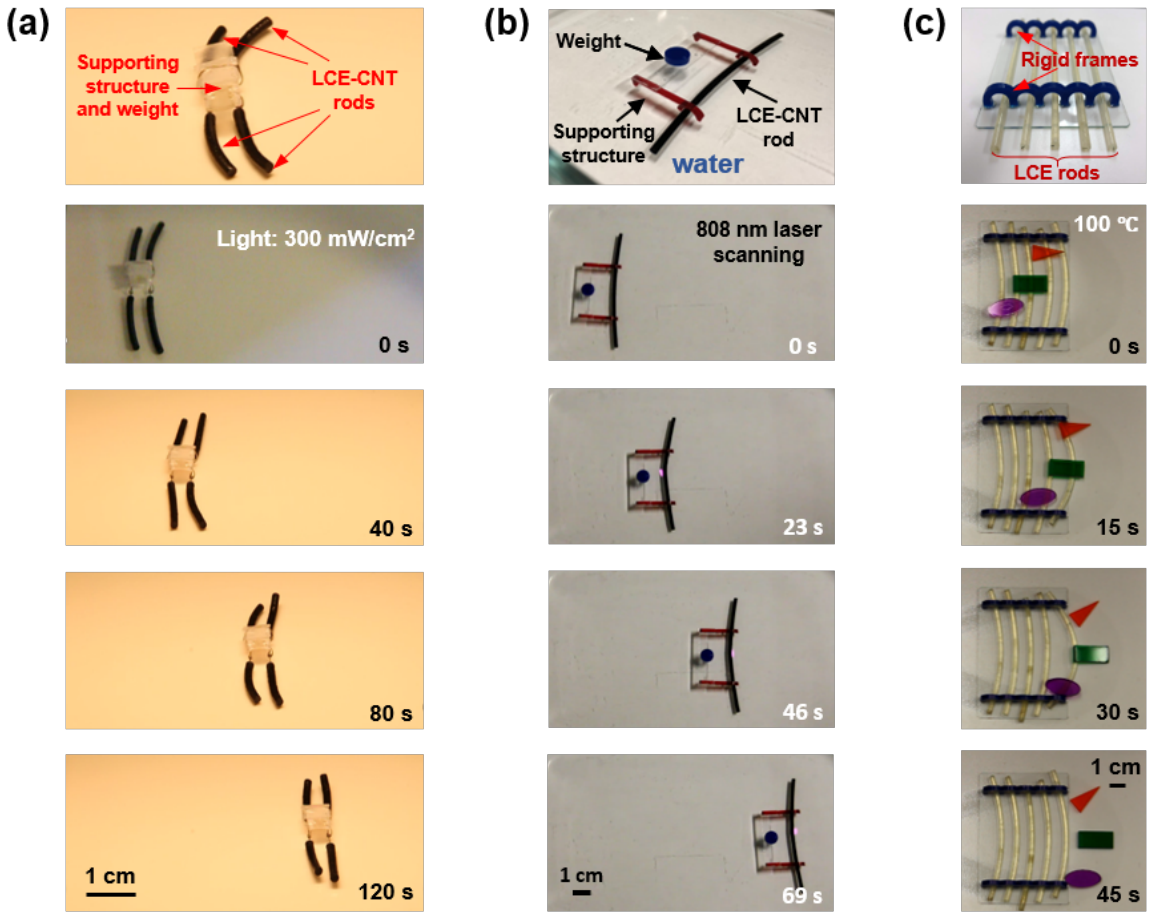

Figure 4.8: Demonstrations of active structures composed of LCE rods as active building blocks. (a) A vehicle composed of four LCE-CNT rod wheels can move on a flat surface under light illumination. (b) LCE-CNT rod rolls under water induced by laser scanning while carrying weight. (c) Thermally-driven LCE conveyor transports weights by its continuous rolling on a hot surface.

4.5 References

1. Hu, W.; Lum, G. Z.; Mastrangeli, M.; Sitti, M. Small-Scale Soft-Bodied Robot with Multimodal Locomotion. *Nature* **554**, 81 (2018)

2. Zhang, L.; Qiu, X.; Yuan, Y.; Zhang, T. Humidity- and Sunlight-driven Motion of a Chemically Bonded Polymer Bilayer with Programmable Surface Patterns. *ACS Appl. Mater. Inter.* **9***,* 41599 (2017)

3. Zeng, H.; Wani, O. M.; Wasylczyk, P.; Priimagi, A. Light-Driven, Caterpillar-Inspired Miniature Inching Robot. *Macromol. Rapid Commun.* **39**, 1700224 (2018)

4. Dai, B.; Wang, J.; Xiong, Z.; Zhan, X.; Dai, W.; Li, C.-C.; Feng, S.-P.; Tang, J. Programmable Artificial Phototactic Microswimmer. *Nat. Nanotechnol.* **11**, 1087 (2016)

5. Wang, E.; Desai, M. S.; Lee, S.-W. Light-Controlled Graphene-Elastin Composite Hydrogel Actuators. *Nano Lett.* **13**, 2826 (2013)

6. Hu, Y.; Liu, J.; Chang, L.; Yang, L.; Xu, A.; Qi, K.; Lu, P.; Wu, G.; Chen, W.; Wu, Y. Electrically and Sunlight-Driven Actuator with Versatile Biomimetic Motions Based on Rolled Carbon Nanotube Bilayer Composite. *Adv. Funct. Mater.* **27**, 1704388 (2017)

7. Wie, J. J.; Shankar, M. R.; White, T. J. Photomotility of Polymers. *Nat. Commun.* **7**, 13260 (2016)

8. Zhang, X.; Yu, Z.; Wang, C.; Zarrouk, D.; Seo, J.-W. T.; Cheng, J. C.; Buchan, A. D.; Takei, K.; Zhao, Y.; Ager, J. W.; Zhang, J.; Hettick, M.; Hersam, M. C.; Pisano, A. P.; Fearing, R. S.; Javey, A. Photoactuators and Motors Based on Carbon Nanotubes with Selective Chirality Distributions. *Nat. Commun.* **5**, 2983 (2013)

9. Gelebart, A. H.; Jan Mulder, D.; Varga, M.; Konya, A.; Vantomme, G.; Meijer, E. W.; Selinger, R. L. B.; Broer, D. J. Making Waves in a Photoactive Polymer Film. *Nature* **546**, 632 (2017)

10. Zeng, H.; Wasylczyk, P.; Wiersma, D. S.; Priimagi, A. Light Robots: Bridging the Gap between Microrobotics and Photomechanics in Soft Materials. *Adv. Mater.* **30***,* 1703554 (2018)

11. Palagi, S.; Mark, A. G.; Reigh, S. Y.; Melde, K.; Qiu, T.; Zeng, H.; Parmeggiani, C.; Martella, D.; Sanchez-Castillo, A.; Kapernaum, N.; Giesselmann, F.; Wiersma, D. S.; Lauga, E.; Fischer, P. Structured Light Enables Biomimetic Swimming and Versatile Locomotion of Photoresponsive Soft Microrobots. *Nat. Mater.* **15**, 647 (2016)

12. Rogóż, M.; Zeng, H.; Xuan, C.; Wiersma, D. S.; Wasylczyk, P. Light-Driven Soft Robot Mimics Caterpillar Locomotion in Natural Scale. *Adv. Opt. Mater.* **4**, 1689 (2016)

13. Jiang, W.; Niu, D.; Liu, H.; Wang, C.; Zhao, T.; Yin, L.; Shi, Y.; Chen, B.; Ding, Y.; Lu, B. Photoresponsive Soft-Robotic Platform: Biomimetic Fabrication and Remote Actuation. *Adv. Funct. Mater.* **24**, 7598 (2014).

14. Camacho-Lopez, M.; Finkelmann, H.; Palffy-Muhoray, P.; Shelley, M. Fast Liquid-Crystal Elastomer Swims into the Dark. *Nat. Mater.* **3**, 307 (2004)

15. Tian, H.; Wang, Z.; Chen, Y.; Shao, J.; Gao, T.; Cai, S. Polydopamine-Coated Main-Chain Liquid Crystal Elastomer as Optically Driven Artificial Muscle. *ACS Appl. Mater. Inter.* **10**, 8307 (2018)

16. Shin, B.; Ha, J.; Lee, M.; Park, K.; Park, G. H.; Choi, T. H.; Cho, K.-J.; Kim, H.-Y. Hygrobot: A Self-Locomotive Ratcheted Actuator Powered by Environmental Humidity. *Sci. Robot.* **3**, 2629 (2018)

17. Maeda, S.; Hara, Y.; Sakai, T.; Yoshida, R.; Hashimoto, S. Self-Walking Gel. *Adv. Mater.* **19***,* 3480 (2007)

18. Maggi, C.; Saglimbeni, F.; Dipalo, M.; De Angelis, F.; Di Leonardo, R. Micromotors with Asymmetric Shape that Efficiently Convert Light into Work by Thermocapillary Effects. *Nat. Commun.* **6**, 7855 (2015)

19. Tang, R.; Liu, Z.; Xu, D.; Liu, J.; Yu, L.; Yu, H. Optical Pendulum Generator Based on Photomechanical Liquid-Crystalline Actuators. *ACS Appl. Mater. Inter.* **7***,* 8397 (2015)

20. Yu, L.; Yu, H. Light-Powered Tumbler Movement of Graphene Oxide/Polymer Nanocomposites. *ACS Appl. Mater. Inter.* **7***,* 3834 (2015)

21. Zeng, H.; Wasylczyk, P.; Parmeggiani, C.; Martella, D.; Burresi, M.; Wiersma, D. S. Light-Fueled Microscopic Walkers. *Adv. Mater.* **27**, 3883 (2015)

22. Yamada, M.; Kondo, M.; Miyasato, R.; Naka, Y.; Mamiya, J.-i.; Kinoshita, M.; Shishido, A.; Yu, Y.; Barrett, C. J.; Ikeda, T. Photomobile Polymer Materials-Various Three-Dimensional Movements. *J. Mater. Chem.* **19**, 60 (2009)

23. Hu, Y.; Wu, G.; Lan, T.; Zhao, J.; Liu, Y.; Chen, W. A Graphene-Based Bimorph Structure for Design of High Performance Photoactuators. *Adv. Mater.* **27**, 7867 (2015)

24. Ostrom, H.; Oberg, H.; Xin, H.; LaRue, J.; Beye, M.; Dell'Angela, M.; Gladh, J.; Ng, M. L.; Sellberg, J. A.; Kaya, S.; Mercurio, G.; Nordlund, D.; Hantschmann, M.; Hieke, F.; Kuhn, D.; Schlotter, W. F.; Dakovski, G. L.; Turner, J. J.; Minitti, M. P.; Mitra, A.; Moeller, S. P.; Fohlisch, A.; Wolf, M.; Wurth, W.; Persson, M.; Norskov, J. K.; Abild-Pedersen, F.; Ogasawara, H.; Pettersson, L. G. M.; Nilsson, A. Voxelated Liquid Crystal Elastomers *Science* **347**, 978 (2015)

25. Shahsavan, H.; Salili, S. M.; Jákli, A.; Zhao, B. Smart Muscle-Driven Self-Cleaning of Biomimetic Microstructures from Liquid Crystal Elastomers. *Adv. Mater.* **27**, 6828 (2015)

26. Sawa, Y.; Urayama, K.; Takigawa, T.; DeSimone, A.; Teresi, L. Thermally Driven Giant Bending of Liquid Crystal Elastomer Films with Hybrid Alignment. *Macromolecules* **43**, 4362 (2010)

27. Agrawal, A.; Luchette, P.; Palffy-Muhoray, P.; Biswal, S. L.; Chapman, W. G.; Verduzco, R. Surface Wrinkling in Liquid Crystal Elastomers. *Soft Matter* **8**, 7138 (2012)

28. Ahn, C.; Liang, X.; Cai, S. Inhomogeneous Stretch Induced Patterning of Molecular Orientation in Liquid Crystal Elastomers. *Extreme Mech. Lett.* **5**, 30 (2015)

29. Zeng, H.; Wani, O. M.; Wasylczyk, P.; Kaczmarek, R.; Priimagi, A. Self-Regulating Iris Based on Light-Actuated Liquid Crystal Elastomer. *Adv. Mater.* **29**, 1701814 (2017)

30. Jiang, Z.; Xu, M.; Li, F.; Yu, Y. Red-Light-Controllable Liquid-Crystal Soft Actuators via Low-Power Excited Upconversion Based on Triplet–Triplet Annihilation. *J. Am. Chem. Soc.* **135**, 16446 (2013)

31. Liu, W.; Guo, L.-X.; Lin, B.-P.; Zhang, X.-Q.; Sun, Y.; Yang, H. Near-Infrared Responsive Liquid Crystalline Elastomers Containing Photothermal Conjugated Polymers. *Macromolecules* **49**, 4023 (2016)

32. Kumar, K.; Knie, C.; Bléger, D.; Peletier, M. A.; Friedrich, H.; Hecht, S.; Broer, D. J.; Debije, M. G.; Schenning, A. P. H. J. A Chaotic Self-Oscillating Sunlight-Driven Polymer Actuator. *Nat. Commun.* **7**, 11975 (2016)

33. Ikeda, T.; Nakano, M.; Yu, Y. L.; Tsutsumi, O.; Kanazawa, A. Anisotropic Bending and Unbending behavior of Azobenzene Liquid-Crystalline Gels by Light Exposure. *Adv. Mater.* **15**, 201 (2003)

34. Lee, K. M.; Koerner, H.; Vaia, R. A.; Bunning, T. J.; White, T. J. Light-Activated Shape Memory of Glassy, Azobenzene Liquid Crystalline Polymer Networks. *Soft Matter* **7**, 4318 (2011)

35. van Oosten, C. L.; Bastiaansen, C. W. M.; Broer, D. J. Printed Artificial Cilia from Liquid-Crystal Network Actuators Modularly Driven by Light. *Nat. Mater.* **8**, 677 (2009)

36. Haberl, J. M.; Sánchez-Ferrer, A.; Mihut, A. M.; Dietsch, H.; Hirt, A. M.; Mezzenga, R. Liquid-Crystalline Elastomer-Nanoparticle Hybrids with Reversible Switch of Magnetic Memory. *Adv. Mater.* **25**, 1787 (2013)

37. Song, H. M.; Kim, J. C.; Hong, J. H.; Lee, Y. B.; Choi, J.; Lee, J. I.; Kim, W. S.; Kim, J. H.; Hur, N. H. Magnetic and Transparent Composites by Linking Liquid Crystals to Ferrite Nanoparticles through Covalent Networks. *Adv. Funct. Mater.* **17**, 2070 (2017)

38. Yakacki, C. M.; Saed, M.; Nair, D. P.; Gong, T.; Reed, S. M.; Bowman, C. N. Tailorable and Programmable Liquid-Crystalline Elastomers Using a Two-Stage Thiol–Acrylate Reaction. *RSC Adv.* **5**, 18997 (2015)

39. Li, C.; Liu, Y.; Lo, C.-w.; Jiang, H. Reversible White-Light Actuation of Carbon Nanotube Incorporated Liquid Crystalline Elastomer Nanocomposites. *Soft Matter* **7**, 7511 (2011)

40. Li, C.; Liu, Y.; Huang, X.; Jiang, H. Direct Sun-Driven Artificial Heliotropism for Solar Energy Harvesting Based on a Photo-Thermomechanical Liquid-Crystal Elastomer Nanocomposite. *Adv. Funct. Mater.* **22**, 5166 (2012)

41. Kam, N. W. S.; Connell, M.; Wisdom, J. A.; Dai, H. Carbon Nanotubes as Multifunctional Biological Transporters and Near-Infrared Agents for Selective Cancer Cell Destruction. *P. Natl. Acad. Sci. USA* **102**, 11600 (2005)

42. Fujigaya, T.; Morimoto, T.; Nakashima, N. Isolated Single-Walled Carbon Nanotubes in a Gel as a Molecular Reservoir and its Application to Controlled Drug Release Triggered by Near-IR Laser Irradiation. *Soft Matter* **7**, 2647 (2011)

Chapter 5 Bioinspired design of light-powered crawling, squeezing and jumping of an untethered soft robot

Light, as a special form of energy, has been recently intensively explored to power small-scale robots. However, most existing light-driven locomoting robots have limited mobility. In this article, we demonstrate a bioinspired design of a completely light-powered untethered soft robot, which can crawl on ground, squeeze its way through a small channel and jump over a wall or onto a step above the ground. The soft robot with an arch shape is made up of liquid crystal elastomer-carbon nanotube composite, which can be actuated by the irradiation of visible light. When a light source is scanned over the surface of the robot, it deforms to an asymmetric shape and crawls forward. With the increase of the light scanning speed, the soft robot can deform significantly to enable itself to pass through a small channel. Subjected to certain light irradiation, the soft robot can deform to a closed loop, gradually store elastic energy and suddenly release it to jump over a wall or onto a step at a fast speed.

5.1 Introduction

Because light can be easily controlled remotely and precisely, light-powered moving structures have been increasingly explored in recent studies (*1-5*). Various light-powered locomotion such as rolling (*6-9*), crawling (*10-13*) and swimming (*14-18*) have been successfully realized in different structures composed of various light-responsive materials. For example, a tubular polycarbonate/carbon nanotube bilayer structure can roll on a flat surface under directional light illumination (*6*). By mimicking the locomotion of caterpillar, a liquid crystal elastomer-based mini robot can crawl under periodic light irradiation (*11*). Under a constant UV irradiation, a liquid-crystal network film can generate continuous waves that propagate away from the light source to enable its movement (*12*). However, most existing light-driven locomoting structures have limited mobility.

Multimodal locomotion of a robot (*19*) is highly desired for enhancing its adaptivity in complex environments. In particular, it has been recognized that jumping is an efficient mode for a small-scale robot to overcome obstacles and realize sudden motion (*20*), which is, however, extremely challenging for an untethered soft robot (*21*). This is partially because the actuation power of an untethered soft robot is often not large enough to enable the jumping. Recently, Hu et al. have demonstrated multimodal locomotion of a magneto-elastic soft millirobot by precisely controlling the magnitude and direction of externally applied magnetic field (*19*). Recent studies have also realized combustion-powered jumping of a soft robot (*21-23*), but the total number of the jumping that can be achieved by the robot is still very limited.

In nature, many soft worms can easily achieve different modes of locomotion by using simple actuation mechanisms. Although most soft worms often move slowly due to the small

actuation power of their muscles, some of them can achieve fast jumping by adopting different power-amplifying strategies. For instance, a fruit fly larva can crawl through contracting its longitudinal muscle and anchoring its legs in the posterior and anterior alternately (*24*). To overcome uneven obstacles, a fruit fly larva can achieve fast jumping through a series of actions: bringing its head to the tail to form a closed loop by allowing its mouth hook to grip the cuticle below the posterior spiracles, generating tension in its body through muscle contraction and disengaging its grip to release the stored elastic energy suddenly (*25*). Very similar jumping strategy is also adopted by nematode with a much smaller size (*26, 27*). Such a power-amplifying mechanism can be conceptualized as a spring-motor-latch system (*28*), which has been widely found in different animals (*29-33*) as well as plants *(34, 35)*.

In this article, inspired by the crawling motion of inchworm (Fig. 5.1a) and jumping motion of fruit fly larva (Fig. 5.1b) (or nematode), we build a liquid crystal elastomer (LCE)-carbon nanotube (CNT)-based soft robot in an arch shape, which can crawl on ground, squeeze itself to pass through a small channel, and jump over a wall and onto a step above the ground at a fast speed. We demonstrate that different modes of locomotion of the soft robot can be easily switched from one to another by changing the way of light irradiation as shown in Fig. 5.1c. Because only elastic deformation is involved, different modes of locomotion can be achieved as many times as needed.

5.2 Methods

5.2.1 Materials

LC monomer, 1,4-Bis-[4-(3-acryloyloxypropyloxy)benzoyloxy]-2-methylbenzene (95%, RM257) is purchased from Wilshire Technologies. Crosslinker, pentaerythritol tetrakis(3-mercaptopropionate) (95%, PETMP), spacer, 2,2'-(ethylenedioxy) diethanethiol (95%, EDDET), catalyst, dipropyl amine (98%, DPA), photoinitiator, (2-hydroxyethoxy)-2-methylpropiophenone (98%, HHMP), and multi-walled carbon nanotubes (98%, CNTs) are purchased from Aldrich. All chemicals are used as received without any purification.

5.2.2 Fabrication of soft robot

LCE-CNT composite is prepared by the two-step crosslinking reaction according to the method previously reported by Yakacki et al *(36)*. The Pre-LCE solution is prepared by dissolving RM257 (LC monomer), PETMP (crosslinker), EDDET (spacer), and HHMP (photoinitiator) in toluene followed by heating above LC phase transition temperature and vigorous mixing. The composition of the mixture consists of 53.0 wt% of RM257, 2.5 wt% of PETMP, 12.5 wt% of EDDET, and 0.4 wt% of HHMP in toluene. In the mixture, 0.3 wt% of CNTs are also added to be dispersed by vigorous stirring for 1 h. After the mixture became homogeneous, 0.2 wt% of DPA (catalyst) is added to trigger the reaction. The mixture is placed in the vacuum chamber to remove bubbles trapped inside followed by being transferred into a rectangular shaped mold. The mixture is left overnight at room temperature to be loosely-crosslinked by the thiol-acrylate Michael addition reaction. The loosely-crosslinked LCE-CNT composite is taken out from the mold and placed in the oven at 80 ℃ for 24 h for the evaporation of residual solvent. After the LCE-CNT

composite is dried, it is subjected to uniaxial stretch to align LC molecules in a longitudinal direction and molded into an arch shape under the UV light (365 nm, UVP B-100AP/R) irradiation for 1 h to be fully crosslinked. Finally, the soft robot is prepared by attaching magnet pieces on each end.

5.2.3 Characterization of the light-induced deformation of an LCE-CNT composite film

A free-standing rectangular LCE-CNT composite film with the dimensions of 40 mm × 7 mm × 2 mm is hung on a rod. To tune the intensity of the illuminated light, we turn on a halogen light bulb (100 W) and place it at three different distances (4, 5, and 7 cm) away from the film. When the light-induced bending of the LCE-CNT composite film reaches a steady state, the light bulb is turned off to allow the deformed LCE-CNT composite film to recover to its original shape. It is noted that in the entire experiment, the same halogen light bulb is used as the only light source.

5.2.4 Light-induced crawling and squeezing of the soft robot

The crawling and squeezing of the soft robot is enabled by manually scanning the light over the surface of the soft robot from one end to the other. The distance between the light bulb and the surface of the soft robot is set to be around 2 cm.

5.2.5 Light-induced jumping of the soft robot

In the experiment, the soft robot forms a closed loop after its inner surface is illuminated by light. Once the loop is formed, it can be maintained by the attractive binding force from the two

magnets attached to the ends of the robot, even after the light is turned off. The outer surface of the soft robot is then exposed to light irradiation at a 2 cm distance, which can induce large deformation over time. When the deformation of the soft robot is too large, the two magnets are suddenly separated and a portion of the stored strain energy is released during a short period, which results in the jumping of the robot. Since the deformation of the robot involved in the process is reversible, the soft robot can recover to its original shape and be ready for the next jumping or crawling after its landing.

5.2.6 Thermal-mechanical characterizations of the LCE-CNT composite

We measure the stress-strain diagram of the LCE-CNT composite by using a mechanical testing machine (5965 Dual Column Testing systems, Instron). The LCE-CNT composite film is first cut into rectangles with the dimension of 30 mm × 8 mm × 1.5 mm. The samples are then firmly clamped by the grippers of the machine and subjected to a uniaxial tensile stress. During the test, both strain and stress are automatically recorded by the machine. The accuracy of the strain measurement is within ±0.1%. We conduct the mechanical tests of the composite at two different strain rates (0.1/min and 0.2/min), which are comparable to the strain rate of the composite undergoing the light-induced deformation in the later experiments. We can fit the stress-strain curve predicted by Neo-Hookean model with shear modulus of 1 MPa to the measurements (Fig. 5.2a). We assume the Poisson's ratio (v) of the LCE-CNT composite is 0.49, resulting in the bulk modulus of the material $K=2\mu(1+v)/(3(1-2v))=49.7$ MPa.

To measure thermally-induced contraction in the material, we put a free standing LCE-CNT composite film with the dimension of 50 mm × 8 mm × 0.6 mm, on a hot plate (Corning,

PC-420D) with controllable temperature. The thermally-induced contractive strain in the film is measured from room temperature to about 160 °C with 20 °C intervals as shown in Fig. 5.2b.

5.3 Results and Discussion

5.3.1 Light-induced bending of an LCE-CNT composite film

In this study, we employ LCE-CNT composite as the active material to build a light-powered soft robot. LCE can be regarded as an integration of mesogenic molecules with a polymer network. With the increase of temperature, uniaxially aligned mesogens in a monodomain LCE become disordered, resulting in large and reversible contraction of the material. Through mixing a small amount of CNT with LCE, we can make LCE-CNT composite, which exhibits large reversible actuation under the irradiation of visible light due to the photothermal effect of the embedded CNTs.

As shown in Fig. 5.3a, to fabricate a monodomain LCE-CNT composite film, we first mix pre-LCE solution with CNTs, which is then filled in a sandwiched glass cell and left intact for twelve hours to enable the completion of first-step crosslinking reaction of the polymer. To induce macroscopic alignment of the mesogens in the film, we next apply a uniaxial stretch onto the film, which is then subjected to UV irradiation to trigger the second-step crosslinking reaction. More details of the fabrication of a monodomain LCE-CNT composite film can be found in the Materials and Methods Section.

We show in Fig. 5.3b that an initially flat LCE-CNT composite film can bend toward a visible light source. Under the light irradiation, the temperature in the film is inhomogeneous: the surface of the film directly exposed to the light irradiation has the highest temperature, while the

opposite side of the film has the lowest temperature. The inhomogeneous temperature field in the film can result in inhomogeneous contraction and consequently bending deformation. When the light is turned on, the deflecting angle of the film increases with time till reaches a maximal value. The maximal deflecting angle and the bending dynamics of the film can be changed by varying the light intensity (Fig. 5.3c). When the light is turned off, the deflecting angle of the film gradually reduces to zero. Light-powered multimodal locomotion of the soft robot developed in the current study mainly relies on such light-induced bending of an LCE-CNT composite film.

5.3.2 Light-powered crawling, squeezing and jumping of a soft robot

The soft robot is simply composed of an arch shape LCE-CNT composite film and two magnets attached to its ends as shown in Fig. 5.4a and Fig. 5.5. Along the proceeding path of the robot, we place several types of obstacles including a wall, a channel and a step to mimic complex environment (Fig. 5.4a). By controlling the way of light irradiation, we can realize different locomotion modes of the soft robot as shown in Fig. 5.4b-e. Since the deformation in the active material is elastic and the binding between the two magnets is reversible, different modes of locomotion can be actuated and switched from one to another as many times as needed.

When we scan a light over the surface of the soft robot from one end to the other, the robot crawls to the direction opposite to the direction of light scanning (Fig. 5.4b). The robot can continuously crawl forward on the ground under cyclic light scanning. The crawling speed of the soft robot is around 0.7 mm/s (0.5 body length/min), when the maximal light intensity at the surface of the soft robot is 1.57 Wcm^{-2} (with the light bulb 2cm away from the surface of the robot), and the light scanning speed is around 15 mm/s with 10s of interval between every two adjacent light scanning cycles. The mechanism for the light-powered crawling of the soft robot can be

understood as following (Fig. 5.6): subject to light irradiation, the soft robot bends inward greatly near the region with the highest light intensity. With the movement of the light source, the region with maximal inward bending moves accordingly. Due to the inward-bending, the shape of the soft robot becomes asymmetric, resulting in uneven supporting forces in the vertical direction on its two ends. Such a symmetry breaking is essential for the soft robot to move to one direction. Meanwhile, with the light-induced bending, two horizontal forces of the same magnitude but opposite directions are also applied onto the two ends of the soft robot. As the light-induced deformation increases, the horizontal reactive force can finally exceed the maximum force of static friction of one end, leading to the sliding of it. With the movement of the light source and the correspondent inward-bending region, the two ends of the soft robot move to one direction alternatively.

Large deformability has been recognized as one of the unique advantages of a soft robot (*37*-*40*). During the crawling, the height of the soft robot can decrease dramatically. Both of the crawling speed and the height of the robot can be changed by varying the time interval between two adjacent light scanning cycles. As shown in Fig. 5.4d, when the time interval between every two adjacent light scanning is decreased to 1 s, the soft robot can squeeze itself to pass through a small channel, which is around 25% smaller than the initial height of the robot. More quantitative understanding of the relationship between the light scanning speed/time interval and the crawling speed/vertical deformation of the soft robot can be found in the following mathematical modelling section.

In addition to the crawling and squeezing, the soft robot can also jump over a wall (Fig. 5.4c) and onto a step above the ground (Fig. 5.4e), powered by the same light source. Similar to the jumping of the fly larva shown in Fig. 1b, to achieve fast jumping, the soft robot first bends

itself to a closed loop with the light irradiation onto its inner surface. After the light is turned off, the closed loop can still be maintained because of the attractive binding force generated by the two magnets. Subsequently, the outer surface of the loop is exposed to light irradiation with the maximal intensity of 1.57 Wcm^{-2}, leading to large deformation. When the deformation or the stored elastic energy in the soft robot reaches a critical level after around 20 s of the light irradiation, the closed loop is suddenly opened. During the opening of the loop, the stored elastic energy is released in a short period. The sudden cascading of elastic energy enables power amplification and triggers jumping of the soft robot. The jumping height of the robot can reach around 80mm and the jumping distance is around 130mm. Although a fruit fly larva (8.5 mm in body length) can jump 8 times body length high and 14 times body length far, the weight of a fruit fly larva is around 2 orders of magnitude smaller than that of the current soft robot *(25)*.

5.4 Conclusion

In summary, we demonstrate that a soft robot made up of LCE-CNT composite film can crawl, squeeze and jump, entirely powered by light. Although light-powered locomoting robots have been widely explored in the previous studies, their mobilities are often very limited. In particular, light-powered motions are usually slow. For the soft robot with an arch shape developed in the current study, we can easily realize multimodal locomotion of it by only using a light bulb. When the light bulb is scanned over the surface of the robot, it can crawl at the speed of 0.7 mm/s (0.5 body length/min). With the reduction of time interval between two adjacent light scanning cycles, the robot can reduce its height by 25% to pass a small channel during crawling. To achieve light-powered jumping of the robot, we adopt a power-amplifying mechanism inspired by the jumping of fruit-fly larva or nematode. We demonstrate that the soft robot developed in the current

work can jump as high as 80 mm (3 times of its height) and as far as 130 mm (4 times of its height).

Chapter 5, in part or in full, is a reprint of the following material:

C. Ahn, X. Liang, S. Cai "Bioinspired design of light-powered crawling, squeezing and jumping of an untethered soft robot" (*submitted*). The dissertation author was the primary investigator and author of this paper.

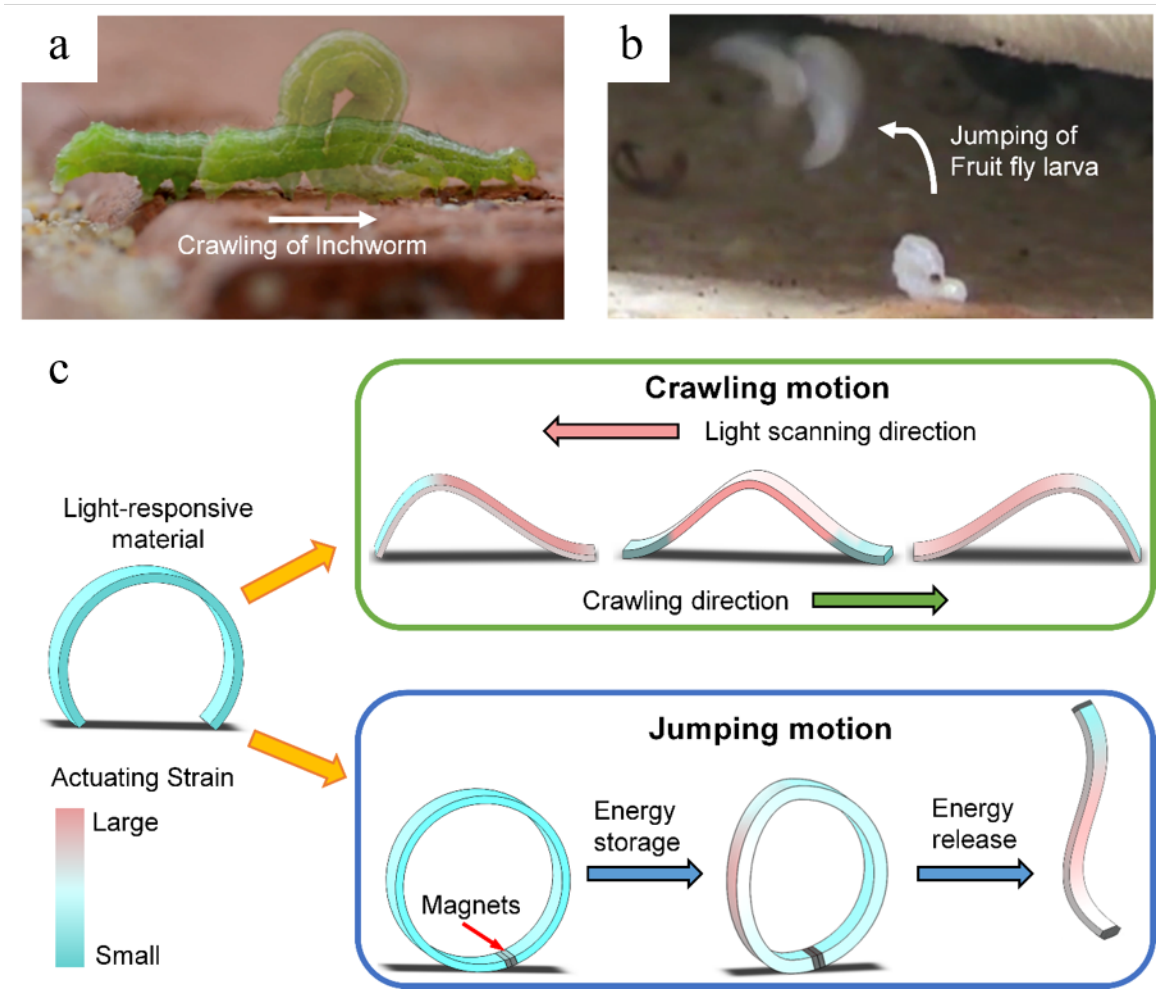

Figure 5.1: Bioinspired design of light-powered crawling, squeezing and jumping of a soft robot. (a) Two overlapped snapshots of a crawling inchworm (*Geometridae larva*). The inchworm bends its body through muscle contraction to achieve directional crawling. (b) Three overlapped snapshots of a fruit fly larva (*Ceratitis capitat*) jumping from the ground. The fruit fly larva realizes jumping motion by first bending its body to form a closed loop, storing elastic energy through muscle contraction and finally releasing the stored energy in a short time. (c) Bioinspired design of an arch shape soft robot that can crawl and jump, powered by light. The soft robot is made up of a light-responsive material. When a light is scanned over the surface of the soft robot from one end to the other, it can bend and move forward, similar to the crawling motion of an inchworm. The soft robot with two magnets attached to the ends (gray area) can also jump by first forming a closed loop through magnetic force, storing elastic energy under light irradiation and suddenly releasing the stored energy, which closely resembles the jumping of fruit fly larva.

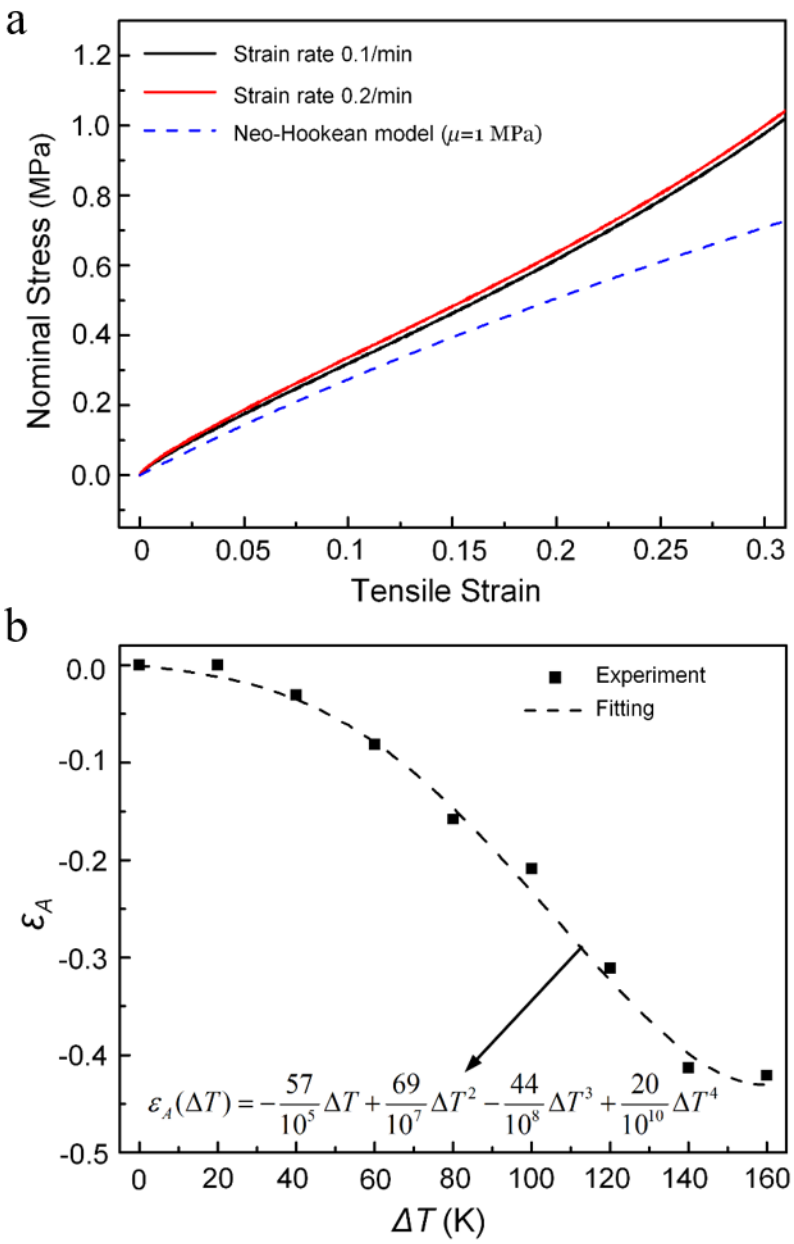

Figure 5.2: Characterizations of the properties of the LCE-CNT composite. (a) Stress-strain curves of the LCE-CNT composite film during uniaxial tensile tests with strain rates of 0.1/min and 0.2/min (solid lines). The stress-strain relationship predicted by a Neo-Hookean model with the shear modulus of 1 MPa is represented by the dashed line. (b) Uniaxial thermal-contraction of a free standing LCE-CNT film on a hot surface at different temperatures. The thermal contraction strain ε_A is fitted with a fourth-order polynomial function of temperature change ΔT as shown with a dashed line. The temperature-dependent thermal contraction coefficient α_A can be then obtained as: $\alpha_A(\Delta T)=\varepsilon_A/\Delta T$.

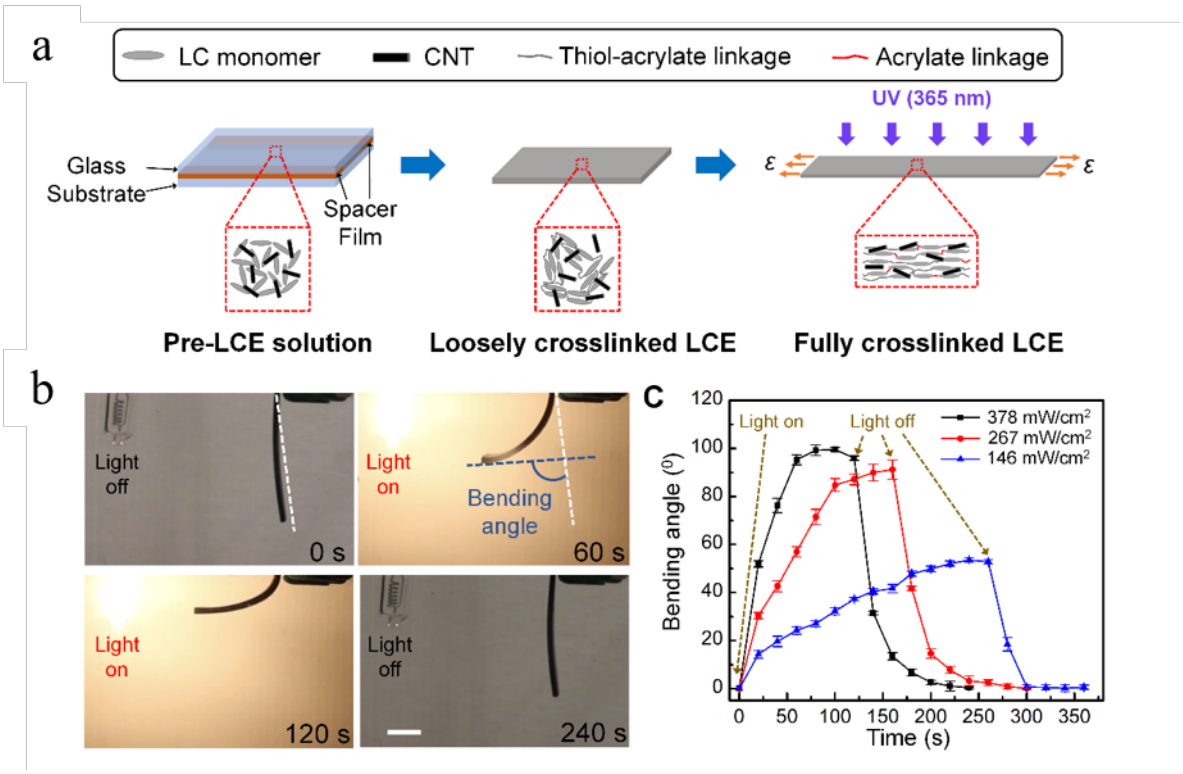

Figure 5.3: Fabrication process and light driven deformation of an LCE-CNT composite film. (a) To obtain a loosely crosslinked LCE-CNT composite film, we first fill pre-LCE solution containing CNT in a sandwiched glass cell, which is then left intact for 12 hours for the completion of the first-step crosslinking reaction of the polymer chains. We next apply a uniaxial stretch to the film and place it under UV irradiation (365 nm) to trigger the second-step crosslinking reaction. After UV irradiation for 40 mins, we can obtain an LCE-CNT composite film in monodomain state with macroscopically-aligned mesogens. (b) Light-induced reversible bending of the LCE-CNT composite film (Scale bar, 1 cm). (c) The bending angle of the LCE-CNT film as a function of time under the light irradiation with different light intensities, and the recovery of the film to the initially straight state after the light is turned off.

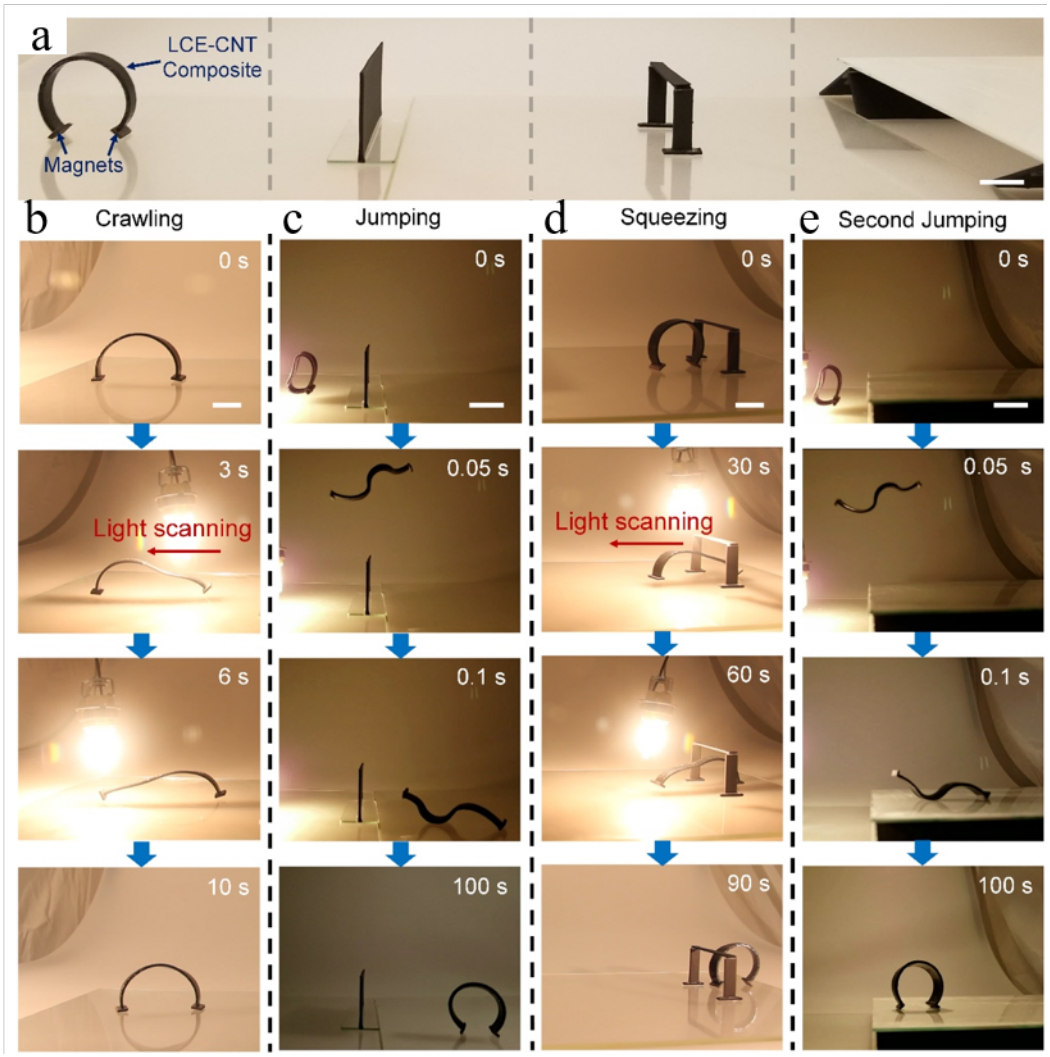

Figure 5.4: Multimodal locomotion of the soft robot powered by light. (a) The soft robot is composed of an arch shape LCE-CNT composite sheet, together with two small magnets attached to the ends. A wall, a channel and a step are placed on the proceeding path of the soft robot. (b) When a light bulb is placed around 2 cm above the soft robot with light intensity of 1.57 Wcm^{-2} and scanned over it from one end to the other in 10 s, the soft robot can crawl forward. (c) To jump over a wall, the soft robot first deforms to a closed loop that is held by the magnetic force through light irradiation on its inner surface, then gradually stores elastic energy with light irradiation (1.57 Wcm^{-2}) around 2 cm away from its outer surface for 20 s, and finally releases the stored energy in a short time. After landing on the ground, the soft robot can almost fully recover to its initial configuration. (d) By applying a cyclic light scanning, the robot can deform significantly to reduce its height and enables itself to pass through a small channel. (e) Since the deformation involved in the previous crawling, jumping and squeezing of the soft robot is elastic, the robot can jump again and land on a step above the ground. (Scale bars, 2 cm)

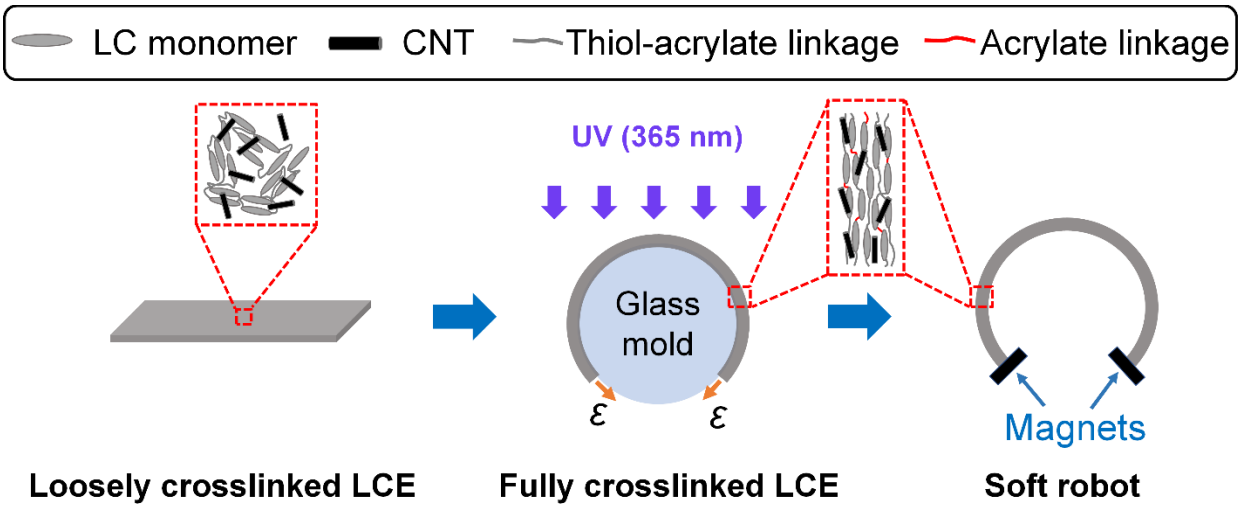

Figure 5.5: Fabrication process of the soft robot. A loosely crosslinked LCE-CNT film is stretched, wrapped around a cylindrical glass rod and subject to UV irradiation. After UV irradiation for 40 mins, the LCE film is fixed to an arch shape and mesogens inside the LCE are well aligned. We then attach two small magnets to the two ends of the LCE film to make the soft robot.

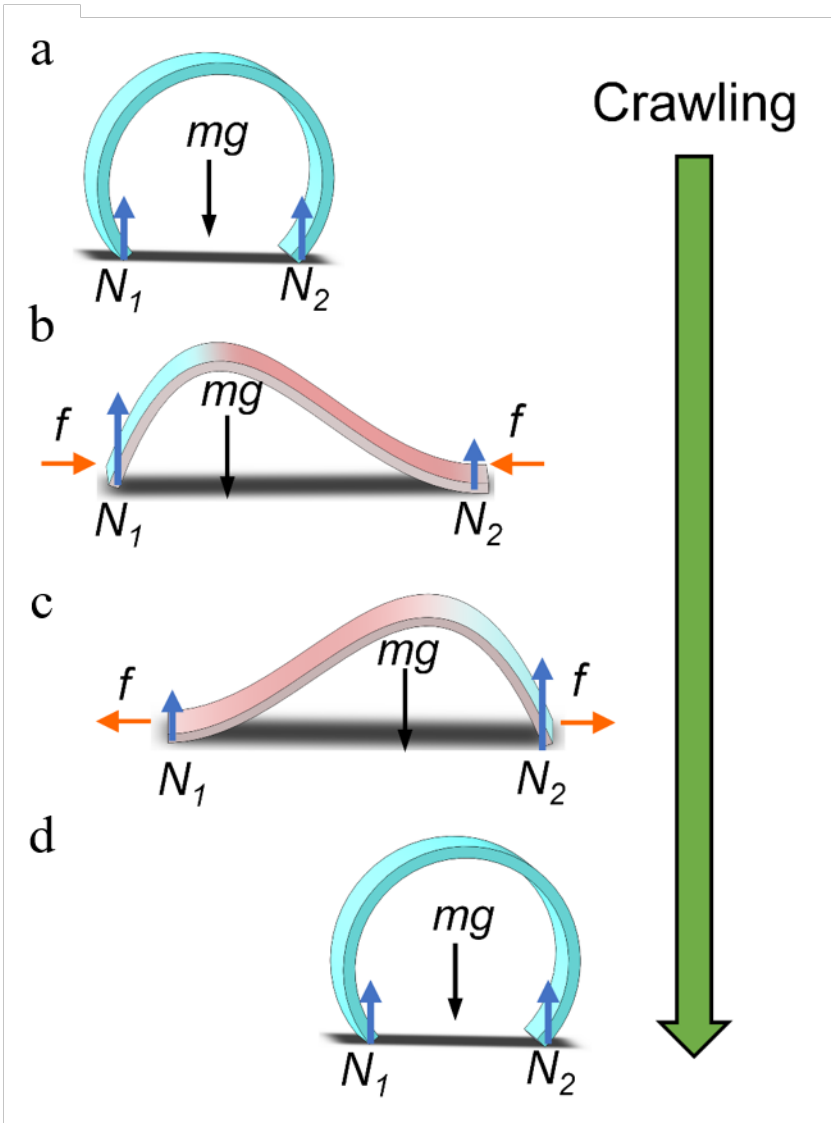

Figure 5.6: Schematics of light-powered crawling of the soft robot. (a) In the initial state, the gravity of the soft robot is balanced by the two supporting forces on its two ends (N_1 and N_2) of the same magnitude. (b) With the light irradiation, the soft robot deforms to an asymmetric shape, resulting in two unequal supporting forces: N_1 and N_2 ($N_1 > N_2$), as well as two horizontal reactive forces: f. When the horizontal force exceeds the maximal static friction of the right end, namely $f > \mu_f N_2$, it slides to the right. (c) As the light is moved to the left of the robot, the supporting force is smaller on the left end ($N_1 < N_2$), leading to its sliding. (d) The soft robot almost completely recovers to its initial shape after the light is off.

5.5 References

1. C. Ohm, M. Brehmer, R. Zentel, Liquid crystalline elastomers as actuators and sensors. *Adv. Mater.* **22**, 3366 (2010).

2. H. Zeng, P. Wasylczyk, C. Parmeggiani, D. Martella, M. Burresi, D. S. Wiersma, Light-fueled microscopic walkers. *Adv. Mater.* **27**, 3883 (2015).

3. E. Uchida, R. Azumi, Y. Norikane, Light-induced crawling of crystals on a glass surface. *Nat. Commun.* **6**, 7310 (2015).

4. D.-D. Han, Y.-L. Zhang, J.-N. Ma, Y.-Q. Liu, B. Han, H.-B. Sun, Light-mediated manufacture and manipulation of actuators. *Adv. Mater.* **28**, 8328 (2016).

5. H. Zeng, O. M. Wani, P. Wasylczyk, R. Kaczmarek, A. Priimagi, Self-regulating iris based on light-actuated liquid crystal elastomer. *Adv. Mater.* **89**, 1701814 (2017).

6. X. Zhang, Z. Yu, C. Wang, D. Zarrouk, J.-W. T. Seo, J. C. Cheng, A. D. Buchan, K. Takei, Y. Zhao, J. W. Ager, J. Zhang, M. Hettick, M. C. Hersam, A. P. Pisano, R. S. Fearing and A. Javey, Photoactuators and motors based on carbon nanotubes with selective chirality distributions. *Nat. Commun.* **5**, 2983 (2013).

7. J. J. Wie, M. R. Shankar, T. J. White, Photomotility of polymers. *Nat. Commun.* **7**, 13260 (2016).

8. Y. Hu, G. Wu, T. Lan, J. Zhao, Y. Liu, W. Chen, A graphene-based bimorph structure for design of high performance photoactuators. *Adv. Mater.* **27**, 7867 (2015).

9. C. Ahn, K. Li, S. Cai, Light or Thermally Powered Autonomous Rolling of an Elastomer Rod. *ACS Appl. Mater. Inter.* **10**, 25689 (2018).

10. M. Rogóż, H. Zeng, C. Xuan, D. S. Wiersma, P. Wasylczyk, Light-driven soft robot mimics caterpillar locomotion in natural scale. *Adv. Opt. Mater.* **4**, 1689 (2016).

11. H. Zeng, O. M. Wani, P. Wasylczyk, A. Priimagi, Light-driven, caterpillar-inspired miniature inching robot. *Macromol. Rapid Commun.* **39**, 1700224 (2018).

12. A. H. Gelebart, D. J. Mulder, M. Varga, A. Konya, G. Vantomme, E. W. Meijer, R. L. B. Selinger and D. J. Broer, Making waves in a photoactive polymer film. *Nature* **546**, 632 (2017).

13. M. Yamada, M. Kondo, R. Miyasato, Y. Naka, J.-i. Mamiya, M. Kinoshita, A. Shishido, Y. Yu, C. J. Barrett, T. Ikeda, Photomobile polymer materials-various three-dimensional movements. *J. Mater. Chem.* **19**, 60 (2009).

14. S. Palagi, A. G. Mark, S. Y. Reigh, K. Melde, T. Qiu, H. Zeng, C. Parmeggiani, A. Martella, A. Sanchez-Castillo, N. Kapernaum, F. Giesselmann, D. S. Wiersma, E. Lauga and P.

Fischer, Structured light enables biomimetic swimming and versatile locomotion of photoresponsive soft microrobots. *Nat. Mater.* **15**, 647 (2016).

15. M. Camacho-Lopez, H. Finkelmann, P. Palffy-Muhoray, M. Shelley, Fast liquid-crystal elastomer swims into the dark. *Nat. Mater.* **3**, 307 (2004).

16. W. Jiang, D. Niu, H. Liu, C. Wang, T. Zhao, L. Yin, Y. Shi, B. Chen, Y. Ding, and B. Lu, Photoresponsive soft-robotic platform: biomimetic fabrication and remote actuation. *Adv. Funct. Mater.* **24**, 7598 (2014).

17. B. Dai, J. Wang, Z. Xiong, X. Zhan, W. Dai, C.-C. Li, S.-P. Feng and J. Tang, Programmable artificial phototactic microswimmer. *Nat. Nanotechnol.* **11**, 1087 (2016).

18. H. Tian, Z. Wang, Y. Chen, J. Shao, T. Gao and S. Cai, Polydopamine-Coated Main-Chain Liquid Crystal Elastomer as Optically Driven Artificial Muscle. *ACS Appl. Mater. Inter.* **10**, 8307 (2018).19. W. Hu, G. Z. Lum, M. Mastrangeli, M. Sitti, Small-scale soft-bodied robot with multimodal locomotion. *Nature* **554**, 81 (2018).

20. M. Kovač, M. Schlegel, J.-C. Zufferey, D. Floreano, Steerable miniature jumping robot. *Auton. Robot.* **28**, 295 (2010).

21. N. W. Bartlett, M. T. Tolley, J. T. B. Overvelde, J. C. Weaver, B. Mosadegh, K. Bertoldi, G. M. Whitesides, R. J. Wood, A 3D-printed, functionally graded soft robot powered by combustion. *Science* **349**, 161 (2015).

22. M. T. Tolley, R. F. Shepherd, M. Karpelson, N. W. Bartlett, K. C. Galloway, M. Wehner, R. Nunes, G. M. Whitesides and R. J. Wood, An untethered jumping soft robot. *IEEE/RSJ International Conference on Intelligent Robots and Systems*. 561 (2014)

23. L. Michael, S. C. M., L. U. B., S. W. J., An untethered, jumping roly-poly soft robot driven by combustion. *Soft Robot.* **2**, 33 (2015).

24. S. Camazine, Leaping Locomotion in Mycetophila cingulum (Diptera: Mycetophilidae): Prepupation Dispersal Mechanism1. *Ann. Entomol. Soc. Am.* **79**, 140 (1986).

25. D. P. Maitland, Locomotion by jumping in the Mediterranean fruit-fly larva Ceratitis capitata. *Nature* **355**, 159 (1992).

26. A. P. J. M., T. Seth, Hopping locomotion in a nematode: Functional anatomy of the caudal gland apparatus of Theristus caudasaliens sp. n. *J. Morphol.* **164**, 265 (1980).

27. E. M. Reed, H. R. Wallace, Leaping Locomotion by an Insect-parasitic Nematode. *Nature* **206**, 210 (1965).

28. M. Ilton, M. Saad Bhamla, Xiaotian Ma, Suzanne M. Cox, Leah L. Fitchett, Yongjin Kim, Je-sung Koh, Deepak Krishnamurthy, Chi-Yun Kuo, Fatma Zeynep Temel, Alfred J. Crosby, Manu Prakash, Gregory P. Sutton, Robert J. Wood, Emanuel Azizi, Sarah

Bergbreiter, S. N. Patek, The principles of cascading power limits in small, fast biological and engineered systems. *Science* **360**, 397 (2018).

29. C. Thomas, C. Elliot, P. S. N., Modularity and scaling in fast movements: Power amplification in mantis shrimp. *Evolution* **65**, 443 (2011).

30. S. N. Patek, B. N. Nowroozi, J. E. Baio, R. L. Caldwell, A. P. Summers, Linkage mechanics and power amplification of the mantis shrimp's strike. *J. Exp. Biol.* **210**, 3677 (2007).

31. S. D. Magdalena, Snap! Trap-jaw ants in Borneo also jump using their legs. *Front. Ecol. Environ.* **13**, 574 (2015).

32. F. J. Larabee, A. V. Suarez, Mandible-powered escape jumps in trap-jaw ants increase survival rates during predator-prey encounters. *PLOS ONE* **10**, 0124871 (2015).

33. F. J. Larabee, W. Gronenberg, A. V. Suarez, Performance, morphology and control of power-amplified mandibles in the trap-jaw ant Myrmoteras (Hymenoptera: Formicidae) *J. Exp. Biol.* **220**, 3062 (2017).

34. Y. Forterre, J. M. Skotheim, J. Dumais, L. Mahadevan, How the Venus flytrap snaps. *Nature* **433**, 421 (2005).

35. X. Noblin, N. O. Rojas, J. Westbrook, C. Llorens, M. Argentina, J. Dumais, The fern sporangium: A unique catapult. *Science* **335**, 1322 (2012).

36. C. Laschi, B. Mazzolai, M. Cianchetti, Soft robotics: Technologies and systems pushing the boundaries of robot abilities. *Sci. Robot.* **1**, 3690 (2016).

37. S. Kim, C. Laschi, B. Trimmer, Soft robotics: a bioinspired evolution in robotics. *Trends Biotechnol.* **31**, 287 (2013).

38. D. Rus, M. T. Tolley, Design, fabrication and control of soft robots. *Nature* **521**, 467 (2015).

39. W. G. M., Soft robotics. *Angewandte Chemie International Edition* **57**, 4258 (2018).

40. A. F. Mills, *Basic heat and mass transfer*. (Prentice hall, 1999), vol. 2.

41. J. E. Shigley, C. R. Mischke, *Machine design fundamentals: a mechanical designers' workbook*. (McGraw-Hill Companies, 1989).

42. J. Burdick, P. Fiorini, Minimalist Jumping Robots for Celestial Exploration. *Int. J. Robot. Res.* **22**, 653 (2003).

43. C. M. Yakacki, M. Saed, D. P. Nair, T. Gong, S. M. Reed and C. N. Bowman, Tailorable and programmable liquid-crystalline elastomers using a two-stage thiol–acrylate reaction. *RSC Adv.* **5**, 18997 (2015).

Chapter 6 Conclusion

Soft actuators have attracted emerging research interests in recent years because of their salient features such as simpler structure for converting external energy into mechanical energy, larger degree of freedom, generally low production cost, and human compatibility compared to conventional rigid actuators. Another advantage of soft actuators is capability of tetherless structure without any rigid energy supplier on it since the material consisting itself can directly convert incoming energy sources such as heat or light into mechanical energy. Among different types of soft actuating materials, LCE is one of the most promising material due to their high anisotropy which can trigger thermally or optically induced large macroscopic deformation by manipulation of molecular level orientation.

We firstly show the patterning programming on LCE with simple strain engineering technique. Programmable soft materials and structures have been intensively studied recent years. But, usually the patterning process is complicated and requires sophisticated instruments. Compared to other patterning method, our strain engineering technique is facile and effective to program pattern LC molecules in a LCE. We can realize the radially patterned LCE with different active deformation modes when subjected to different external stimuli. By applying uniaxial strain on partially crosslinked LCE manually followed by UV curing process without any special setup, the radial pattern on LCE can be achieved. As a result, the radially patterned LCE shows fully reversible undulated deformation when subjected to heat which is induced by constrained expansion of LCE in hoop direction. In addition, larger undulated deformation can be obtained on radially patterned LCE when it is submerged in a solvent as the migration of solvent molecules into LCE network induces anisotropic swelling in radial and hoop direction. We only showed

simple radial patterning on LCE in this study, but more complex patterning is expected to be programmed using strain engineering technique by applying inhomogeneous strain in different ways.

Using the strain engineering technique, we next prepared light-induced multi-directional bending LCE-CNT rod. In this study, we incorporated CNT in the pre-LCE solution to get LCE-CNT composite material which endows photosensitivity on LCE matrix by the photothermal effect of CNT. The LCE-CNT rod is prepared in a tube shape mold followed by applying uniaxial strain under the UV curing to get fully programmed monodomain LCE-CNT rod. The LCE-CNT rod is aligned along its longitudinal direction, so it can bend concave toward light due to the strain gradient along its thickness. LCE-CNT rod exhibits fully reversible heliotropic deformation under the visible light different from conventional bending deformation reported from other LCE actuators. Therefore, we can tune the bending direction of the LCE-CNT rod intentionally tuned with the alteration of the position of light. In addition to the bending deformation induced by light, LCE-CNT rod shows localized and amplified bending deformation under the nIR laser irradiation, which may make it possible to control the bending behavior of LCE-CNT rod more precisely. We also show the soft gripper demonstration with manipulating function using LCE-CNT rod connected with arch shape LCE-CNT structure which can be fully driven by the light. The optically driven soft gripper demonstrated in study can perform the full operational function of gripping, moving, and releasing different from previous light-induced soft grippers which are limited to only gripping and releasing function.

Next, by using a same LCE or LCE-CNT rod structure, we show a discovery of unusual autonomous rolling phenomenon with an extremely simple setup. Our observation is that the LCE rod can roll while keeping their curved shape continuously on a flat hot surface with

homogeneously elevated temperature or under the homogeneous light illumination using a CNT incorporated LCE rod. The key reason for the unusual rolling is a combination of thermally driven active deformation and the heat transfer between LCE rod and surroundings. When LCE rod is subjected to heat either by direct heating or photothermal effect, the bending deformation triggers deviation of supporting force and gravity center of LCE rod which generates torque. Therefore, LCE rod can roll while generating new curvature every single moment, which may be regarded as LCE rod keep its curvature statically. We can confirm this by comparing the curvature direction of rolling LCE-CNT rod induced by heat or light, which show opposite curvature direction due to the opposite position of each external stimuli. In addition, we can control the rolling direction of thermally driven LCE-CNE rod by illuminating light from its moving direction to be reversed. We also show the demonstration of a light-powered weight-carrying vehicle and a thermally-powered conveyor using LCE-CNT rod as an active building block material.

Diverse types of light-induced actuation modes have been reported so far using soft actuating materials, but their motions are usually limited in one function for each soft actuating structure. We demonstrate a soft robot that can crawl, squeeze, and jump prepared from photosensitive LCE-CNT composite structure. Inspired by the locomotion of inchworm and jumping of fly larva, we created soft robot in arch shape with magnets at each end. By scanning the light on the soft robot, we can induce crawling motion induced by the deformation traveling on the top surface of it. When we reduce the interval between two adjacent light scanning cycles, the soft robot can deform more significantly with its height reduced by 25% of its initial height, so it can pass a small channel while crawling by squeezing its body. In addition to the crawling motion, the soft robot can perform jumping motion. We adopted a power-amplifying mechanism to achieve jumping motion by fixing each end of soft robot with magnetic force to make the soft robot in a

closed loop shape followed by light illumination on its outer surface. The strain energy can be stored under the continuous light irradiation on soft robot can be released in a very short time once the accumulated energy becomes large enough to open the closed structure constrained by magnetic force. As a result, the soft robot can jump by the amplified power as far as 4 times of its initial height. The light-induced crawling, squeezing, and jumping motion of soft robot is fully reversible, so it can proceed path with obstacles with different motions driven by light only.

Soft actuation is an attractive research area due to its intrinsic advantages over traditional actuators based on rigid materials. Although there have been notable developments in soft actuation last decades, it is still challenging to apply soft actuation in practical purposes. I wish this dissertation can contribute a small, but meaningful vision for the research and development of wirelessly controllable soft actuators, and their successful use for real world applications.